# DAMPING POWER SYSTEM OSCILLATIONS USING A STATCOM AND A PHASE IMBALANCED HYBRID SERIES CAPACITIVE COMPENSATION SCHEME

A Thesis

Submitted to the College of Graduate Studies and Research

in Partial Fulfillment of the Requirements

For the Degree of Master of Science

in the Department of Electrical and Computer Engineering

University of Saskatchewan

Saskatoon, Saskatchewan

By

Raed Bakhsh

# PERMISSION TO USE

I agree that the Library, University of Saskatchewan, may make this thesis freely available for inspection. I further agree that permission for copying of this thesis for scholarly purpose may be granted by the professor or professors who supervised the thesis work recorded herein or, in their absence, by the Head of the Department or the Dean of the College in which the thesis work was done. It is understood that due recognition will be given to me and to the University of Saskatchewan in any use of the material in this thesis. Copying or publication or any other use of this thesis for financial gain without approval by the University of Saskatchewan and my written permission is prohibited.

Request for permission to copy or to make any other use of the material in this thesis in whole or part should be addressed to:

Head of the Department of Electrical and Computer Engineering
57 Campus Drive
University of Saskatchewan
Saskatoon, Saskatchewan
Canada S7N 5A9

# ABSTRACT

Interconnection of remotely power systems with large generation capacity and system load is progressively widespread due to the increase of the power exchanges between countries as well as regions within countries in many parts of the world. In the cases of long distance AC transmission, as in interconnected power systems, care has to be taken for maintaining synchronism as well as stable system voltages, particularly in conjunction with system faults and line switching. With series compensation, bulk AC power transmission over very long distances (1000 km and more) is in existence today. These long distance power transfers cause, however, the system low-frequency oscillations, typically within the range of 0.4 to 2 Hz, to become more lightly damped. For this reason, many power network operators and utilities are taking steps to add supplementary controls in their systems to provide extra system damping aiming to improve the system security by damping these undesirable oscillations.

This thesis reports the results of time-domain simulation studies that are carried out to investigate the effectiveness of supplemental controls of a phase imbalance hybrid single-phase-Thyristor Controlled Series Capacitor (TCSC) compensation scheme and a static synchronous compensator in damping power system oscillations. In this context, studies are conducted on a typical large power system incorporating several series capacitor compensated transmission lines and large load centers with their reactive power support provided by static synchronous compensators (STATCOM).

Several case studies investigating the effects of the location of the hybrid single-phase-TCSC compensation scheme, the degree of compensation provided by the scheme, the stabilizing signals of the supplemental controls, the fault clearing time, as well as the fault location on the damping of power system oscillations are documented. The results of the investigations conducted in this thesis demonstrate that the supplemental controls are very effective in damping power system oscillations resulting from clearing system faults. The time-domain simulation studies are conducted using the ElectroMagnetic Transients program Restructured Version (EMTP-RV).

# ACKNOWLEDGMENTS

My first debt of appreciation must go to my Supervisor, Dr. Faried who patiently provided me with the vision, encouragement and the advice necessary for me to keep through the Master program and complete my thesis.

My fellow graduate students, faculty and staff of the Department of Electrical and Computer Engineering also deserve my sincerest thanks. Their friendship and assistance has meant more to me than I could ever express.

# TABLE OF CONTENTS

# LIST OF FIGURES

# LIST OF TABLES

# LIST OF SYMBOLS

| | |
|---|---|
| $C$ | capacitor |
| $C_{TCSC}$ | fixed capacitor of TCSC |
| $C_s$ | capacitor of the RC snubber circuit |
| d | direct axis |
| $E_{fd}$ | exciter output voltage |
| $E_R$ | output voltage of the voltage regulator amplifier |
| $E_{ref}$ | reference voltage of the excitation system |
| $E_{SB}$ | feedback stabilizing signal of the excitation system |
| *Fixed C* | Transmission lines are series capacitor compensated |
| $e_d$, $e_q$ | d- and q- axis stator voltages |
| $e_{fd}$ | field voltage |
| $G_p(s)$ | transfer function of a proportional type TCSC supplemental controller |
| $G_{L\text{-}L}(s)$ | transfer function of a lead-lag type TCSC supplemental controller |
| *Hybrid* | Transmission lines are compensated with the hybrid single-phase-TCSC compensation scheme |
| $I_{STATCOM}$ | STATCOM current |
| $I_{dc}$ | Capacitor dc current |
| $I_{CC}$ | STATCOM capacitive current |
| $I_{CC\_max}$ | STATCOM maximum capacitive current |
| $I_{LL}$ | STATCOM inductive current |
| $I_{LL\_max}$ | STATCOM maximum inductive current |
| $i_d$, $i_q$ | d- and q- axis stator currents |
| $i_{fd}$ | field winding current |
| $i_{1d}$, | d-axis damper winding current |
| $i_{1q}$, $i_{2q}$ | q-axis damper winding currents |
| *IMG* | imaginary part of a complex number |
| $K_A$ | gain of the voltage regulator amplifier |
| $K_E$ | exciter gain |
| $K_{FE}$ | feedback stabilizing loop gain of the excitation system |

| | |
|---|---|
| $K_G$ | supplemental controller gain |
| $K_P$ | proportional controller gain |
| $K_i$ | integral controller gain |
| $K_{Idc}$ | STATCOM dc capacitor voltage control integration gain |
| $K_{pdc}$ | Proportional gain (STATCOM controller) |
| $K_{mv}$ | STATCOM voltage control gain |
| $L_{TCSC}$ | fixed inductor of TCSC |
| $L_{ad}$ | d-axis magnetizing inductance |
| $L_{aq}$ | q-axis magnetizing inductance |
| $L_d$, $L_q$ | d- and q-axis synchronous inductances |
| $L_{ffd}$ | self-inductance of the field winding |
| $L_{11d}$ | self-inductance of the d-axis damper winding |
| $L_{11q}$, $L_{22q}$ | self-inductances of the q-axis damper winding |
| $m_{max}$ | Maximum limit of the STATCOM modulation ratio |
| $m_{min}$ | Minimum limit of the STATCOM modulation ratio |
| $P$ | real power |
| $PI$ | proportional integral |
| $P_{L1}$ *and* $P\_L1$ | real power flow in transmission line $L_1$ |
| $P_{L2}$ *and* $P\_L2$ | real power flow in transmission line $L_2$ |
| $P_m$ | mechanical power |
| $Q$ | reactive power |
| q | quadrature axis |
| $R_L$ | resistance of the series capacitor compensated transmission line |
| $R_a$ | armature resistance |
| $R_{fd}$ | field winding resistance |
| $R_{1d}$ | d-axis damper winding resistance |
| $R_{1q}$, $R_{2q}$ | q-axis damper winding resistances |
| $r_s$ | resistance of the RC snubber circuit |
| s | Laplace transformation operator |
| $T$ | superscript to denote matrix transpose |
| t | time |
| $T_F$ | forward thyristor |

| | |
|---|---|
| $T_R$ | reverse thyristor |
| $T_A$, $T_E$, $T_{FE}$ | time constants in the excitation system |
| $T_{ELEC}$ | air-gap torque |
| $T_{Idc}$ | STATCOM dc capacitor voltage control time constant |
| $T_m$ | supplemental controller low-pass filter time constant |
| $T_{mv}$ | STATCOM voltage control time constant |
| $T_{MECH}$ | mechanical torque |
| $T_1$, $T_2$ | Time constants (SVC/STATCOM controllers) |
| $T_1$, $T_{2,}$ $T_3$, $T_4$ | lead-lag network time constants |
| $T_w$ | washout filter time constant |
| $V_C$ | voltage across the series capacitor of the compensated transmission line |
| $V_{Cd}$, $V_{Cq}$ | voltages across the series capacitor in the d-q reference frame |
| $V_L$ | voltage across the inductance of the series capacitor compensated transmission line |
| $V_{Ld}$, $V_{Lq}$ | voltages across the inductance in the d-q reference frame |
| $V_R$ | voltage across the resistance of the series capacitor compensated transmission line |
| $V_{Rd}$, $V_{Rq}$ | voltages across the resistance in the d-q reference frame |
| $V_{Rmax}$, $V_{Rmin}$ | maximum and minimum ceiling voltages of the excitation system respectively |
| $V_b$ | infinite-bus voltage |
| $V_t$ | generator terminal voltage |
| $V_{td}$, $V_{tq}$ | d- and q- axis generator terminal voltages |
| $X_C$ | series capacitor reactance |
| $X_L$ | inductive reactance of the series capacitor compensated transmission line |
| $X_{-max}$, $X_{-min}$ | maximum and minimum TCSC reactances respectively |
| $X_{order}$ | dynamic reactance of TCSC |
| $X_{TCSCo}$ | initial net reactance of TCSC |
| $\alpha$ | thyristor firing angle |
| $\Psi_d$, $\Psi_q$ | d- and q- axis stator flux linkages |
| $\Psi_{fd}$ | field winding flux linkage |

| | |
|---|---|
| $\Psi_{1d}$ | d-axis damper winding flux linkage |
| $\Psi_{1q}$, $\Psi_{2q}$ | q-axis damper winding flux linkages |
| $\delta$ | generator power (load) angle |
| $\delta_{21}$ *and d21* | generator 2 load angle measured with respect to generator 1 load angle |
| $\delta_{31}$ *and d31* | generator 3 load angle measured with respect to generator 1 load angle |
| $\omega$ | angular velocity |
| $\omega_0$ $(f_0)$ | synchronous frequency (377 rad/sec) |
| $\omega_{21}$ | generator 2 speed measured with respect to generator 1 speed |
| $\omega_{31}$ | generator 3 speed measured with respect to generator 1 speed |
| $\Delta\theta_{dcmax}$ | Maximum phase lag angle change (STATCOM controller) |
| $\Delta\theta_{dcmin}$ | Minimum phase lag angle change (STATCOM controller) |
| $_0$ | suffix to denote the initial operating condition |
| $^{-1}$ | superscript to denote matrix inversion |

# Chapter 1

# INTROUDUCTION

## 1.1 General

Development of electric power transmission facilities is constrained despite the fact that bulk power transfers and use of transmission systems by third parties are increasing. Transmission bottlenecks, non-uniform utilization of facilities and unwanted parallel-path or loop flows are not uncommon. Transmission system expansion is needed, but not easily accomplished. Factors that contribute to this situation include a variety of environmental, land-use and regulatory requirements. As a result, the utility industry is facing the challenge of efficient utilization of the existing AC transmission lines. Thus, the transmission systems are being pushed to operate closer to their stability and thermal limits. Although electricity is a highly engineered product, it is increasingly being considered and handled as a commodity. Thus, the focus on the quality of power delivered is also greater than ever.

Series capacitive compensation of power transmission lines is an important and the most economical way to improve power transfer capability, especially when large amounts of power must be transmitted through long transmission lines. However, one of the hindering factors for the increased utilization of series capacitive compensation is the potential risk of Subsynchronous Resonance (SSR), where electrical energy is exchanged with turbine-generator shaft systems in a growing manner which can result in shaft damage [1]. Figure 1.1 shows a typical time response of a turbine-generator shaft torsional torque during and after clearing a fault on a series capacitive compensated transmission line in the presence of the SSR phenomenon. It is worth noting here that this shaft is designed to withstand a maximum torsional torque of 4 per unit. Another limitation of series capacitive compensation is its inability to provide adequate damping to power system oscillations after clearing and high-speed reclosing of system faults. Figure 1.2 shows a typical time response of a generator load angle, measured with respect to a reference generator load angle, during and after clearing a three-phase fault on a series capacitive compensated transmission line. As it can be seen from this figure, the

oscillations are not completely damped after the first few seconds from fault clearing which results in degrading the power quality of the system.

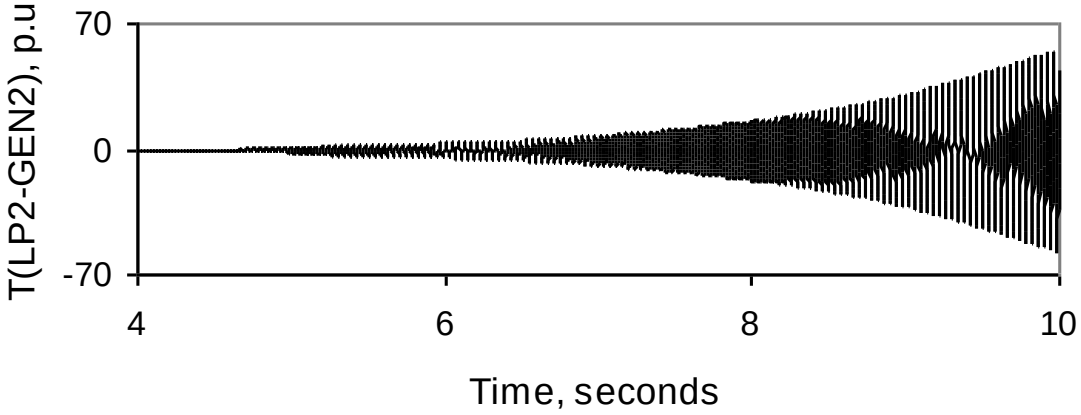


**Figure 1.1:** Transient time response of a turbine-generator shaft torsional torque during and after clearing a system fault on a series capacitive compensated transmission line.

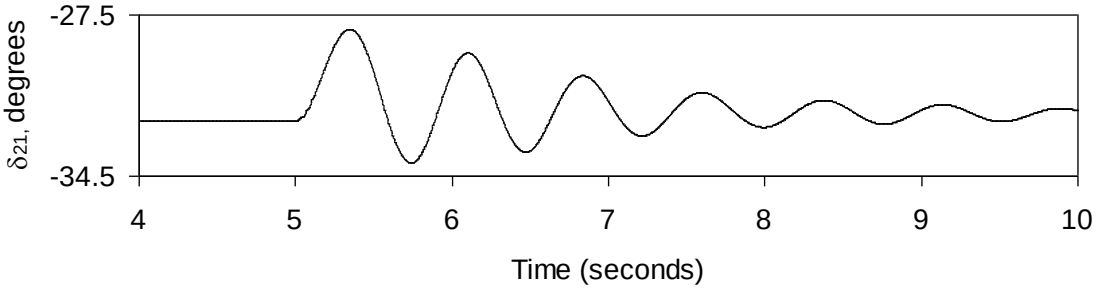


**Figure 1.2:** Transient time response of a generator load angle, measured with respect to a reference generator load angle, during and after clearing a system fault on a series capacitive compensated transmission line.

## 1.2 Transmission Line Series Compensation

The main purpose of series compensation in a power system is the virtual reduction of line reactance in order to enhance power system stability and increase the loadability of transmission corridors [2]. The principle is based on the compensation of the distributed line reactance by the insertion of a series capacitor. The reactive power generated by the capacitor is continuously proportional to the square of the line current. This means that the series capacitor has a self-regulating effect. When the system loading increases, the reactive power generated by the series capacitor increases as well. The response of the series capacitor is automatic, instantaneous and continuous as long as the capacitor current remains within the specified operating limits. The following are some of the major benefits of incorporating series capacitors in transmission systems:

### 1.2.1 Increase the power transfer capability by raising the first swing stability limit

A substantial increase in the stability margin is achieved by installing a series capacitor. The series compensation will improve the situation in two ways: it will decrease the initial generator load angle corresponding to a specific power transfer and it will also shift the power-load angle (P-δ) characteristic upwards. This will result in increasing the transient stability margin.

### 1.2.2 Increase in power transfer

The increase in the power transfer capability as a function of the degree of compensation for a transmission line can be illustrated using the circuit and the vector diagram shown in Figure 1.3. The power transfer on the transmission line is given by:

$$P = \frac{|V_s||V_R|}{X_{line} - X_c}\sin\delta = \frac{|V_s||V_R|}{X_{line}(1-k)}\sin\delta \qquad (1.1)$$

where $k$ is the degree of compensation defined as

$$k = \frac{X_c}{X_{line}}$$

The effect on the power transfer when a constant load angle difference is assumed is shown in Figure 1.4. Practical compensation degrees range from 20 to 70 percent. Transmission capability increases of more than two times can be obtained in practice.

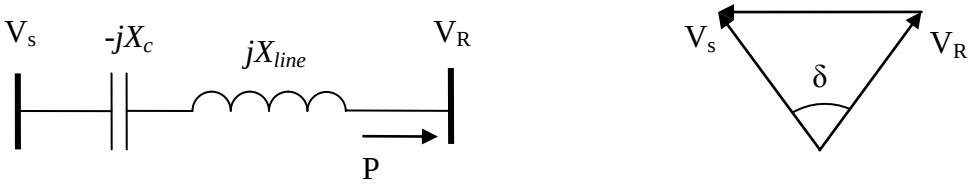


**Figure 1.3:** Transmission line with series capacitor.

### 1.2.3 Active load sharing between parallel circuits

When two transmission lines are connected in parallel, the natural power sharing between them is dictated by their respective impedances. If the two lines are of different configurations (and consequently of different thermal ratings), their impedances could still be very close. Therefore, the power transmitted in each line will be similar. The voltage drops in

both circuits are identical, and therefore, the relationship between the line currents $I_{L1}$ and $I_{L2}$ can be expressed as:

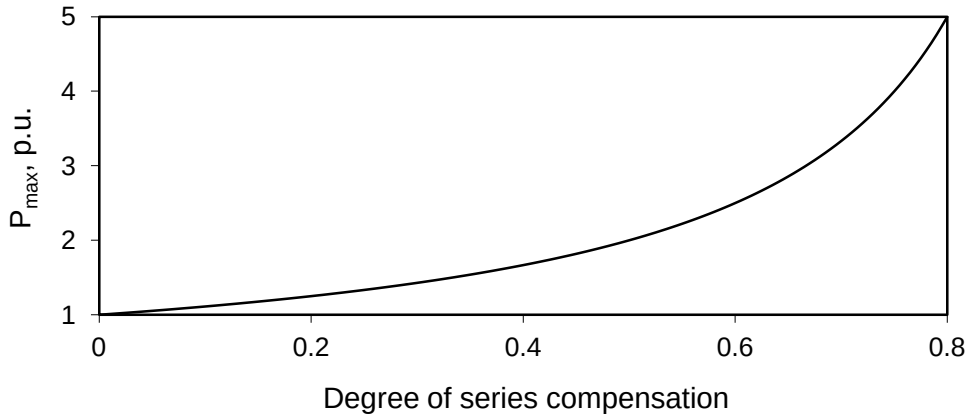


**Figure 1.4:** Maximum power transmitted over a transmission line as a function of the degree of series compensation ($|V_s| = |V_R| = 1\ p.u., X_{line} = 1\ p.u.$).

$$I_{L1}Z_{L1} = I_{L2}Z_{L2} \tag{1.2}$$

If overloading the lower thermal rating line, ($L_2$, Figure 1.5) is to be avoided (i.e., $I_{L2} \le I_{L2\max}$), then the full power capacity of the other line, $L_1$, will never be reached (i.e. $I_{L1} < I_{L1\max}$). For example, consider the case when $L_1$ is a four conductor bundle (quad) circuit configuration, whereas $L_2$ has a two conductor bundle (twin) circuit configuration. If the conductors of the two bundles are identical, then $L_1$ has twice the rating of $L_2$. The inductive reactances of the two lines, however, are very close. If a series capacitor is installed in the higher thermal rating line, both transmission lines can operate at their maximum capacity when the appropriate degree of compensation is provided (50% in this case) [3].

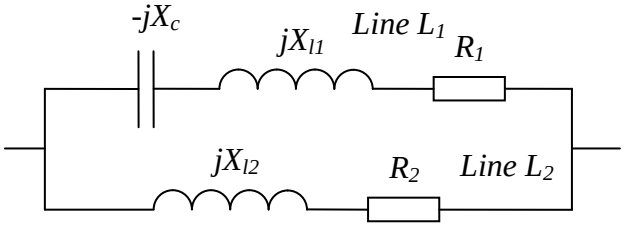


**Figure 1.5:** Adjusting the power sharing between two parallel lines using a series capacitor.

## 1.3 Series Capacitor Location

The optimum location for a single series capacitor bank, in terms of the most effective use of the series capacitive reactance, is at the middle of the transmission line [2]. The "effectiveness", which is based on the distributed parameter theory of transmission lines, is the figure of merit for the reduction of the series inductive reactance by a series capacitor. One Canadian installation that has the capacitors located at the middle of the transmission line is the B.C. Hydro 500 kV system described in [4]. A number of utilities, especially in the U.S., have tended to utilize two series capacitor banks and locate them at the ends of the transmission lines, in order to take advantage of existing land and the availability of service personnel at the line terminals [2]. In some situations, there may be valid reasons (geographical restrictions or specific benefits) for selecting other locations. For example, B.C. Hydro has a 605 Mvar, 500 kV single capacitor bank installed at McLeese substation which is located "nearly" mid-line between Williston and Kelly Lake substations (180 km from Williston and 130 km from Kelly Lake) [5].

## 1.4 Power System Oscillations

Many electric utilities world-wide are experiencing increased loadings on portions of their transmission systems, which can, and sometimes do, lead to poorly damped, low-frequency oscillations (0.5 – 2 Hz). These oscillations can severely restrict system operation by requiring the curtailment of electric power transfers as an operational measure. They can also lead to widespread system disturbances if cascading outages of transmission lines occur due to oscillatory power swings, like during the blackout in Western North America on August 10, 1996 [6].

Damping is defined as the energy dissipation properties of a material or a system. Power system oscillations can be damped, when extra energy is injected into the system which is instantaneously decelerated, and/or when extra energy is consumed in the system which is instantaneously accelerated. The damping energy is obtained by the modulation of load or generation for a period of time, typically in the range of five to ten seconds. The damping energy must have the correct phase shift relative to the accelerated/decelerated system as incorrect phase angles can excite the oscillations. Figure 1.6 shows different possibilities to damp power system oscillations [7].

## 1.5 Flexible AC Transmission Systems

All of the above discussed advantages of series compensation can be achieved without the risks of SSR phenomenon if series Flexible AC Transmission Systems (FACTS) devices are used instead of series capacitors. These devices are also able to provide adequate and fast damping to power system oscillations.

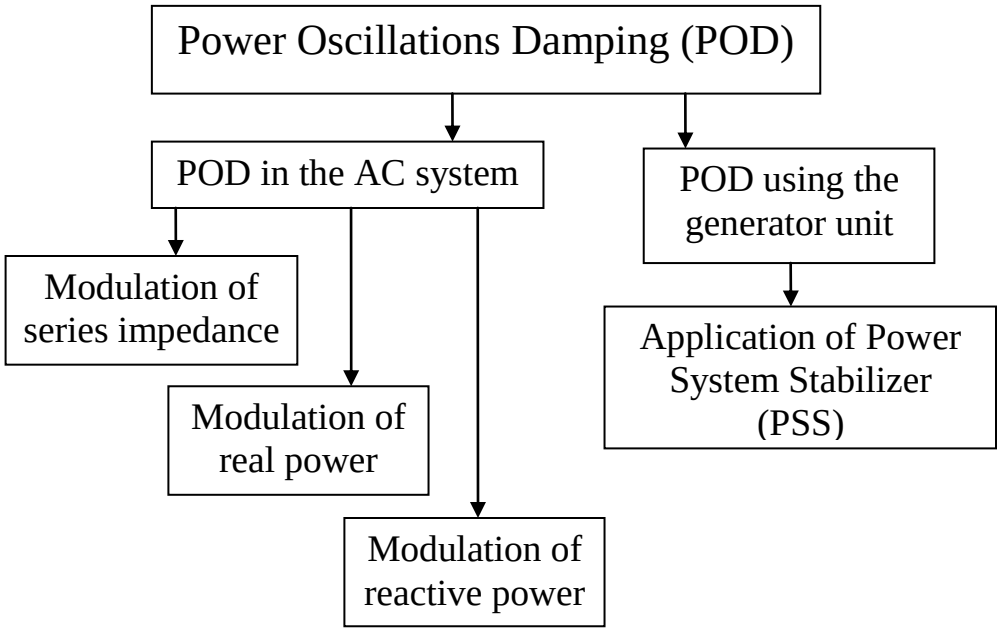


**Figure 1.6:** Strategies to damp power system oscillations.

FACTS controllers are power electronic based controllers which can influence transmission system voltages, currents, impedances and/or phase angles rapidly [8], [9]. These controllers have the flexibility of controlling both real and reactive power, which could provide an excellent capability for improving power system dynamics. FACTS technology provides an unprecedented way for controlling transmission grids and increasing transmission capacity.

FACTS controllers may be based on thyristor devices with no gate turn-off (only with gate turn-on), or with power devices with gate turn-off capability. In general, the principal controllers with gate turn-off devices are based on dc to ac converters, which can exchange active and/or reactive power with the ac system. In the studies conducted in this thesis, a series FACTS controller based on thyristor switches as well as a shunt FACTS controller based on power devices with gate turn-off capability are considered. The series FACTS controller, shown in Figure 1.7, is called a Thyristor Controlled Series Capacitor (TCSC) whereas the shunt

FACTS controller, shown in Figure 1.8, is called Static Synchronous Compensator (STATCOM) [8], [9].

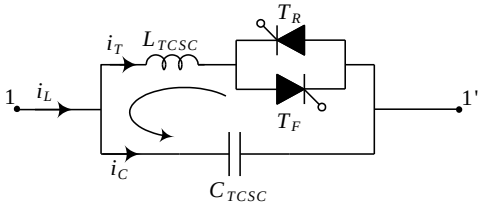


**Figure 1.7:** A schematic diagram of the TCSC.

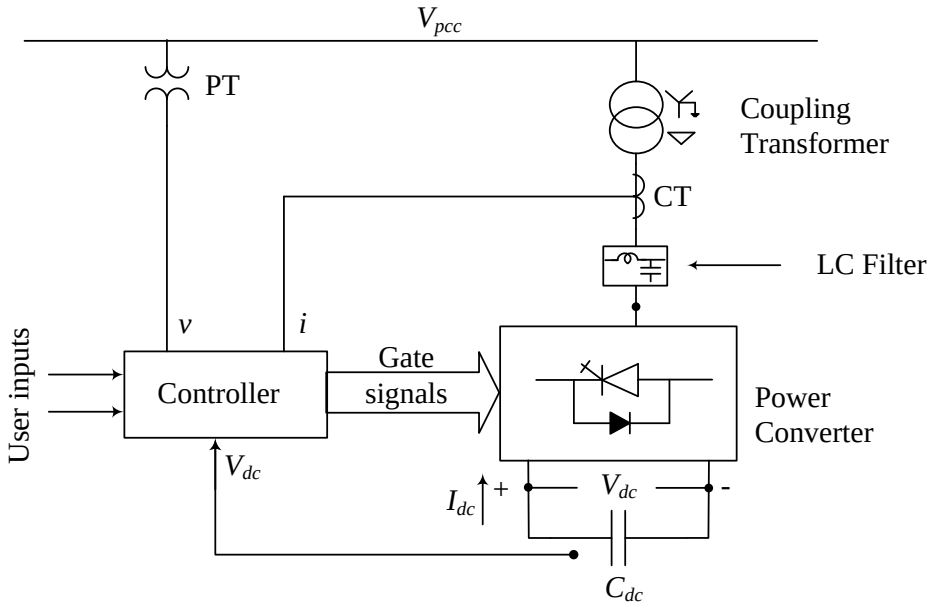


**Figure 1.8:** A STATCOM schematic block diagram connected to the ac grid.

The STATCOM and TCSC which will be discussed in details in Chapters 2 and 3 respectively, have been installed and operated successfully by utilities in several countries. One example of a TCSC installation is the Brazilian North-South interconnection (a 500 kV, 1020 km transmission line with a rated transmitted power of 1300 MW), where a hybrid three-phase-TCSC connects the North and South systems [10], [11]. Such a hybrid three-phase-TCSC, shown in Figure 1.9, consists of five fixed capacitors (distributed equally along the line length) and two TCSC modules (located at the sending and receiving ends). The degree of compensation of the interconnection is 66% (1100 Mvar capacitive), where the fixed capacitors provide 54% and each TCSC module provides 6%. The task of the TCSC modules is purely damping the low-frequency, inter-area power oscillations between the two systems. These oscillations would, otherwise, provide a threat to the stability of the interconnected system. On

the other hand, an example of a STATCOM installation for voltage support as a dynamic reactive power (var) source is the ± 100 MVAr STATCOM at the Sullivan Substation in North-Eastern Tennessee [9].

## 1.6 Research Objective and Scope of the Thesis

The recently proposed phase imbalanced series capacitive compensation concept has been shown to be effective in enhancing power system dynamics as it has the potential of damping power swing as well as subsynchronous resonance oscillations [12] - [14]. Figure 1.10 shows two schemes for a phase imbalanced capacitive compensation. They are *"hybrid"* series compensation schemes, where the series capacitive compensation in one phase is created using a single-phase TCSC (Scheme I) or a single-phase Static Synchronous Series Compensator (SSSC) (Scheme II) in series with a fixed capacitor ($C_c$), and the other two phases are compensated by fixed series capacitors (C). The TCSC and SSSC controls are initially set such that their equivalent compensations at the power frequency combined with the fixed capacitor yield a resultant compensation equal to the other two phases. Thus, the phase balance is maintained at the power frequency while at any other frequency, a phase imbalance is created. To further enhance power oscillations damping, the TCSC and SSSC are equipped with supplementary controllers.

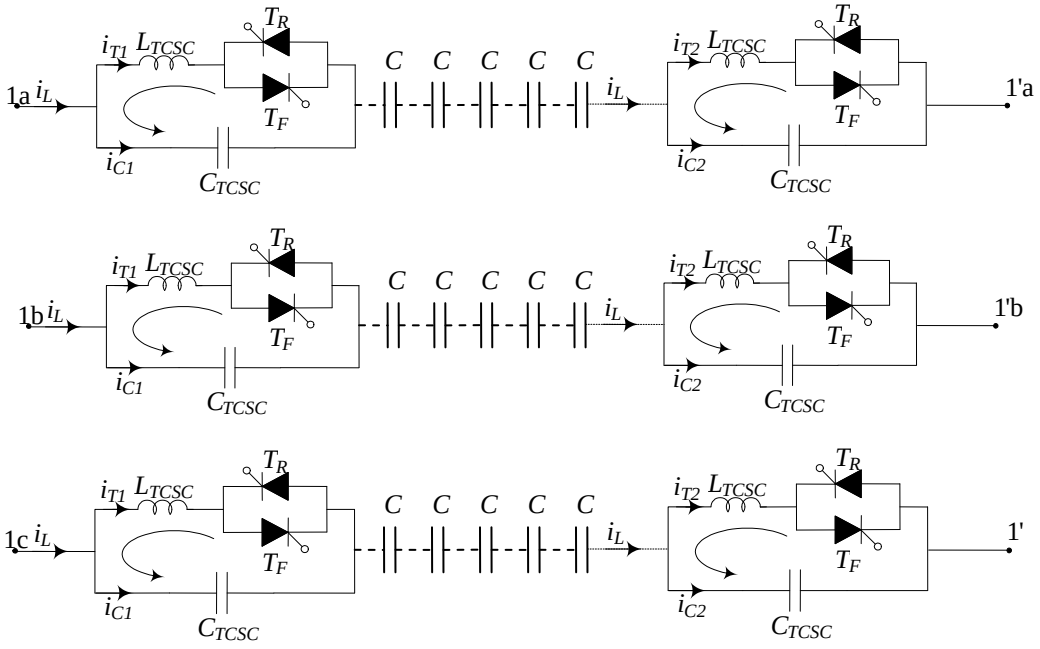


**Figure 1.9:** A three-line diagram of a hybrid three-phase-TCSC.

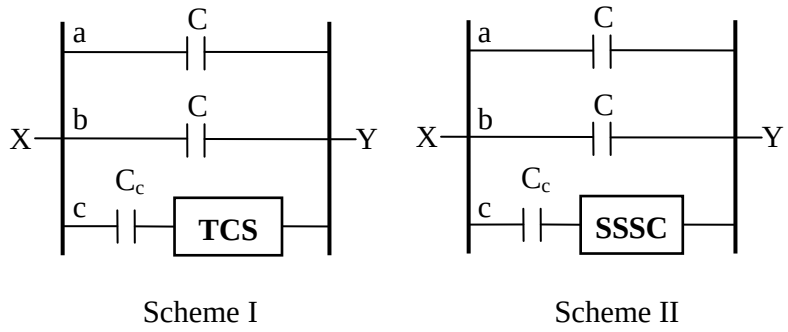


**Figure 1.10:** Schematic diagrams of the hybrid series capacitive compensation schemes.

The three-phase TCSC and the hybrid three-phase-TCSC which are already employed by several utilities for power flow control and damping low-frequency and SSR oscillations have shown superior performance through field tests and analytical and simulation studies [15] – [29]. The main objective of this research work is to investigate the potential use of a supplemental control of a STATCOM combined with a phase imbalanced hybrid series capacitive compensation scheme, namely Scheme I for damping power system oscillations resulting from large disturbances (mainly transmission line faults) in multi-machine power systems.

There are five chapters in this thesis. The main topics of each chapter are as follows:

Chapter 1 introduces the fundamental benefits of series compensation of transmission lines. Brief introductions to SSR, FACTS controllers and the TCSC are also presented. The objective of the research is also presented in this chapter.

In Chapter 2, the system used for the investigations conducted in this thesis is described and the detailed dynamic models of its individual components are also presented in this chapter. The results of the digital time-domain simulations of a case study for the system during a three-phase fault are presented at the end of this chapter.

Chapter 3 presents a comprehensive description of the TCSC, its three modes of operation and the analysis of its net reactance. The phase imbalanced hybrid single-phase-TCSC compensation scheme (Scheme I) and its modeling in the ElectroMagnetic Transient Program (EMTP-RV) are also presented.

Chapter 4 demonstrates the effectiveness of the supplemental controllers of the hybrid single-phase- TCSC compensation scheme (Scheme I) and the STATCOM in damping power

system oscillations through time-domain simulation studies. The performance of the controllers under different stabilizing signals is also investigated.

Chapter 5 summarizes the research described in this thesis and presents some conclusions.

# Chapter 2

# POWER SYSTEM MODELING FOR LARGE DISTURBANCE STUDIES

## 2.1 General

In this chapter, the system used for the studies reported in this thesis is described and the mathematical models of its various components are presented. A digital time-domain simulation of a case study of the system during a three-phase fault is presented at the end of this chapter.

## 2.2 System under Study

The system used in the investigations of this thesis is shown in Figure 2.1. It consists of four large generating stations ($G_1$, $G_2$, $G_3$ and $G_4$) supplying two load centers ($S_1$ and $S_2$) through seven 500 kV transmission lines. The two double-circuit transmission lines $L_1$ and $L_2$ are series compensated with fixed capacitor banks located in the middle of the lines. The compensation degree of $L_1$ and $L_2$ is 50%. The total installed capacity and peak load of the system are 5600 MVA and 4590 MVA respectively. Shunt capacitor banks are installed at bus 4 while a STATCOM is installed at bus 5 to maintain their voltages within 1±0.05 p.u. The system data are given in Appendix A.

## 2.3 Power System Modeling

The nonlinear differential equations of the system under study are derived by developing individually the mathematical models which represent the various components of the system, namely the synchronous generator, the excitation system, the transmission line and the system load. Knowing the mutual interaction among these models, the whole system differential equations can be formed.

### 2.3.1 Modeling of the synchronous machine

In a conventional synchronous machine, the stator circuit consisting of a three-phase winding produces a sinusoidally space distributed magnetomotive force. The rotor of the machine carries the field (excitation) winding which is excited by a dc voltage. The electrical damping due to the

eddy currents in the solid rotor and, if present, the damper winding is represented by three equivalent damper circuits; one on the direct axis (d-axis) and the other two on the quadrature axis (q-axis). The performance of the synchronous machine can be described by the equations given below in the d-q reference frame [30]. In these equations, the convention adopted for the signs of the voltages and currents are that *v* is the impressed voltage at the terminals and that the direction of positive current *i* corresponds to generation. The sign of the currents in the equivalent damper windings is taken positive when they flow in a direction similar to that of the positive field current.

With time $t$ expressed in seconds, the angular velocity $\omega$ expressed in rad/s ( $\omega_0 = 377\ rad\ /\sec$) and the other quantities expressed in per unit, the stator equations become:

$$e_d = \frac{1}{\omega_0}\frac{d\Psi_d}{dt} - \frac{\omega}{\omega_0}\Psi_q - R_a i_d \tag{2.1}$$

$$e_q = \frac{1}{\omega_0}\frac{d\Psi_q}{dt} + \frac{\omega}{\omega_0}\Psi_d - R_a i_q \tag{2.2}$$

The rotor equations:

$$e_{fd} = \frac{1}{\omega_0}\frac{d\Psi_{fd}}{dt} + R_{fd} i_{fd} \tag{2.3}$$

$$0 = \frac{1}{\omega_0}\frac{d\Psi_{1d}}{dt} + R_{1d} i_{1d} \tag{2.4}$$

$$0 = \frac{1}{\omega_0}\frac{d\Psi_{1q}}{dt} + R_{1q} i_{1q} \tag{2.5}$$

$$0 = \frac{1}{\omega_0}\frac{d\Psi_{2q}}{dt} + R_{2q} i_{2q} \tag{2.6}$$

The stator flux linkage equations:

$$\Psi_d = -L_d i_d + L_{ad} i_{fd} + L_{ad} i_{1d} \tag{2.7}$$

$$\Psi_q = -L_q i_q + L_{aq} i_{1q} + L_{aq} i_{2q} \tag{2.8}$$

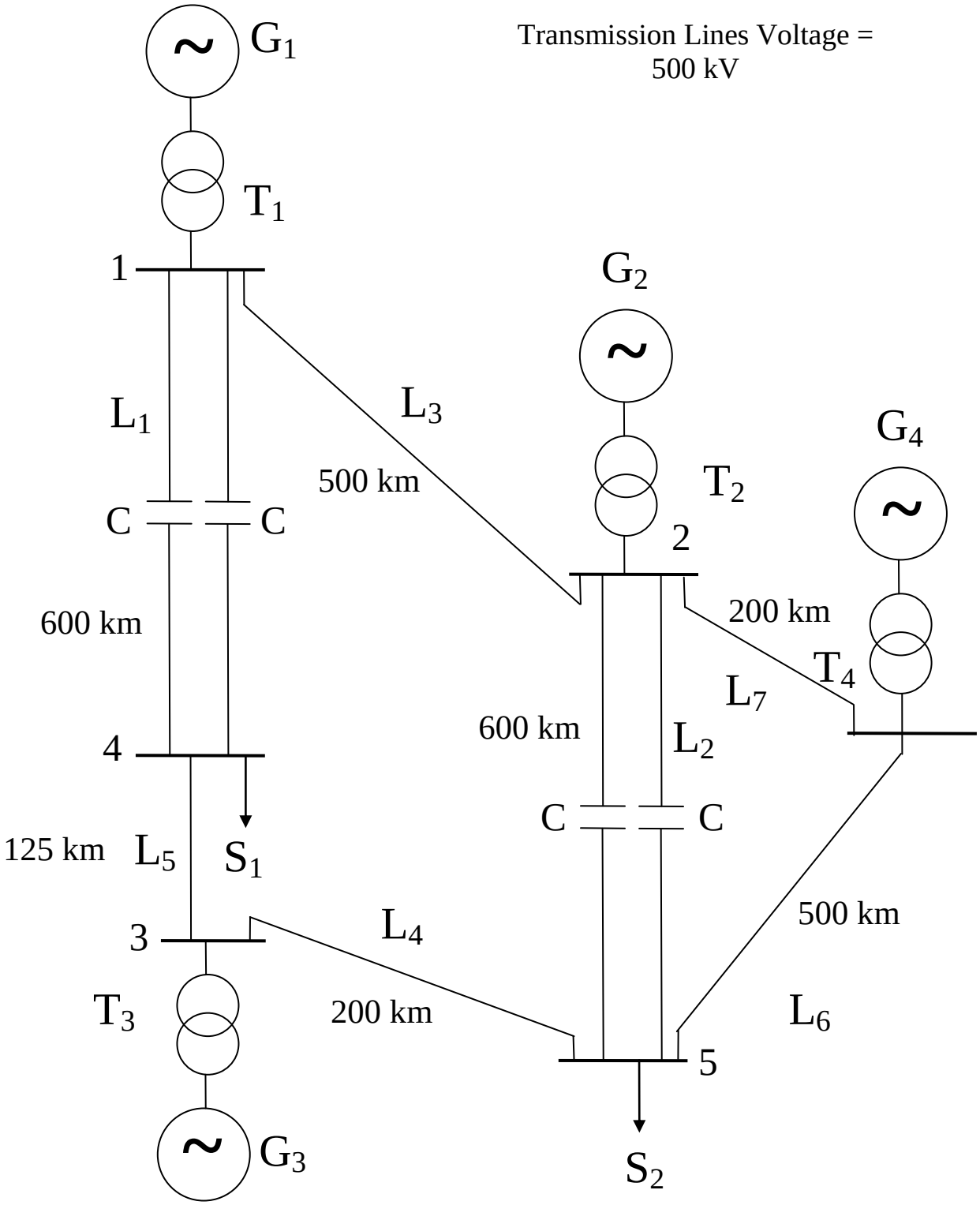


**Figure 2.1:** System under study.

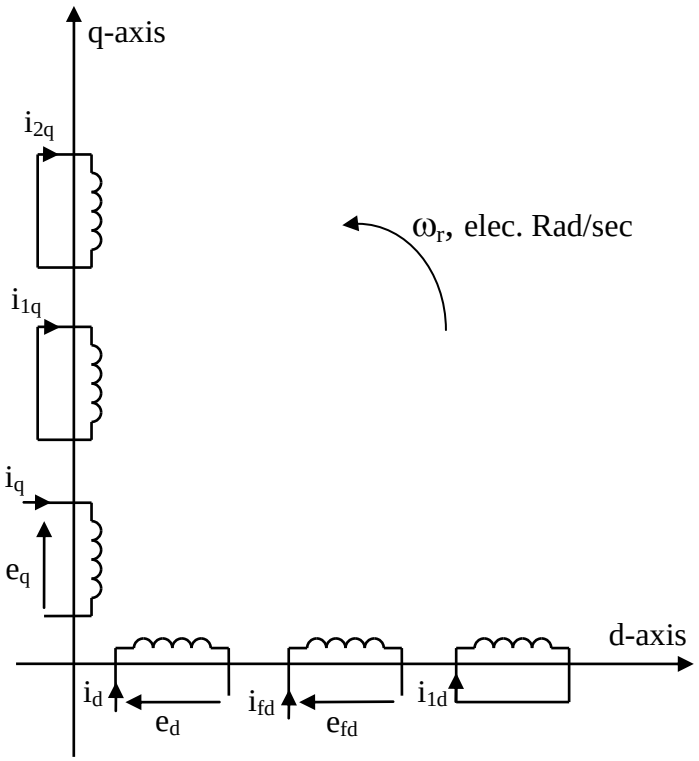


**Figure 2.2:** Modeling of the synchronous machine in the d-q reference frame.

The rotor flux linkage equations:

$$\Psi_{fd} = L_{ffd}\, i_{fd} + L_{ad}\, i_{1d} - L_{ad}\, i_d \tag{2.9}$$

$$\Psi_{1d} = L_{ad}\, i_{fd} + L_{11d}\, i_{1d} - L_{ad}\, i_d \tag{2.10}$$

$$\Psi_{1q} = L_{11q}\, i_{1q} + L_{aq}\, i_{2q} - L_{aq}\, i_q \tag{2.11}$$

$$\Psi_{2q} = L_{aq}\, i_{1q} + L_{22q}\, i_{2q} - L_{aq}\, i_q \tag{2.12}$$

The air-gap torque equation:

$$T_{ELEC} = \Psi_d\, i_q - \Psi_q\, i_d \tag{2.13}$$

The overall differential equations which describe the transient performance of the synchronous machine are given by the following matrix equation:

$$\left[\frac{dX_{syn}}{dt}\right] = \left[At_{syn}\right]\left[X_{syn}\right] + \left[Bt_{syn}\right]\begin{bmatrix} V_{td} \\ V_{tq} \\ e_{fd} \end{bmatrix} \tag{2.14}$$

where

$$\left[X_{syn}\right] = \left[i_d \quad i_q \quad i_{fd} \quad i_{1q} \quad i_{1d} \quad i_{2q}\right]^T$$

$$\left[At_{syn}\right] = \left[L\right]^{-1}\left[Qt\right]$$

$$\left[Bt_{syn}\right] = \left[L\right]^{-1}\left[Rt\right]$$

$$\left[L\right] = \begin{bmatrix} -L_d & 0 & L_{ad} & 0 & L_{ad} & 0 \\ 0 & -L_q & 0 & L_{aq} & 0 & L_{aq} \\ -L_{ad} & 0 & L_{ffd} & 0 & L_{ad} & 0 \\ 0 & -L_{aq} & 0 & L_{11q} & 0 & L_{aq} \\ -L_{aq} & 0 & L_{ad} & 0 & L_{11d} & 0 \\ 0 & -L_{aq} & 0 & L_{aq} & 0 & L_{22q} \end{bmatrix} \tag{2.15}$$

$$\left[Qt\right] = \begin{bmatrix} \omega_0 R_a & -\omega L_q & 0 & \omega L_{aq} & 0 & \omega L_{aq} \\ \omega L_d & \omega_0 R_a & -\omega L_{ad} & 0 & -\omega L_{ad} & 0 \\ 0 & 0 & -\omega_0 R_{fd} & 0 & 0 & 0 \\ 0 & 0 & 0 & -\omega_0 R_{1q} & 0 & 0 \\ 0 & 0 & 0 & 0 & -\omega_0 R_{1d} & 0 \\ 0 & 0 & 0 & 0 & 0 & -\omega_0 R_{2q} \end{bmatrix}$$

$$\left[Rt\right] = \begin{bmatrix} \omega_0 & 0 & 0 \\ 0 & \omega_0 & 0 \\ 0 & 0 & \omega_0 \\ 0 & 0 & 0 \\ 0 & 0 & 0 \\ 0 & 0 & 0 \end{bmatrix}$$

here, the superscript $^T$ means matrix transpose.

The synchronous machine swing equation can be written as:

$$\frac{2H}{\omega_o}\frac{d\omega}{dt} = T_{MECH} - T_{ELEC} \tag{2.16}$$

$$\frac{d\delta}{dt} = \omega - \omega_o \tag{2.17}$$

In the above two equations (2.16 and 2.17), $\omega$ is in radians per second, the inertia constant H is in seconds, and the load angle δ is in radians, $\omega_o$ is the synchronous frequency (377 rad/sec) and the mechanical and electrical torques $T_{MECH}$ and $T_{ELEC}$ are in per unit.

In developing the equations of multi-machine systems, the equations of each synchronous machine expressed in its own d-q reference frame which rotates with its rotor must be expressed in a common reference frame. Usually, a reference frame rotating at synchronous speed is used as the common reference. Axis transformation equations are used to transform between the individual machine (d-q) reference frames and the common (R-I) reference frame [30].

### 2.3.2 Modeling of the transmission line

A series capacitor-compensated transmission line may be represented by the *RLC* circuit shown in Figure 2.3 [31]. In the voltage phasor diagram shown in Figure 2.4, the rotor angle $\delta$ is the angle (in elec. rad) by which the q-axis leads the reference voltage $V_b$. The differential equations for the circuit elements, after applying Park's transformation [31], can be expressed in the d-q reference frame by the following matrix expressions.

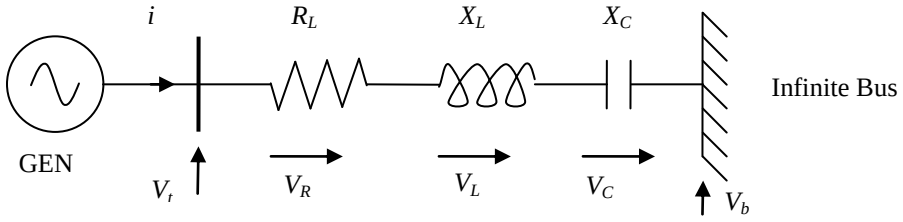


**Figure 2.3:** A series capacitor-compensated transmission line.

The voltage across the resistance:

$$\begin{bmatrix} V_{Rd} \\ V_{Rq} \end{bmatrix} = \begin{bmatrix} R_L & 0 \\ 0 & R_L \end{bmatrix} \begin{bmatrix} i_d \\ i_q \end{bmatrix} \tag{2.18}$$

The voltage across the inductance:

$$\begin{bmatrix} V_{Ld} \\ V_{Lq} \end{bmatrix} = \begin{bmatrix} 0 & -\frac{\omega}{\omega_0} X_L \\ \frac{\omega}{\omega_0} X_L & 0 \end{bmatrix} \begin{bmatrix} i_d \\ i_q \end{bmatrix} + \begin{bmatrix} \frac{X_L}{\omega_0} & 0 \\ 0 & \frac{X_L}{\omega_0} \end{bmatrix} \begin{bmatrix} \frac{di_d}{dt} \\ \frac{di_q}{dt} \end{bmatrix} \tag{2.19}$$

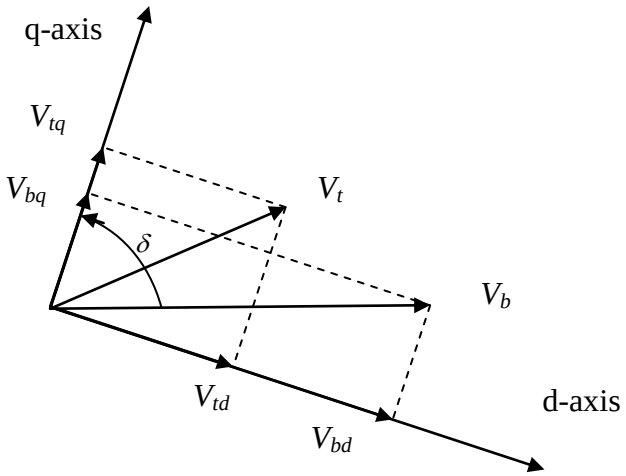


**Figure 2.4:** Voltage phasor diagram.

The voltage across the capacitor:

$$\begin{bmatrix} \frac{dV_{Cd}}{dt} \\ \frac{dV_{Cq}}{dt} \end{bmatrix} = \begin{bmatrix} \omega_0 X_C & 0 \\ 0 & \omega_0 X_C \end{bmatrix} \begin{bmatrix} i_d \\ i_q \end{bmatrix} + \begin{bmatrix} 0 & \omega \\ -\omega & 0 \end{bmatrix} \begin{bmatrix} V_{Cd} \\ V_{Cq} \end{bmatrix} \tag{2.20}$$

The overall equations of the transmission line can be written as

$$\begin{bmatrix} \frac{dV_{Cd}}{dt} \\ \frac{dV_{Cq}}{dt} \\ V_{td} \\ V_{tq} \end{bmatrix} = [Att] \begin{bmatrix} V_{Cd} \\ V_{Cq} \end{bmatrix} + [Rt1] \begin{bmatrix} \frac{di_d}{dt} \\ \frac{di_q}{dt} \end{bmatrix} + [Rt2] \begin{bmatrix} i_d \\ i_q \end{bmatrix} + [Btt][V_b] \tag{2.21}$$

where

$$[Att] = \begin{bmatrix} 0 & \omega \\ -\omega & 0 \\ 1 & 0 \\ 0 & 1 \end{bmatrix}$$

$$[Rt1] = \begin{bmatrix} 0 & 0 \\ 0 & 0 \\ \frac{X_L}{\omega_0} & 0 \\ 0 & \frac{X_L}{\omega_0} \end{bmatrix}$$

$$[Rt\,2] = \begin{bmatrix} \omega_0 X_C & 0 \\ 0 & \omega_0 X_C \\ R_L & -\dfrac{\omega}{\omega_0} X_L \\ \dfrac{\omega}{\omega_0} X_L & R_L \end{bmatrix} \tag{2.22}$$

$$[Btt] = \begin{bmatrix} 0 \\ 0 \\ \sin\delta \\ \cos\delta \end{bmatrix}$$

### 2.3.3 Excitation system

The block diagram representation of the excitation system used in this study is shown in Figure 2.5, and the corresponding data are given in Appendix A [31].

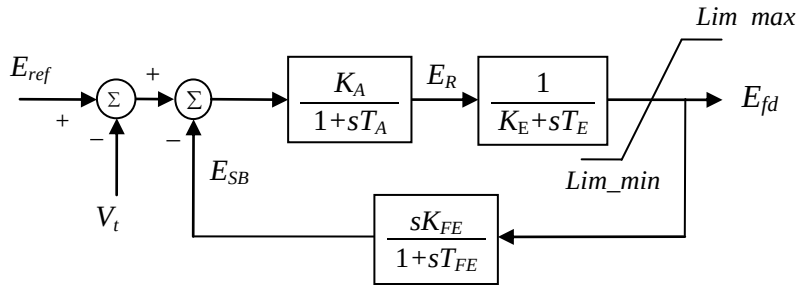


**Figure 2.5:** Block diagram of the excitation system.

Utilizing the relationship between the excitation system output voltage and the field voltage given by $E_{fd} = \dfrac{L_{ad}}{R_{fd}} e_{fd}$, the state-space equation of the excitation system can be derived from its block diagram and is given by

$$\begin{bmatrix} \dfrac{dX_v}{dt} \end{bmatrix} = [At_v][X_v] + [Bt_v] \begin{bmatrix} V_t \\ E_{ref} \end{bmatrix} \tag{2.23}$$

where

$$[X_v] = \begin{bmatrix} e_{fd} & E_R & E_{SB} \end{bmatrix}^T$$

$$[At_v] = \begin{bmatrix} -\frac{K_E}{T_E} & \frac{1}{T_E}\frac{R_{fd}}{L_{ad}} & 0 \\ 0 & -\frac{1}{T_A} & -\frac{K_A}{T_A} \\ -\frac{K_E K_F}{T_E T_F}\frac{L_{ad}}{R_{fd}} & \frac{K_F}{T_F T_E} & -\frac{1}{T_F} \end{bmatrix} \tag{2.24}$$

$$[Bt_v] = \begin{bmatrix} 0 & 0 \\ -\frac{K_A}{T_A} & \frac{K_A}{T_A} \\ 0 & 0 \end{bmatrix}$$

### 2.3.4 Modeling of the transformer

The three-phase transformer is constructed by using three single-phase transformers connected in Delta (LV side)/Y grounded (HV side). The transformer leakage and magnetizing reactances as well as the winding resistances and core loss are represented in the model.

### 2.3.5 Modeling of system loads

The system loads are modeled in these studies by constant impedances. The formula, which is used in calculating the load impedances, is given by [32]:

$$Z_{Load} = \frac{|V_{Load}|^2}{P_{Load} - jQ_{Load}} \tag{2.25}$$

where

$Z_{Load}$ = load impedance.

$V_{Load}$ = load voltage.

$P_{Load}$ = load real power.

$Q_{Load}$ = load reactive power.

## 2.4 The Static Synchronous Compensator

The STATCOM is a shunt connected reactive power compensation FACTS Controller that is capable of generating and/or absorbing reactive power and in which the output can be varied to control specific parameters of an electric power system. It is, in general, a solid-state switching converter capable of generating or absorbing independently controllable real and reactive power at its output terminals when it is fed from an energy source or energy-storage device at its input

terminals. More specific, the STATCOM is a voltage-source converter (VSC) that, from a given input of dc voltage, produces a set of three-phase ac output, each in phase and coupled to the corresponding ac system voltage through a relatively small reactance (which is provided by either an interface reactor or the leakage inductance of a coupling transformer). The dc voltage is provided by an energy storage capacitor. The principle of operation of VSCs is discussed in Appendix B [33].

### 2.4.1 STATCOM principle of operation

The STATCOM is a controlled reactive power source. It provides the desired reactive power generation or absorption entirely by means of electronic processing of the voltage and current waveforms in a VSC. A single-line diagram of a STATCOM power circuit is shown in Figure 2.6(a), where a VSC is connected to a utility bus through magnetic coupling [34].

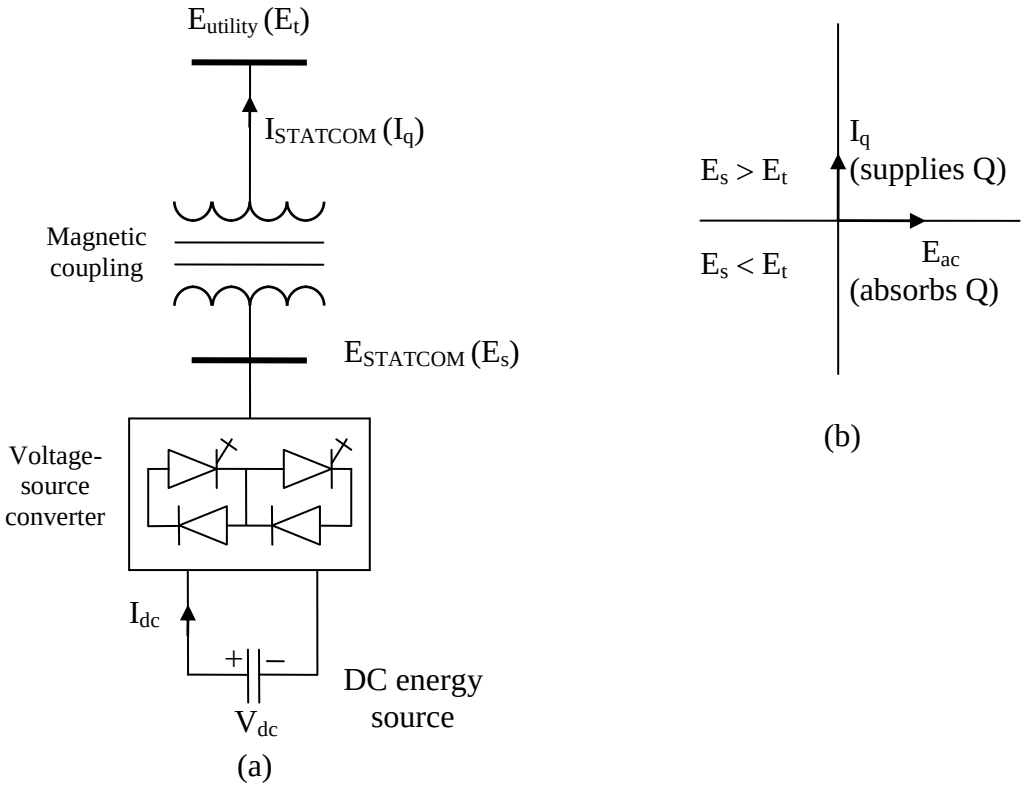


**Figure 2.6:** The STATCOM principle diagram: (a) power circuit, (b) reactive power exchange.

The exchange of the reactive power between the converter and the ac system can be controlled by varying the amplitude of the three-phase output voltage, $E_s$, of the converter, as illustrated in

Figure 2.6(b). That is, if the amplitude of the output voltage is increased above that of the utility bus voltage, $E_t$, then a current flows through the reactance from the converter to the ac system and the converter generates capacitive-reactive power for the ac system. If the amplitude of the output voltage is decreased below the utility bus voltage, then current flows from the ac system to the converter and the converter absorbs inductive-reactive power from the ac system. If the output voltage equals the ac system voltage, the reactive power exchange becomes zero, in which case, the STATCOM is said to be in a floating state.

The VSC has the same rated current capacity when it operates with the capacitive or inductive current. Therefore, a VSC having a certain MVA rating gives the STATCOM twice the dynamic range in MVAR. The magnitude of the capacitor is chosen so that the dc voltage across its terminal remains fairly constant to prevent it from contributing to the ripples in the dc current.

The VSC may be a 2- level or 3-level type, depending on the required output power and voltage [9], [34]. A number of VSCs are combined in a multi-pulse connection to form the STATCOM. At steady-state, the VSCs operate with fundamental frequency switching to minimize converter losses. However, during transient conditions caused by line faults, a Pulse Width Modulation (PWM) mode is used to prevent the fault current from entering the VSCs. In this way, the STATCOM is able to withstand transients on the ac side without blocking.

### 2.4.2 STATCOM V-I characteristic

A typical V-I characteristic of a STATCOM is depicted in Figure 2.7 [34]. As can be seen, the STATCOM can be operated over its full output current range even at very low system voltage levels (typically 0.2 p.u.). In other words, the maximum capacitive or inductive output current of the STATCOM can be maintained independently of the ac system voltage. Moreover, the STATCOM maximum Var generation or absorption changes linearly with the ac system voltage.

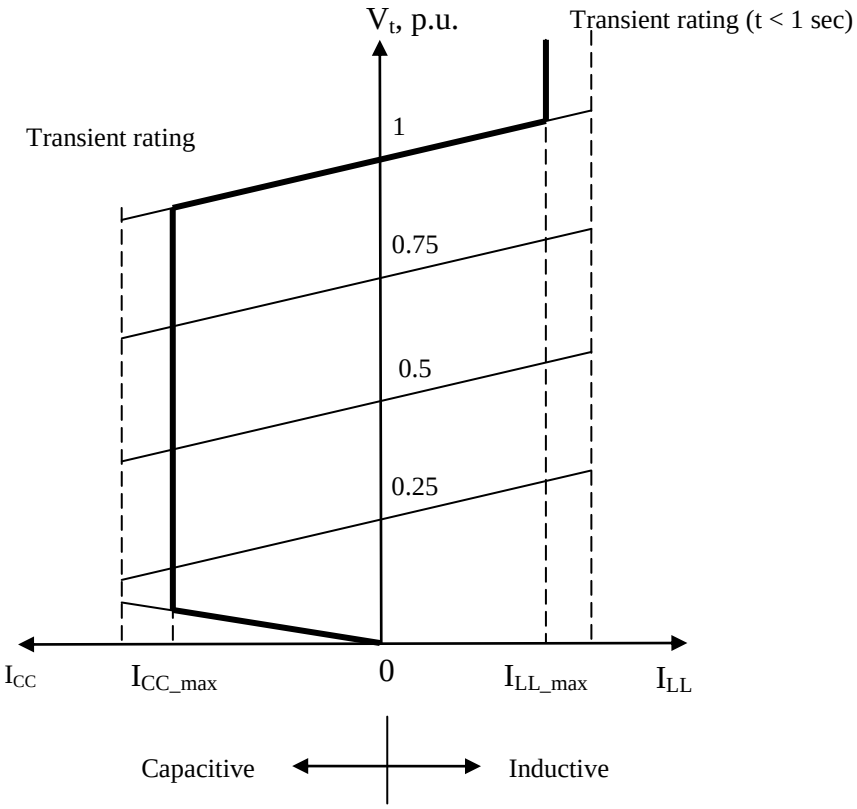


**Figure 2.7:** The STATCOM V-I characteristic.

### 2.4.3 STATCOM controller

The main function of a STATCOM, as with an SVC, is to regulate the transmission line voltage at the point of connection. Figure 2.8(a) shows the block diagrams of a STATCOM voltage controller where $E_s$ is controlled by varying the modulation ratio $m$ (Appendix B).

For a proper operation of the STATCOM, the dc bus voltage must be maintained within a pre-specified range. At steady state, $E_s$ lags $E_t$ by a small angle (less than one degree) in order to charge the dc capacitor and supply the VSC losses. The control of the dc capacitor voltage is achieved by implementing a proportional-integral (PI) controller as shown in Figure 2.8(b). The output of this controller, "$\Delta\theta_{dc}$" is added to the phase angle between $E_s$ and $E_t$.

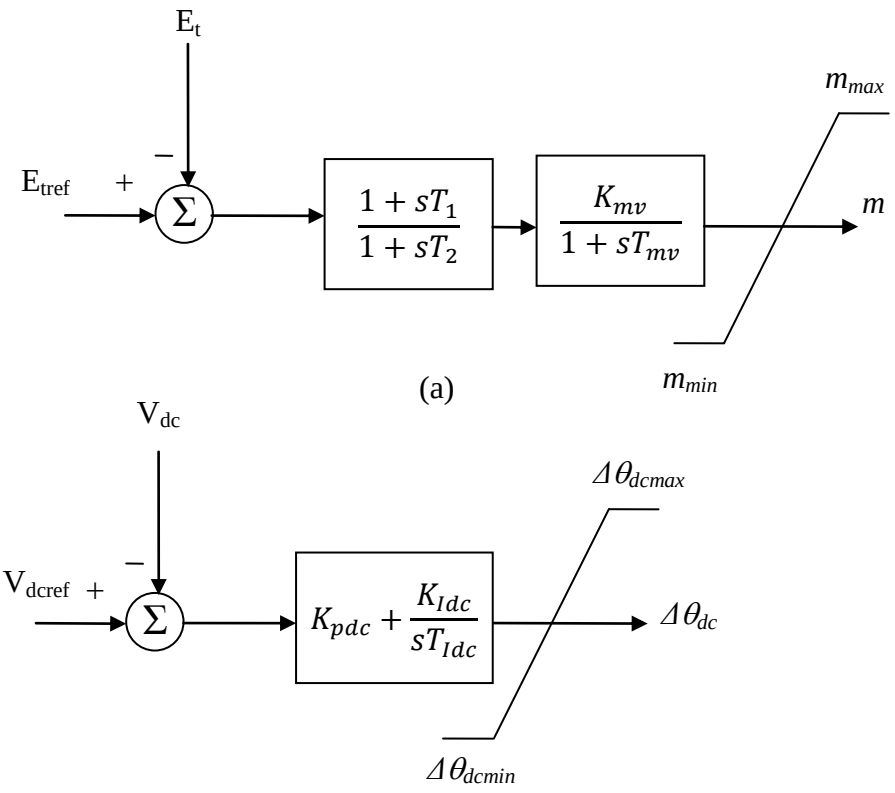


**Figure 2.8:** A STATCOM controller: (a) voltage control, (b) dc capacitor voltage control.

## 2.5 A Sample Case Study

In the studies conducted in this thesis, the ElectroMagnetic Transient Program (EMTP-RV) is used for modeling the various system components and producing the time-domain simulation results [35]. Due to the initialization process in the EMTP-RV, simulation results will be displayed starting at time equal fifteen seconds. Moreover, faults are assumed to occur at t = 16 seconds.

Figure 2.9 shows the power flow results for the bus voltages and the line real power flows of the system under study. Figure 2.10 shows the transient time responses of the generator load angles and speeds (measured respectively with respect to the load angle and speed of generator 1), the bus voltages and the real power flows in the transmission lines during and after clearing a three-cycle, three-phase fault at bus 3. The following observations can be made from examining these two figures:

1. The power flow results show heavy power transfers along the two compensated lines $L_1$ and $L_2$.
2. The system is stable after fault clearing. The generator load angles and speeds reach steady states. The bus voltages drop immediately at the instant of fault inception but recover after fault clearing.
3. The low frequency oscillations in the generator load angles and speeds are poorly damped.
4. The system under study has four generators; therefore, it has three natural modes of oscillations [29]. In general, synchronous machines respond to disturbances by complex oscillations that involve several natural frequencies, but a particular machine or group of coherent machines may tend to favor one mode over all others [2]. This is the case for generators 2, 3 and 4. As it can be seen from the load angle responses of these three generators, measured with respect to the load angle of generator 1 (Figure 2.10), generators 2, 3 and 4 tend to oscillate at a single frequency (approximately 1.4 Hz).

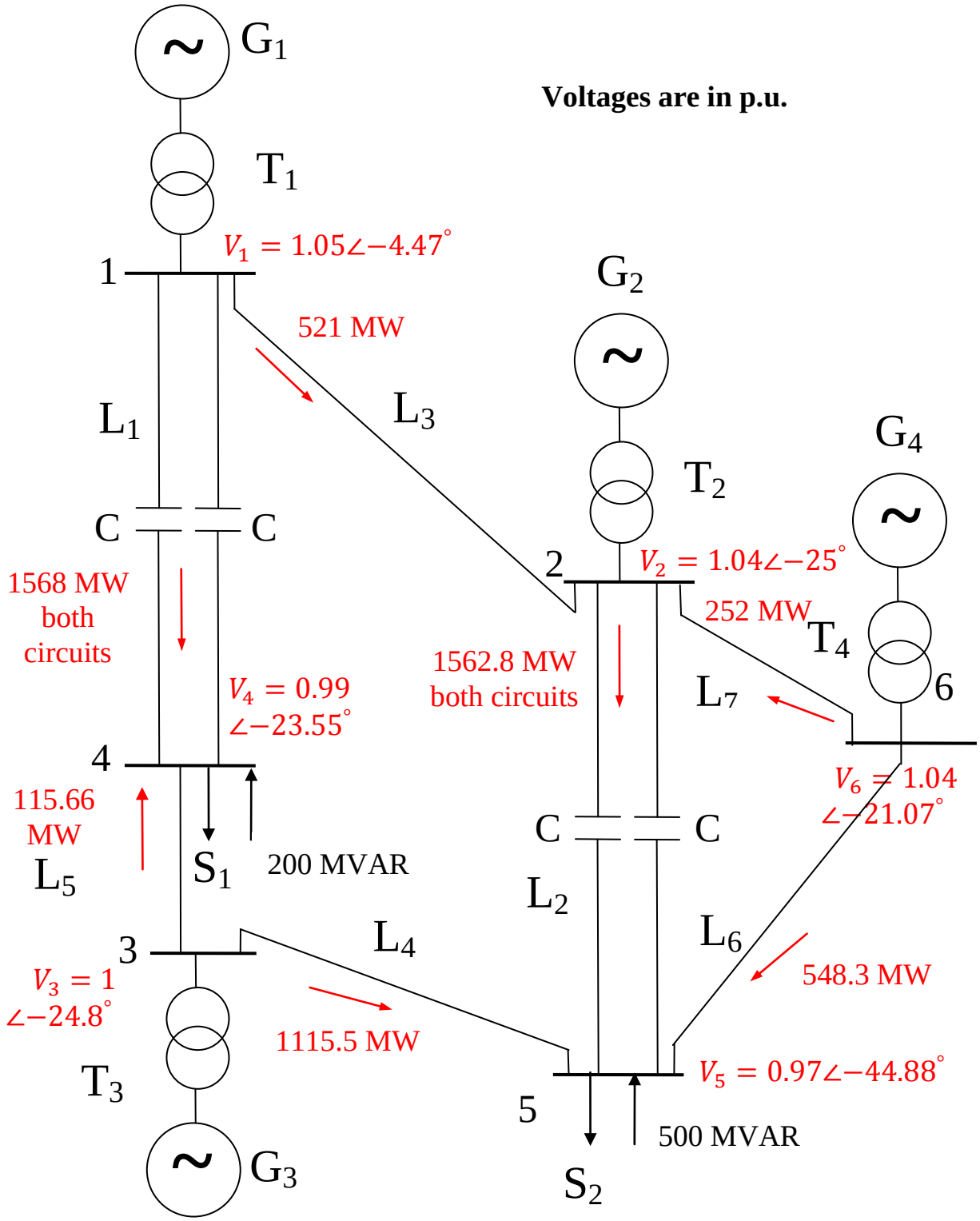


**Figure 2.9:** Power flow results of bus voltages and line real power flows of the system under study.

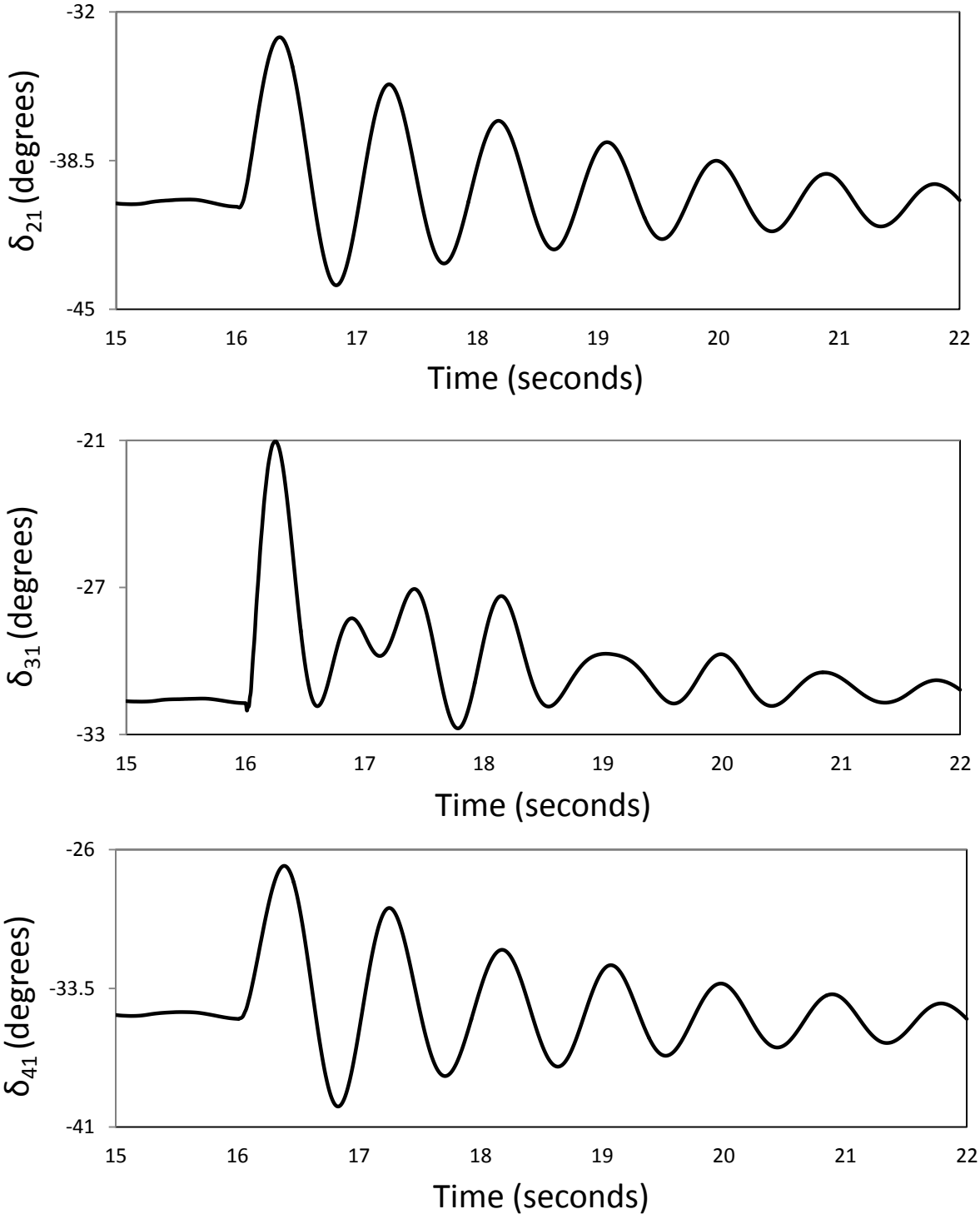


**Figure 2.10:** Transient time responses of the power system during and after clearing a three-cycle, three-phase fault at bus 3.

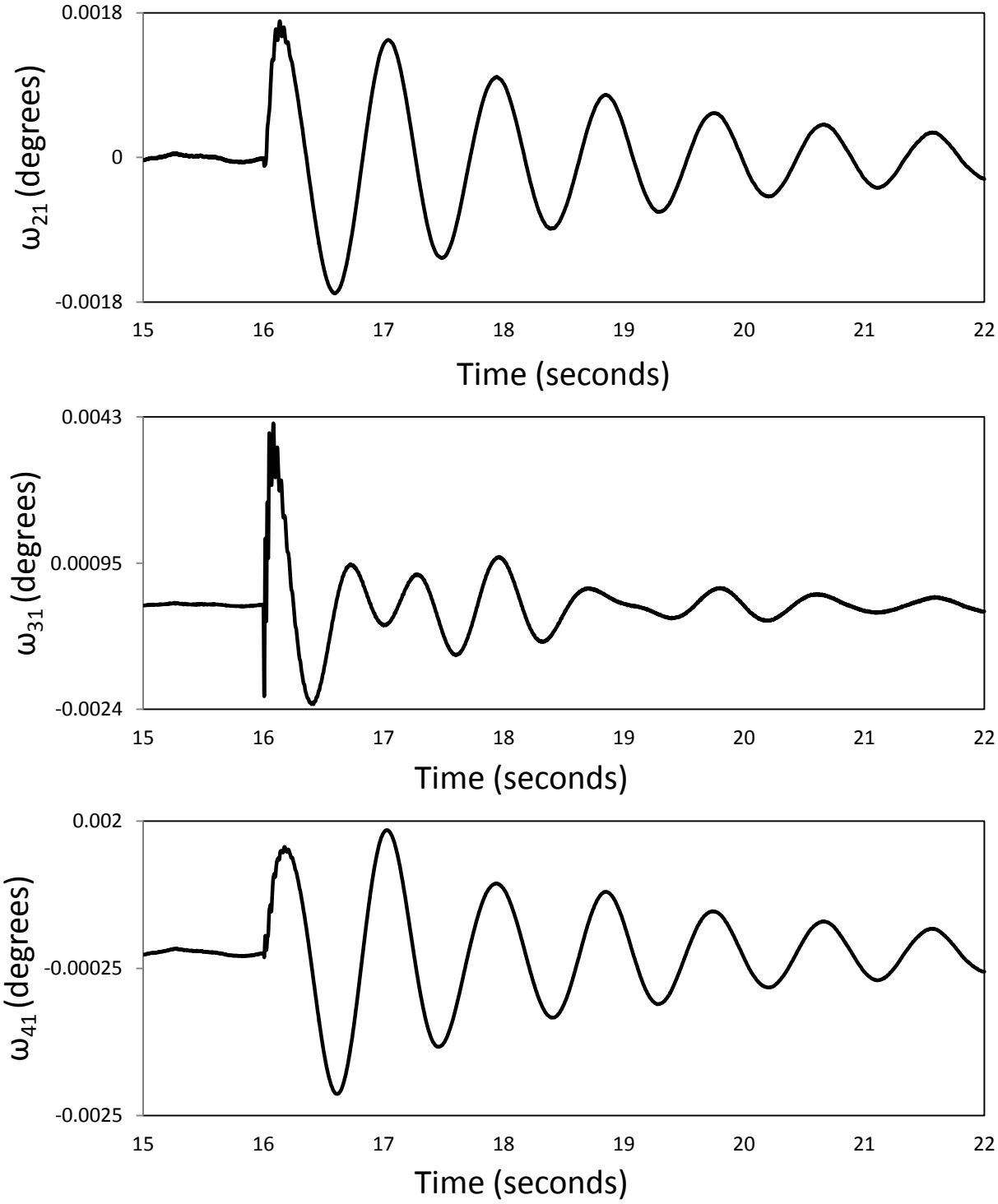


**Figure 2.10:** Continued.

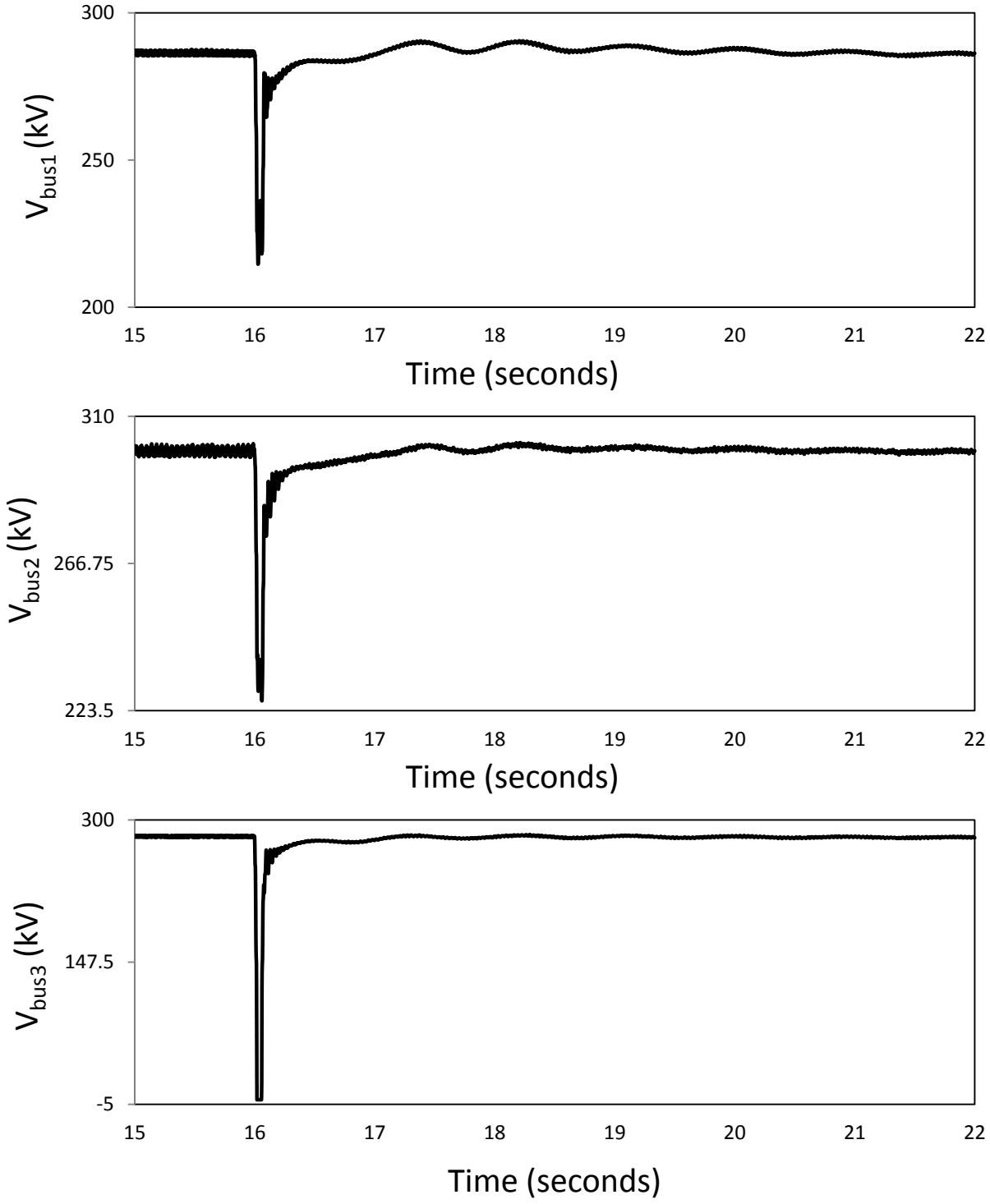


**Figure 2.10:** Continued.

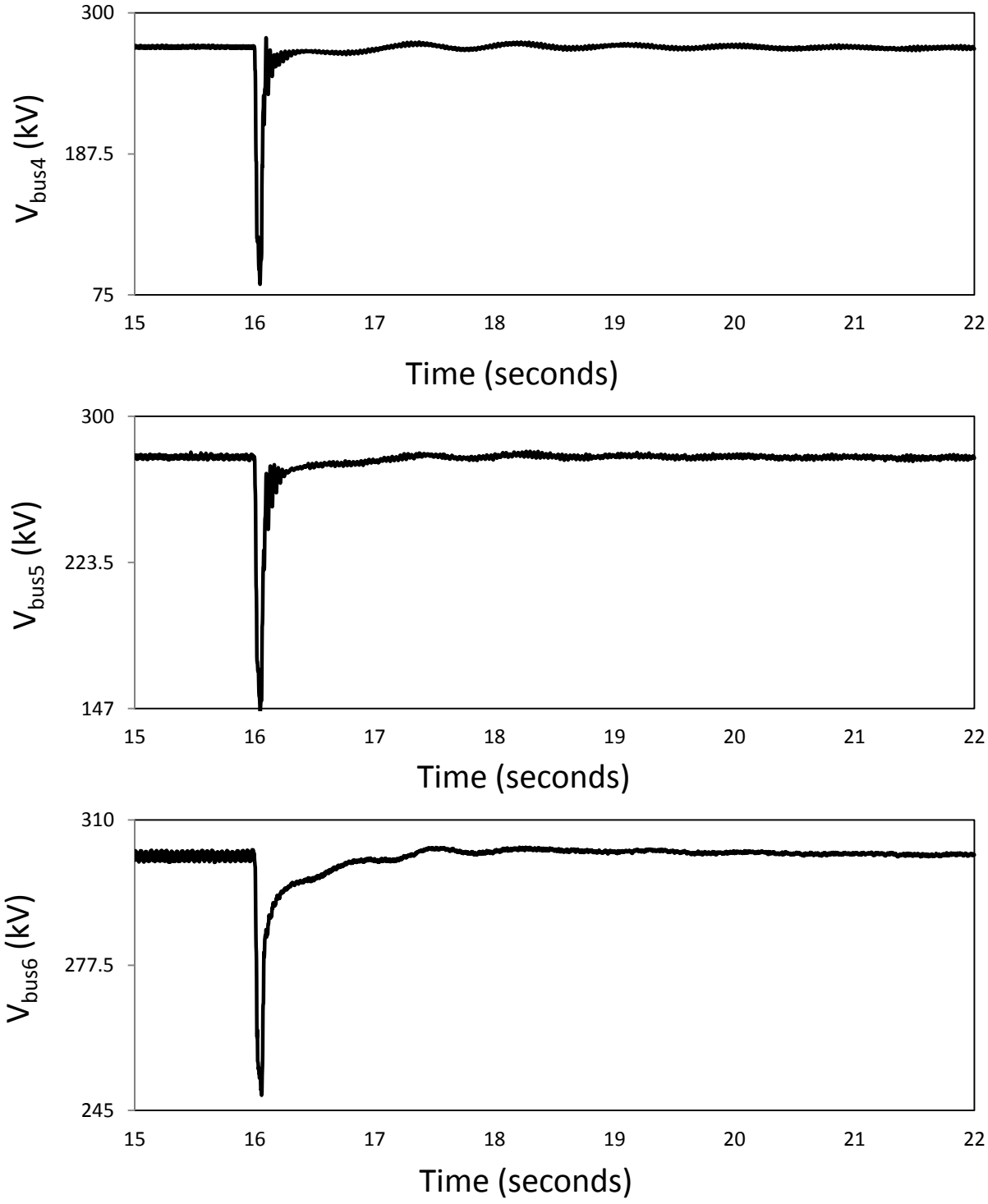


**Figure 2.10**: Continued.

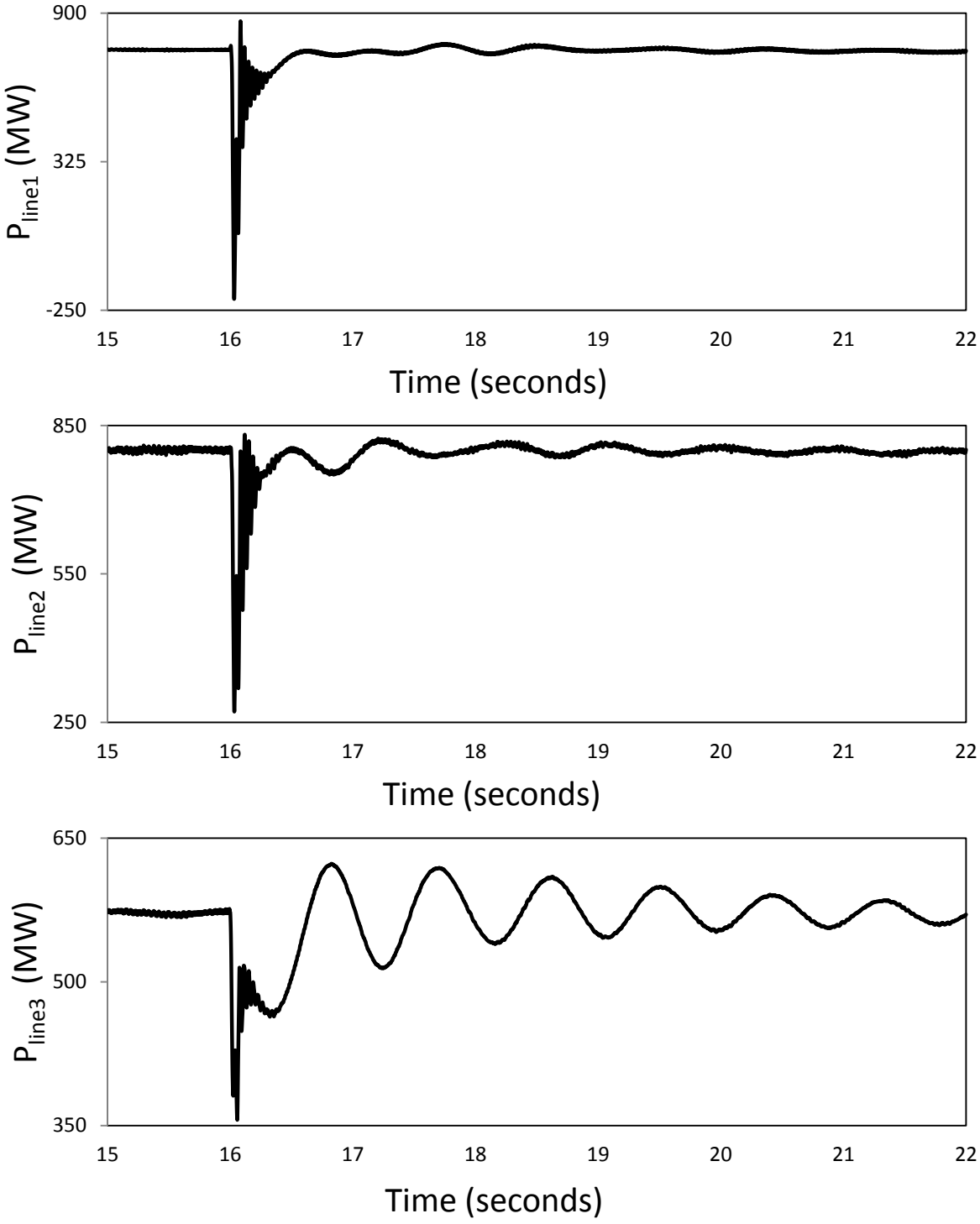


**Figure 2.10:** Continued.

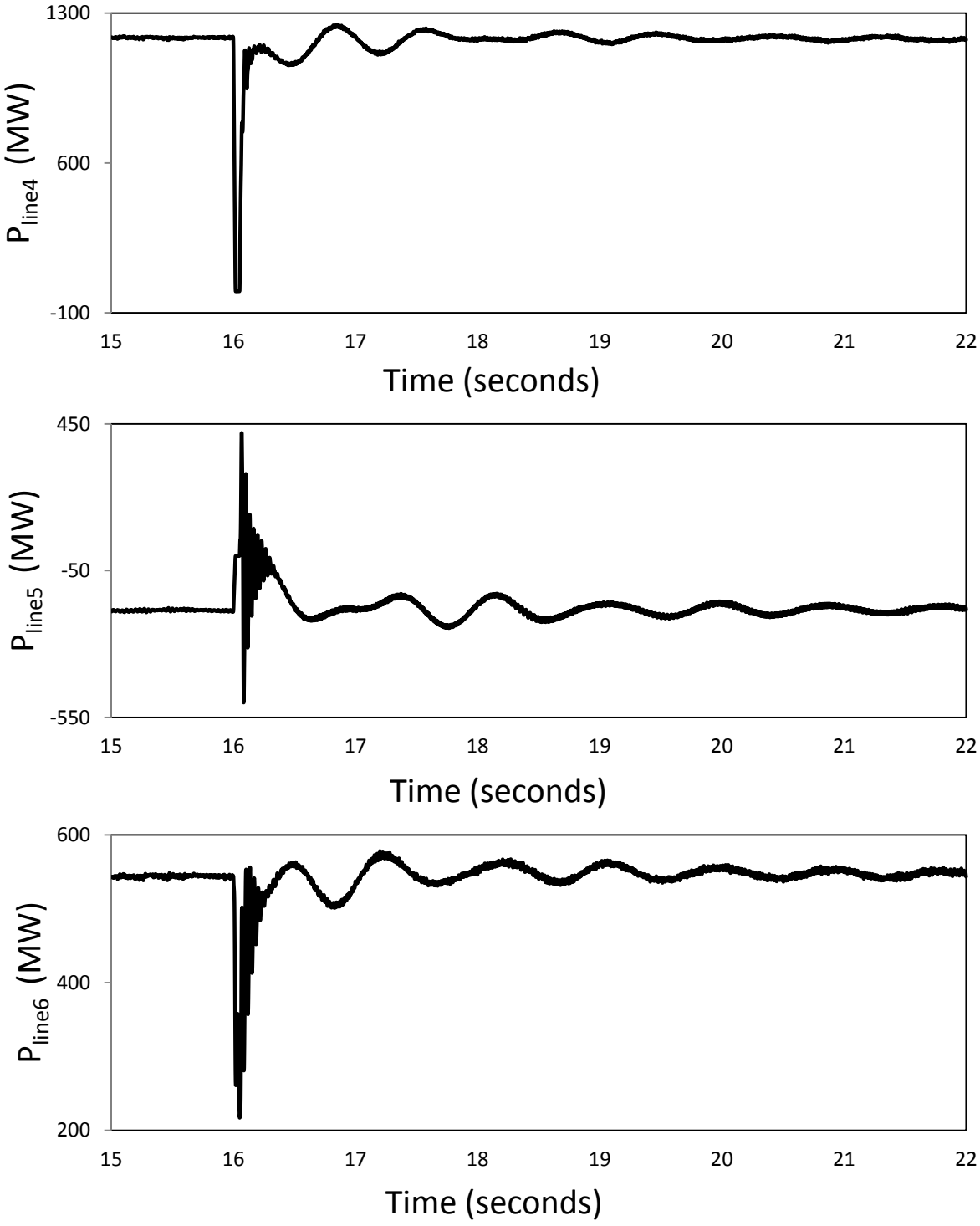


**Figure 2.10:** Continued.

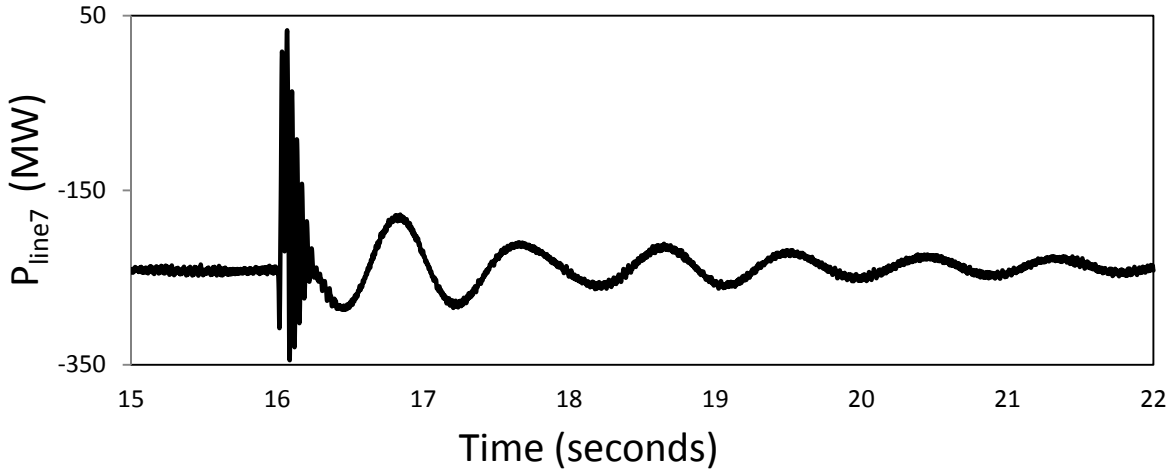


**Figure 2.10:** Continued.

## 2.6 Summary

This chapter introduced the system used for the studies reported in this thesis and presented the mathematical models of its various components. A digital time-domain simulation of a case study of the system during a three-phase fault is also presented and some observations are noted.

# Chapter 3

# THE THYRISTOR CONTROLLED SERIES CAPACITOR AND THE HYBRID SINGLE-PHASE- TCSC COMPENSATION SCHEME

## 3.1 General

This chapter presents the description and the basic principles of the TCSC as well as the derivation of its mathematical model. Modeling the hybrid single-phase-TCSC scheme in the ElectroMagnetic Transient Program (EMTP-RV) is also presented.

## 3.2 Thyristor Controlled Series Capacitor

The TCSC shown in Figure 3.1 consists of a number of series connected modules. In each module, the capacitor bank is provided with a parallel thyristor controlled inductor that circulates current pulses which add in phase with the line current. This boosts the capacitor voltage beyond the level that would be obtained by the line current alone. A Zinc oxide varistor is included in each module for secure overvoltage protection of the TCSC. Each thyristor is triggered once per cycle and has a conduction interval that is shorter than a half-cycle of the rated frequency. If the additional voltage created by the circulating current pulses is controlled to be proportional to the line current, the transmission system will perceive the TCSC as having a virtually increased reactance beyond the physical reactance of the capacitor. This feature which is referred to "vernier control" can be used for short-time transient control. The upper limit for vernier operation is a function of the line current magnitude and time spent at the operating point. Moreover, this scheme can provide an accurate setting of the compensation degree with a high resolution as well as a subsynchronous resonance immune series compensation even at high compensation degrees [36], [37].

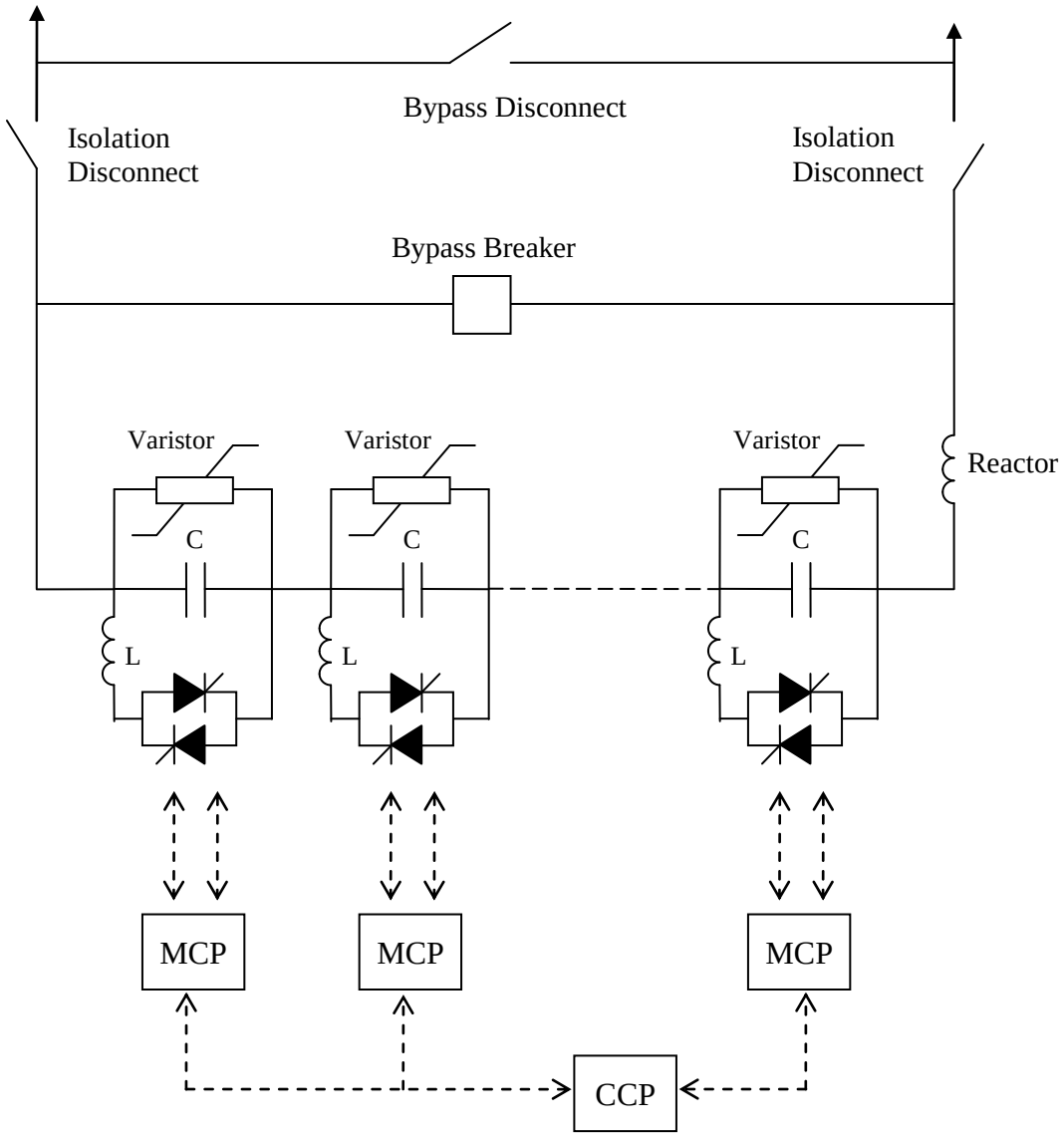


**Figure 3.1:** A multi-module TCSC.

The control and protection of TCSC are partitioned in two levels; common and module. Commands for both control and protective operations flow from the common level to the module levels. Status information is sent back from each module level. The design concept is to permit any module or combination of modules to be out of service while still being able to operate the remaining modules to benefit the power system.

The common-level protection detects problems affecting all modules, and as such, generally requires bypassing all modules with the bypass breaker. The module-level protection detects problems affecting a single-module and as such, may only initiate protective actions within the affected module. The thyristor switches allow for bypassing individual modules by continuous gating the thyristors, and this is an effective protective action for many potential internal failures (e.g., capacitor failure). However, for some serious problems within a module (e.g., varistor failure), protective actions may involve bypassing all modules with the bypass breaker.

## 3.3 Operation of the TCSC

### 3.3.1 Basic principles [34]

A simple understanding of TCSC functioning can be realized by analyzing the behavior of the circuit shown in Figure 3.2 which consists of a variable inductor connected in parallel with a fixed capacitor. The equivalent impedance, $Z_{eq}$, of this LC combination is expressed as:

$$Z_{eq} = -j\frac{1}{\omega C - \frac{1}{\omega L}} \tag{3.1}$$

The impedance of the capacitor alone, however, is given by $X_c = -j\frac{1}{\omega C}$.

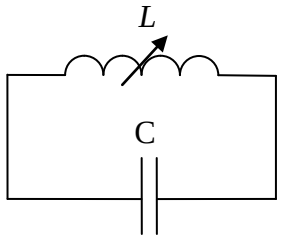


**Figure 3.2:** A variable inductor connected in parallel with a fixed capacitor.

If $\omega C - \left(\frac{1}{\omega L}\right) > 0$ or, in other words, $\omega L > \frac{1}{\omega C}$, the reactance of the fixed capacitor is less than that of the parallel-connected variable reactor and that this combination provides a variable-capacitive reactance are both implied. Moreover, this inductor increases the equivalent-capacitive reactance of the LC combination above that of the fixed capacitor.

If $\omega C - \left( \frac{1}{\omega L} \right) = 0$, a resonance develops that results in an infinite-capacitive impedance. If, however, $\omega C - \left( \frac{1}{\omega L} \right) < 0$, the LC combination provides inductance above the value of the fixed inductor. This situation corresponds to the inductive-vernier mode of the TCSC operation.

In the variable-capacitive mode of the TCSC, as the inductive reactance of the variable inductor is increased, the equivalent-capacitive reactance is gradually decreased. The minimum equivalent-capacitive reactance is obtained for extremely large inductive reactance or when the variable inductor is open-circuited, in which the value is equal to the reactance of the fixed capacitor itself.

The behavior of the TCSC is similar to that of the parallel LC combination. The difference is that the LC-combination analysis is based on the presence of pure sinusoidal voltage and current in the circuit, whereas in the TCSC, the voltage and current are not sinusoidal because of the thyristor switchings. The analysis in this case is presented in Section 3.4.

### 3.3.2 Modes of TCSC operation

There are three modes of TCSC operation:

1. Bypassed-Thyristor Mode: the thyristors are made to fully conduct resulting in a continuous sinusoid of flow current through the thyristor valves (Figure 3.3(a)). The TCSC module behaves like a parallel capacitor-inductor combination. The net current through the module, however, is inductive, for the susceptance of the reactor is chosen to be greater than that of the capacitor.
2. Blocked-Thyristor Mode: the firing pulses of the thyristor valves are blocked. The TCSC module is reduced to a fixed capacitor (Figure 3.3(b)).
3. Partially Conducting Thyristor or Vernier Mode: This mode allows the TCSC to behave either as a continuously controllable capacitive reactance or as a continuously controllable inductive reactance. It is achieved by varying the thyristor-pair firing angle in an appropriate range. In practice, the TCSC operates only in the *capacitive-vernier-control* mode. In such a mode, the thyristors are fired when the capacitor voltage and the capacitor current have opposite polarity. This condition causes the reactor current to have a direction opposite to that of the capacitor current, thereby, resulting in a loop-

current flow in the TCSC controller. The loop current increases the voltage across the fixed capacitor, effectively enhancing the equivalent capacitive reactance and the series compensation level for the same value of line current. To preclude resonance, the firing angle α of the forward facing thyristor, as measured from the positive reaching a zero crossing of the capacitor voltage, is constrained in the range $\alpha_{\min} \le \alpha \le 180^\circ$. This constraint provides a continuous vernier of the TCSC module reactance. The loop current increases as α is decreased from $180^\circ$ to $\alpha_{\min}$. The maximum TCSC reactance permissible with $\alpha = \alpha_{\min}$ is typically two-and-half to three times the capacitor reactance at fundamental frequency.

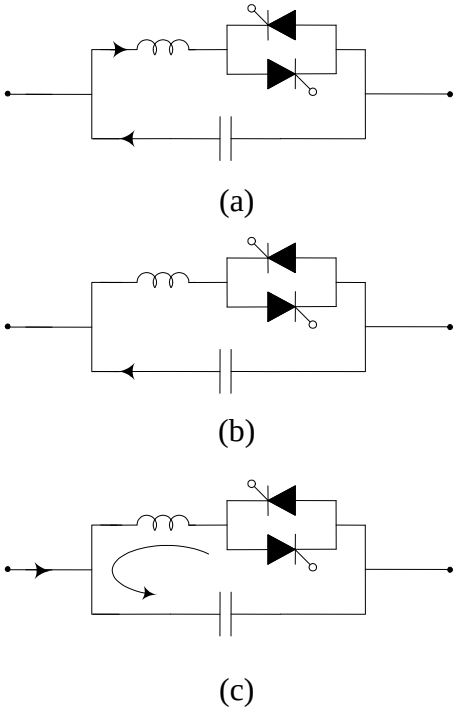


**Figure 3.3:** TCSC modes of operation: (a) bypassed-thyristor mode, (b) blocked-thyristor mode, (c) vernier mode.

### 3.4 Analysis of the TCSC

The following "approximate" analysis of TCSC operation in the vernier-control mode is performed based on the simplified TCSC circuit shown in Figure 3.4 [34]. Transmission line current is assumed to be the independent-input-variable and is modeled as an external current

source, $i_s(t)$. Moreover, it is assumed that the line current is sinusoidal, as field tests have demonstrated that very few harmonics exist in the line current [15].

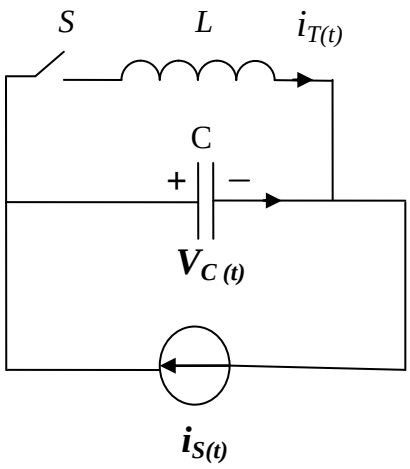


**Figure 3.4:** A simplified TCSC circuit.

The current through the fixed-series capacitor, *C*, is expressed as

$$C\frac{dv_c}{dt} = i_s(t) - i_T(t).u \tag{3.2}$$

The switching variable *u* is equal to 1 when the thyristor valves are conducting (switch S is closed). When the thyristor valves are blocked (switch S is open), *u* = 0. The thyristor current, $i_T(t)$ can be described as

$$L\frac{di_T}{dt} = v_c.u \tag{3.3}$$

Let the line current, $i_s(t)$ be represented by

$$i_s(t) = I_m \cos \omega t \tag{3.4}$$

Equations (3.3) and (3.4) can be solved with the knowledge of the instants of switching. In equidistant firing-pulse control, for balanced TCSC operation, the thyristors are switched on twice in each cycle of the line current at instants $t_1$ and $t_3$ given by

$$t_1 = -\frac{\beta}{\omega} \tag{3.5}$$

$$t_3 = \frac{\pi - \beta}{\omega} \tag{3.6}$$

where β is the angle of advance (before the forward voltage becomes zero). Or,

$$\beta = \pi - \alpha; \qquad 0 < \beta < \beta_{\max} \tag{3.7}$$

The firing angle α is generated using a reference signal that can be in phase with the capacitor voltage. The thyristor switch S turns off at the instant $t_2$ and $t_4$ defined as:

$$t_2 = t_1 + \frac{\sigma}{\omega} \tag{3.8}$$

$$t_4 = t_3 + \frac{\sigma}{\omega} \tag{3.9}$$

where $\sigma$ is the conduction angle and,

$$\sigma = 2\beta \tag{3.10}$$

Solving the TCSC equations (3.2 to 3.4) results in the steady-state thyristor current $i_T$, as:

$$i_T(t) = \frac{k^2}{k^2 - 1} IMG \left[ \cos \omega t - \frac{\cos \beta}{\cos k\beta} \cos \omega_r t \right]; \qquad -\beta \le \omega t \le \beta \tag{3.11}$$

where

$$\omega_r = \frac{1}{\sqrt{LC}} \tag{3.12}$$

$$k = \frac{\omega_r}{\omega} = \sqrt{\frac{1}{\omega L}\frac{1}{\omega C}} = \sqrt{\frac{X_C}{X_L}} \tag{3.13}$$

and $X_C$ is the nominal reactance of the fixed capacitor only. The steady-state capacitor voltage at the instant $\omega t = -\beta$ is expressed by:

$$v_{C1} = \frac{IMG \quad X_C}{k^2 - 1}(\sin \beta - k \cos \beta \tan k\beta) \tag{3.14}$$

At $\omega t = \beta$, $i_T = 0$, and the capacitor voltage is given by:

$$v_C(\omega t = \beta) = v_{C2} = -v_{C1} \tag{3.15}$$

The capacitor voltage is finally obtained as:

$$v_C(t) = \frac{IMG \quad X_C}{k^2 - 1}\left[ -\sin \omega t + k \frac{\cos \beta}{\cos k\beta} \sin \omega_r t \right]; \qquad -\beta \le \omega t \le \beta \tag{3.16}$$

$$v_C(t) = v_{C2} + IMG \quad X_C(\sin \omega t - \sin \beta); \qquad \beta < \omega t < \pi - \beta \tag{3.17}$$

Because the nonsinusoidal capacitor voltage, $v_C$, has odd symmetry about the axis $\omega t = 0$, the fundamental component, $V_{CF}$, is obtained as:

$$V_{CF} = \frac{4}{\pi} \int_0^{\pi/2} v_c(t) \sin \omega t \, d(\omega t) \tag{3.18}$$

The equivalent TCSC reactance is computed as the ratio of $V_{CF}$ to $I_m$:

$$\begin{aligned} X_{TCSC} &= \frac{V_{CF}}{I_m} = X_C - \frac{X_C^2}{(X_C - X_L)} \frac{2\beta + \sin 2\beta}{\pi} \\ &+ \frac{4 X_C^2}{(X_C - X_L)} \frac{\cos^2 \beta}{(k^2 - 1)} \frac{(k \tan k\beta - \tan \beta)}{\pi} \end{aligned} \tag{3.19}$$

The net reactance of the TCSC in per unit of $X_C$, denoted by $X_{net}$ (= $X_{TCSC}/X_C$, sometimes called the boost factor) can be expressed as:

$$\begin{aligned} X_{net} &= 1 - \frac{X_C}{(X_C - X_L)} \frac{\sigma + \sin \sigma}{\pi} + \frac{4 X_C}{(X_C - X_L)} \frac{\cos^2 0.5\sigma}{(k^2 - 1)} \\ &\cdot \frac{(k \tan 0.5\sigma \, k - \tan 0.5\sigma)}{\pi} \end{aligned} \tag{3.20}$$

Because the TCSC is used mainly as a capacitive device, the convention is to define positive reactance as capacitive and negative reactance as inductive. As an example, $X_{net} = +2$ implies that the thyristors are fired so that the resulting circulating current in the fixed capacitor – thyristor controlled reactor loop causes a 60-Hz voltage of $2 X_C I_{line}$ p.u. to appear across the fixed capacitor, which lags the line current by 90°.

The traditional boost control method (constant firing angle delay (CFAD)) controls the firing angle $\beta = \pi - \alpha$ of the thyristor. A rather non-linear relationship exists between the boost factor *kB* and the steady state conduction angle $\sigma = 2\beta$, making *kB* very sensitive to the instant of triggering when the TCSC operates at a high boost factor. Further, at transients, a complicated dynamic characteristic governs the relationship between the firing angle and the conduction angle. Instead of controlling the thyristor firing angle, another control scheme, named 'Synchronous Voltage Reversal' (SVR), is being used. It aims to control the instant when the capacitor voltage crosses zero [38], [39]. This eliminates the non-linearity in the boost control and results in that the TCSC apparent impedance at subsynchronous frequencies appears as inductive. Furthermore, at low boost factors, SVR controlled TCSC can provide much better SSR damping than conventional CFAD control [40]. In the studies conducted in this thesis, the SVR control is used.

### 3.5 The Hybrid Single-Phase-TCSC Compensation Scheme

Figure 3.5 shows a phase imbalanced hybrid series capacitive compensation scheme using a TCSC [41]. In such a scheme, the series capacitive compensation in one phase is created using a single-phase TCSC in series with a fixed capacitor ($C_c$), and the other two phases are compensated by fixed series capacitors (C). The TCSC control is initially set such that its equivalent compensation at the power frequency combined with the fixed capacitor $C_c$ yield a resultant compensation equal to the other two phases. Thus, the phase balance is maintained at the power frequency while at any other frequency, a phase imbalance is created. Mathematically, this can be explained as follows:

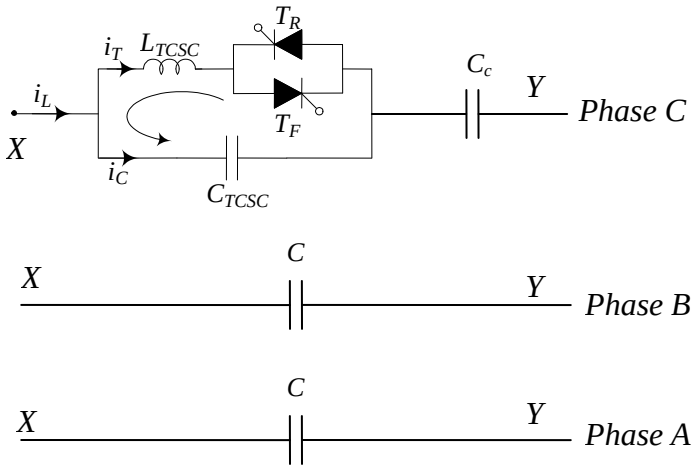


**Figure 3.5:** The hybrid single-phase TCSC compensation scheme.

1) At the power frequency, the series reactance between buses X and Y, in Figure 3.5, in phases a, b, and c are given by:

$$X_a = X_b = \frac{1}{j\omega_o C} \tag{3.21}$$

$$X_c = \frac{1}{j\omega_o C_c} - jX_{TCSCo} \tag{3.22}$$

where $-jX_{TCSCo}$ is the effective capacitive reactance of the TCSC at the power frequency such that $X_a = X_b = X_c$.

2) During any other frequency, $f_e$, including subsynchronous frequencies,

$$X_c = \frac{1}{j\omega_e C_c} - jX_{TCSCo} - j\Delta X_{TCSC} \tag{3.23}$$

The first terms in (3.22) and (3.23) are different because of the difference in frequency. The third term in (3.23) represents the change in the effective capacitive reactance of the TCSC due to the action of the TCSC supplemental controller.

### 3.6 Modeling of the Single-Phase TCSC in the EMTP-RV

The single-phase TCSC is modeled in the EMTP-RV as a single module using an ideal thyristor pair and an RC snubber circuit as shown in Figure 3.6. A Phase Locked Loop (PLL) is used to extract phase information of the fundamental frequency line current, which will be used to synchronize TCSC operation. The thyristor gating control is based on the Synchronous Voltage Reversal (SVR) technique [38] - [40]. The TCSC impedance is measured in terms of a boost factor *kB*, which is the ratio of the apparent reactance of the TCSC seen from the line to the physical reactance of the TCSC capacitor bank. A positive value of *kB* is considered for capacitive operation. A low-pass filter based estimation algorithm is used to estimate the voltage and the current phasors. A boost measurement block performs complex impedance calculations for the boost factor of the TCSC as $kB = \text{Imag}\{\hat{v}_C / \hat{I}_C\} / X_{CTCSC}$, where, $\hat{v}_C$ and $\hat{I}_C$ are the estimated phase voltage and current and $X_{CTCSC}$ is the capacitive reactance of the TCSC capacitor branch at the fundamental frequency. A proportional-integral (PI) control based boost level controller is implemented to control the TCSC boost level to the desired value by adjusting the instant of the expected capacitor voltage zero crossing. The integral part of the controller helps in removing the steady state errors. The controller parameters were determined by performing repeated time domain simulations for the different operating conditions. This algorithm uses the difference between the actual boost level and the reference boost level (*err*) shown in Figure 3.6 as an objective function. The algorithm starts with arbitrary initial values for the control parameters and calculates the values of the objective function each time. The control parameters are incremented for the next iteration and the procedure is repeated until the objective function approaches a minimum value (below a threshold value). The procedure described above is widely used by industry for tuning of controller parameters. The multiple simulations run

based tuning procedure similar to the above was reported in [42], [43]. The optimum values of the parameters obtained for the different compensation degrees are given in Appendix B.

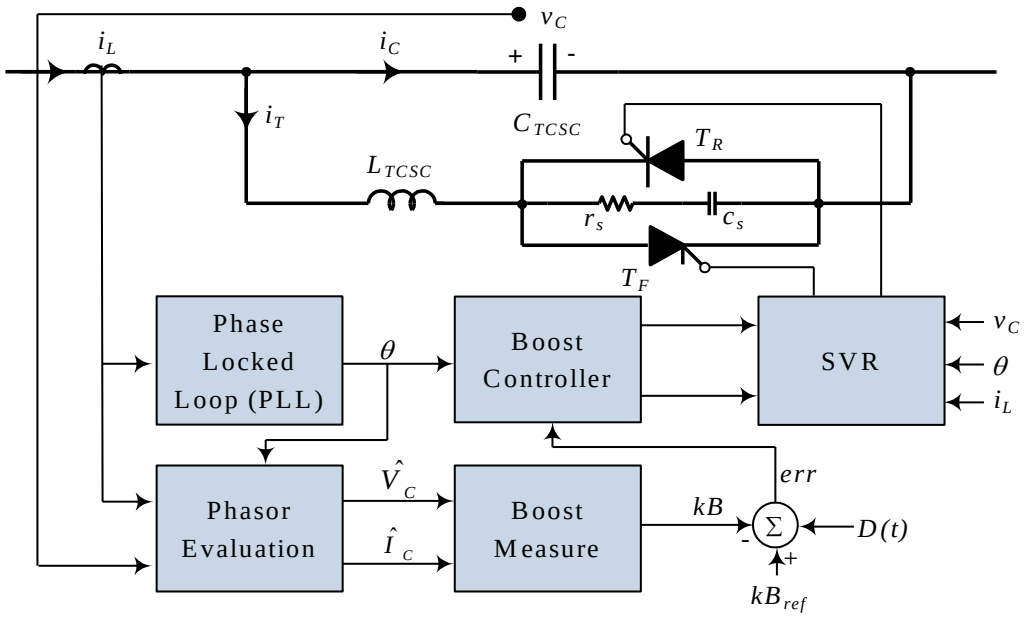


**Figure 3.6:** Block diagram of a TCSC controller.

In Figure 3.6, $kB_{ref}$ is the TCSC boost level set point and $D(t)$ is the supplementary control signal for damping low frequency oscillations. The Synchronous Voltage Reversal block solves for angle $\gamma$ from the non-linear relation, $u_{CZ} = X_o i_{LM} [\lambda\gamma - \tan(\lambda\gamma)]$, where $u_{CZ}$ is the estimated capacitor voltage at the desired instant when the capacitor voltage zero crossing occurs, $i_{LM}$ is the measured value of the line current $i_L$, $X_0$ is the TCSC capacitor reactance at the TCSC resonance frequency, $\lambda$ is the ratio between the TCSC resonance frequency and the system fundamental frequency and $\gamma$ is the angle difference between the firing time and the voltage zero-crossing. The value of $\gamma$ is used to calculate the exact firing instants of the individual thyristors. The non-linear relationship between the boost factor and the thyristor firing angle α is shown in Figure 3.7.

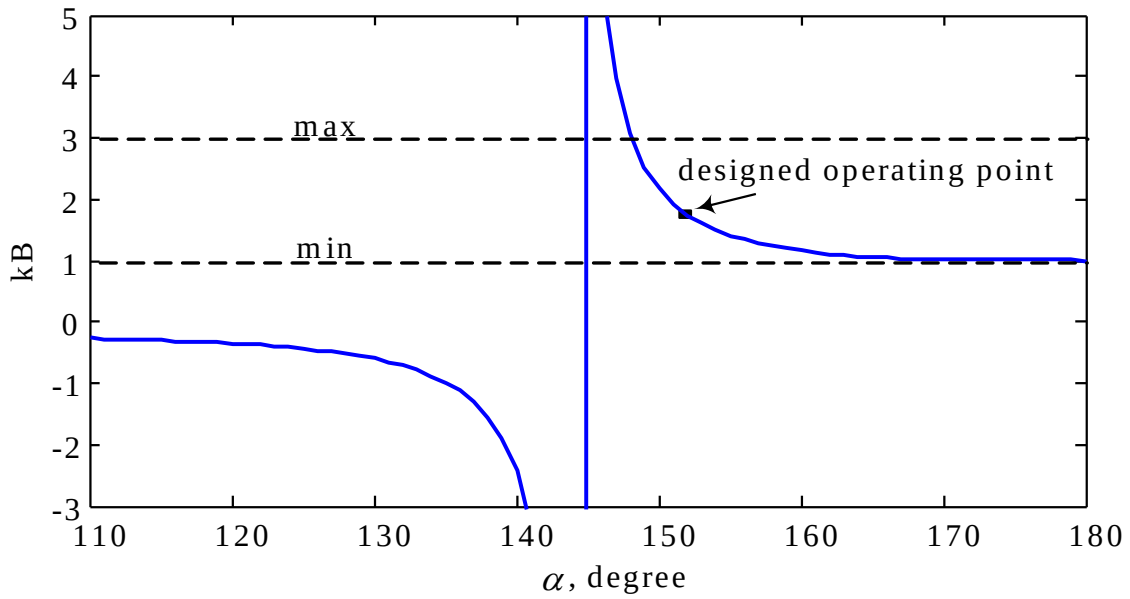


**Figure 3.7:** TCSC boost factor as a function of the thyristor firing angle α.

The most striking feature of the TCSC is that it behaves like an inductor at subsynchronous frequencies. This prevents the occurrence of a series resonance within a certain critical frequency band. On the other hand, the TCSC behaves like a capacitor at the power frequency. The transition of the virtual reactance of the TCSC from inductive to capacitive outside the subsynchronous frequency band is achieved by means of a reactance controller (like the SVR technique), providing a controllable capacitive reactance around the power frequency as shown in Figure 3.8 [44]. The details of the SVR algorithm are given in [38], [39].

## 3.7 Summary

This chapter presents the description, basic principles and the derivation of the mathematical model of the TCSC. Modeling the hybrid single-phase TCSC in the ElectroMagnetic Transient Program (EMTP-RV) is also presented. This model is incorporated in the system under study (Figure 2.1) replacing the fixed compensations in lines $L_1$ and $L_2$. The effectiveness of the hybrid single-phase compensation scheme in damping power system oscillations is investigated in the next chapter.

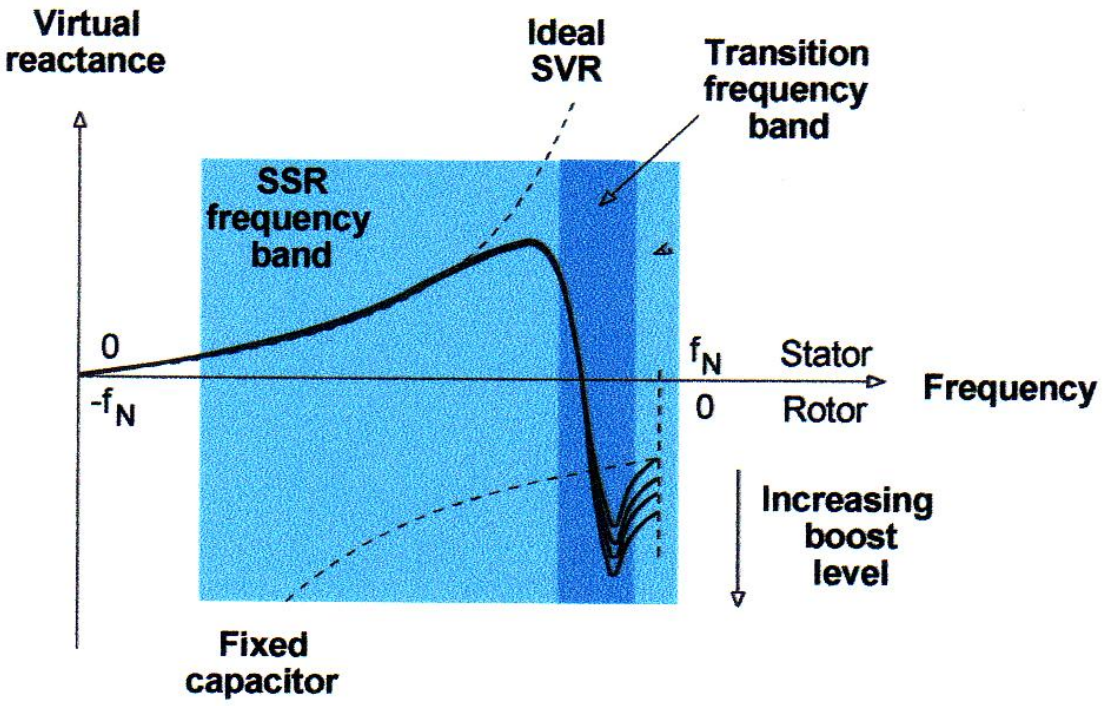


**Figure 3.8:** Effect of the SVR technique on the virtual reactance of the TCSC.

# Chapter 4

# DAMPING POWER SYSTEM OSCILLATIONS USING A STATCOM AND THE HYBRID SINGLE-PHASE-TCSC COMPENSATION SCHEME

## 4.1 General

The control offered by the TCSC is an 'impedance' type control, i.e. the inserted voltage is proportional to the line current. This type of control normally is best suited to applications in power flow corridors, where a well-defined phase angle difference exists between the ends of the transmission line to be compensated and controlled. In addition, the STATCOM can offer voltage regulation by functioning as a very fast variable reactive power generation source. As a result, transient stability improvement and the increase in the maximum real power transmitted can be achieved. TCSC and STATCOM can also be used, however, to provide additional damping to the electromechanical (0.5 - 2 Hz) power oscillations as they provide fast speed of response and executes any switching patterns without such restrictions that might apply for mechanical switches.

In this chapter, the effectiveness of the STATCOM and the hybrid single-phase-TCSC compensation scheme (Scheme I) supplemental controllers in damping power system oscillations is investigated. For this purpose, the scheme is assumed to be installed in one or more circuits of lines $L_1$ and $L_2$ replacing the fixed series capacitor compensations as well as in the uncompensated line $L_3$. The performance of the Scheme I and the STATCOM supplemental controllers is compared to the case with only fixed capacitor compensation in $L_1$ and $L_2$ (Fixed C) as well as to the case when the STATCOM supplemental controller is not activated (TCSC supplemental controller only).

## 4.2 TCSC and STATCOM Power Oscillations Damping Controllers

The TCSC can be made to vary the series-compensation level dynamically in response to the controller-input signal so that the resulting changes in the power flow enhance the system damping. Also, the STATCOM controller consists of two loops which they are: outer regulation loop and inner current loop. They work together to regulate the voltage at the connecting point with the system. Voltage regulation leads to improve the system damping. The traditional type of controller for Power Oscillations Damping (POD) purposes uses cascade-connected washout filters and linear lead-lag compensators to generate the desired reactance modulation signal. The purpose of the wash-out filters is to eliminate the average and extract the oscillating part of the input signal. The lead-lag compensators provide the desired phase shift at the oscillations frequency. Such a controller is illustrated in Figure 4.1 [27], [45], [46]. In some situations, a simple controller consists of only the washout filters can have a better performance than that of the lead-lag controller. Such a controller, shown in Figure 4.2 can be regarded as a proportional type controller.

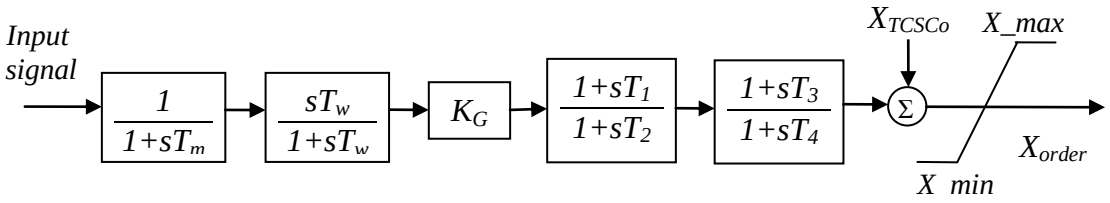


**Figure 4.1:** Structure of a lead-lag POD controller.

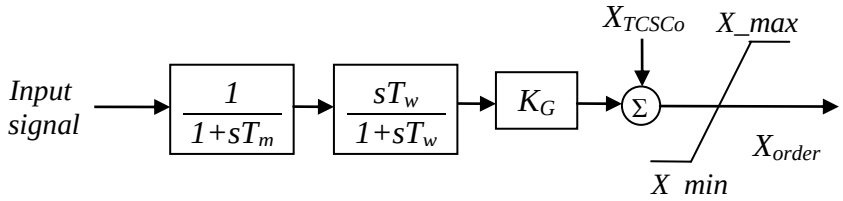


**Figure 4.2:** Structure of a simple POD controller.

The selection of the appropriate input (stabilizing) signal is an important issue in the design of an effective and robust controller. The selected input signal must yield correct control action when a severe fault occurs in the system. As an example, it was reported in [47] that if the real power is used as input signal of a pure derivative controller, the output control signal may cause negative damping effects in the presence of disturbances involving large changes in the generator power angles.

The input signals could be local (e.g. real power flows) or remote (e.g. load angles or speed deviations of remote generators). If a wide-area network of Synchronized Phasor Measurement (SPM) units is available, then the remote signals can be downloaded at the controller in real time without delay [48] - [52]. In the studies conducted in this thesis, the generator load angles and speeds, measured with respect to the load angle and speed of a reference generator are used as input signals.

It is worth noting here that due to the inherent imbalance nature of hybrid single-phase-TCSC compensation scheme during transients, the design of the TCSC supplemental controller using classical linear control techniques would be very difficult, if not, virtually impossible to achieve. However, nonlinear control theories for STATCOM and TCSC applications have been found to have a significant potential in recent years [53]. Some of the examples are; variable-structure controllers (VSCs), model reference adaptive controllers and self-tuning controllers. VSCs are capable of maintaining a desired response characteristic almost independently of the system structure. The design of any of such controllers is, however, beyond the level of being a part of a Master research project. In the studies conducted in this thesis, the supplemental controller parameters are determined by performing multiple time domain simulations with the aim of improving the transient responses of the system. In the case of multiple controllers, simultaneous tuning of the parameters of the controllers is performed to ensure that satisfactory dynamic and steady-state performances are met whilst minimizing or preventing undesirable interactions among controllers.

## 4.3 Case Study I: The Hybrid Single-Phase-TCSC Compensation Scheme is Installed in both Circuits of Line $L_1$

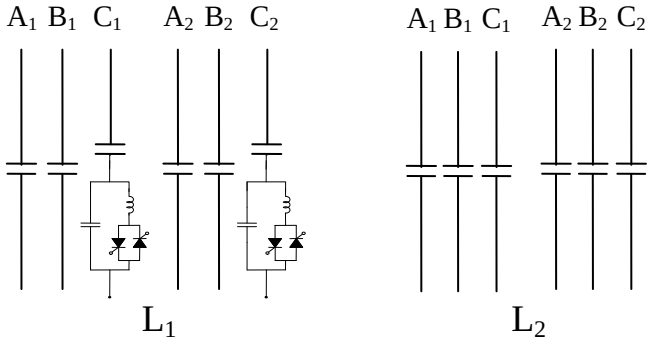


**Figure 4.3:** Case study I: the hybrid single-phase-TCSC compensation scheme is installed in both circuits of line $L_1$.

Each TCSC provides 50% of the total capacitive compensation ($X_{Cc} = X_{TCSC} = 0.5\ X_C$) and the stabilizing signal for their supplemental controllers as well as for the STATCOM supplemental controller is $\delta_{21}$. The generator load angles and speeds, measured with respect to generator 1 load angle and speed, and the transmission line real power flow responses during and after clearing a three-cycle, three-phase fault at bus 3 are illustrated in Figures 4.4 to 4.6 for the case when the TCSC supplemental controllers are of a proportional type with a transfer function given in Equation 4.1 and the STATCOM supplemental controller is not activated as well as for the case when the TCSC supplemental controllers are of a proportional type with a transfer function given in Equation 4.2 and the STATCOM supplemental controller given by Equation 4.3 is activated.

$$G_{P-\delta 21}(s) = \frac{0.5}{(s+0.5)}\frac{2s}{(2s+1)} \tag{4.1}$$

$$G_{P-\delta 21}(s) = 1.5\frac{0.5}{(s+0.5)}\frac{2s}{(2s+1)} \tag{4.2}$$

$$G_{P-\delta 21}(s) = 100\ \frac{10}{(s+10)}\frac{5s}{(5s+1)} \tag{4.3}$$

It can be seen from Figure 4.4 that in the case of fixed capacitor compensation, the system is first swing stable for this fault, but the post-contingency oscillations are not well damped. It can also be seen from Figure 4.4 that the effect of the TCSC supplemental controllers on the first swing is insignificant. The same figure shows, however, that the TCSC supplemental controllers reduce the subsequent swings and provide a better damping than in the case of fixed capacitor compensation. Moreover, Figure 4.4 shows that the STATCOM supplemental controller has a significant contribution to the damping of the system oscillations. Regarding the real line power flows, Figure 4.6 shows that in the case of the hybrid single-phase TCSC scheme and the STATCOM, high spikes occur during the fault period.

### 4.3.1 Effect of the ratio $X_{TCSC}/X_{Cc}$

In order to explore such an effect, each TCSC is set to provide 70% of the total capacitive compensation ($X_{Cc} = 0.3\ X_C$, $X_{TCSC} = 0.7\ X_C$) with a stabilizing signal $\delta_{21}$. Moreover, the STATCOM supplemental controller is not activated in this case study. Figure 4.7 illustrates the transient time responses of the generator load angles, measured with respect to generator 1 load

angle during and after clearing a three-cycle, three-phase fault at bus 3. It can be seen from this figure that increasing the proportion of the single-phase-TCSC to the fixed capacitor of its phase (phase C) results in improving the damping of system oscillations.

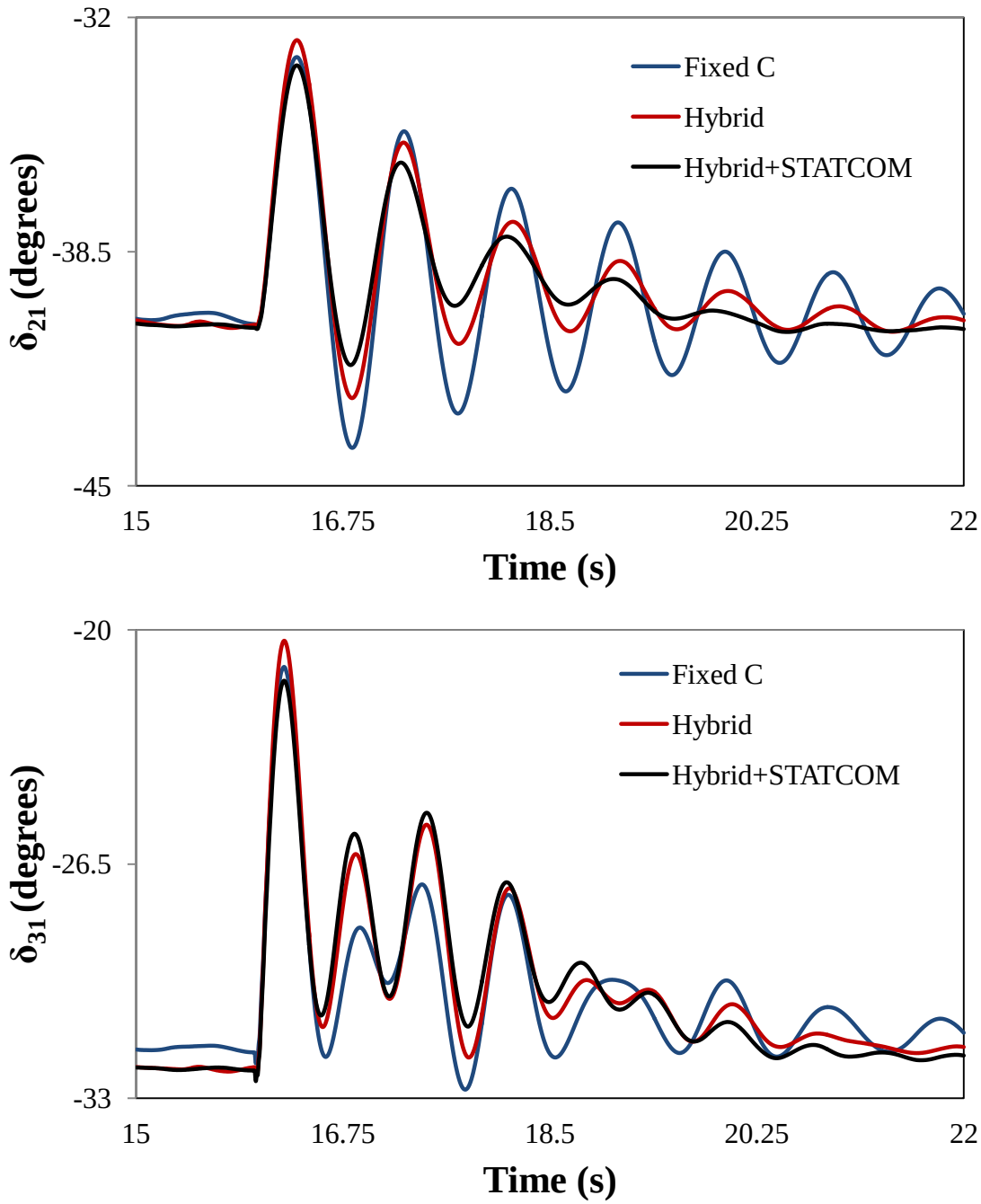


**Figure 4.4:** Generator load angles, measured with respect to generator 1 load angle, during and after clearing a three-cycle, three-phase fault at bus 3 (case study I).

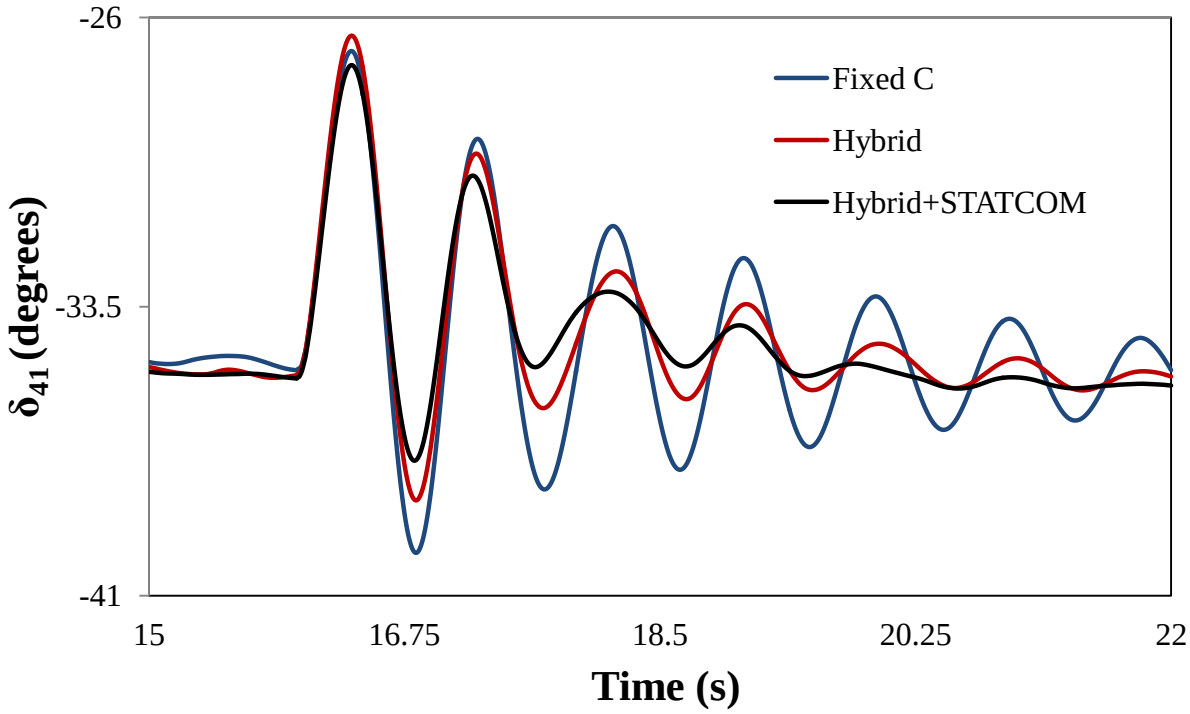


**Figure 4.4:** Continued.

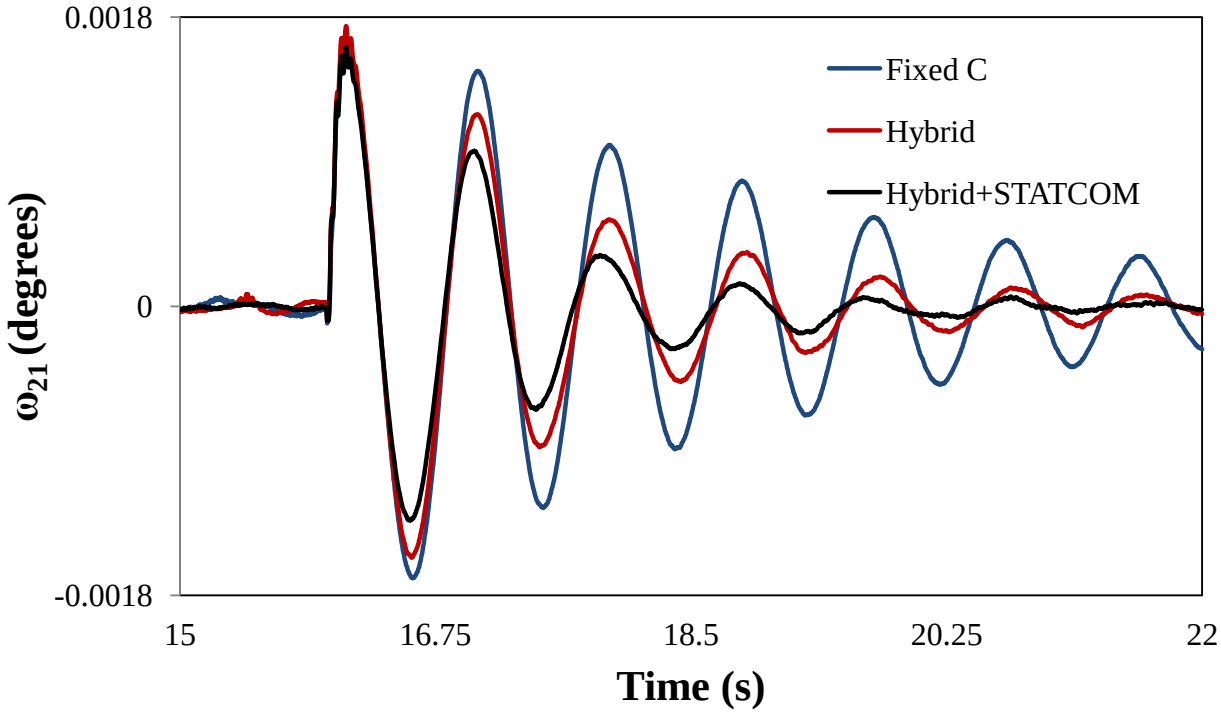


**Figure 4.5:** Generator speeds, measured with respect to generator 1 speed, during and after clearing a three-cycle, three-phase fault at bus 3 (case study I).

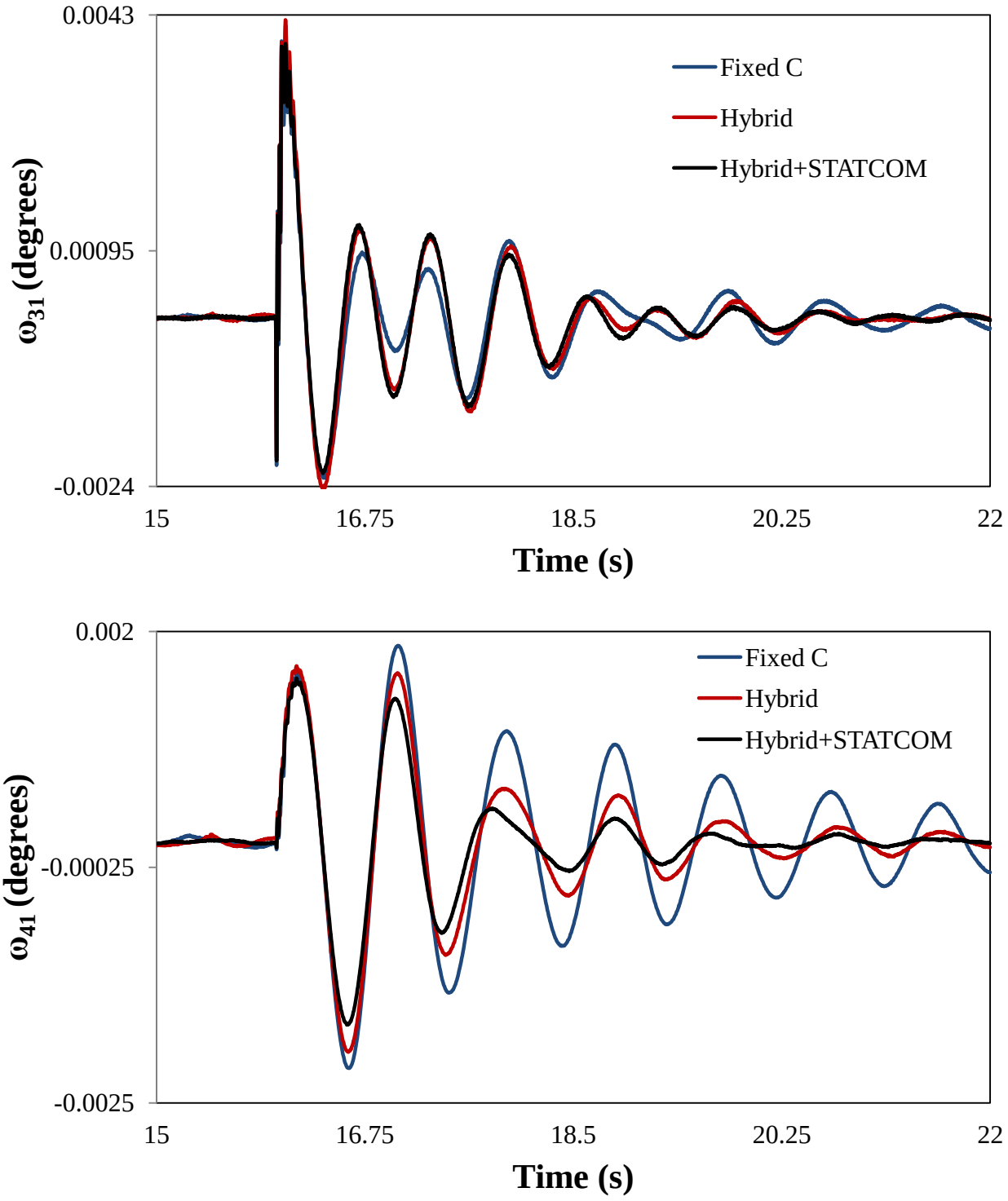


**Figure 4.5:** Continued.

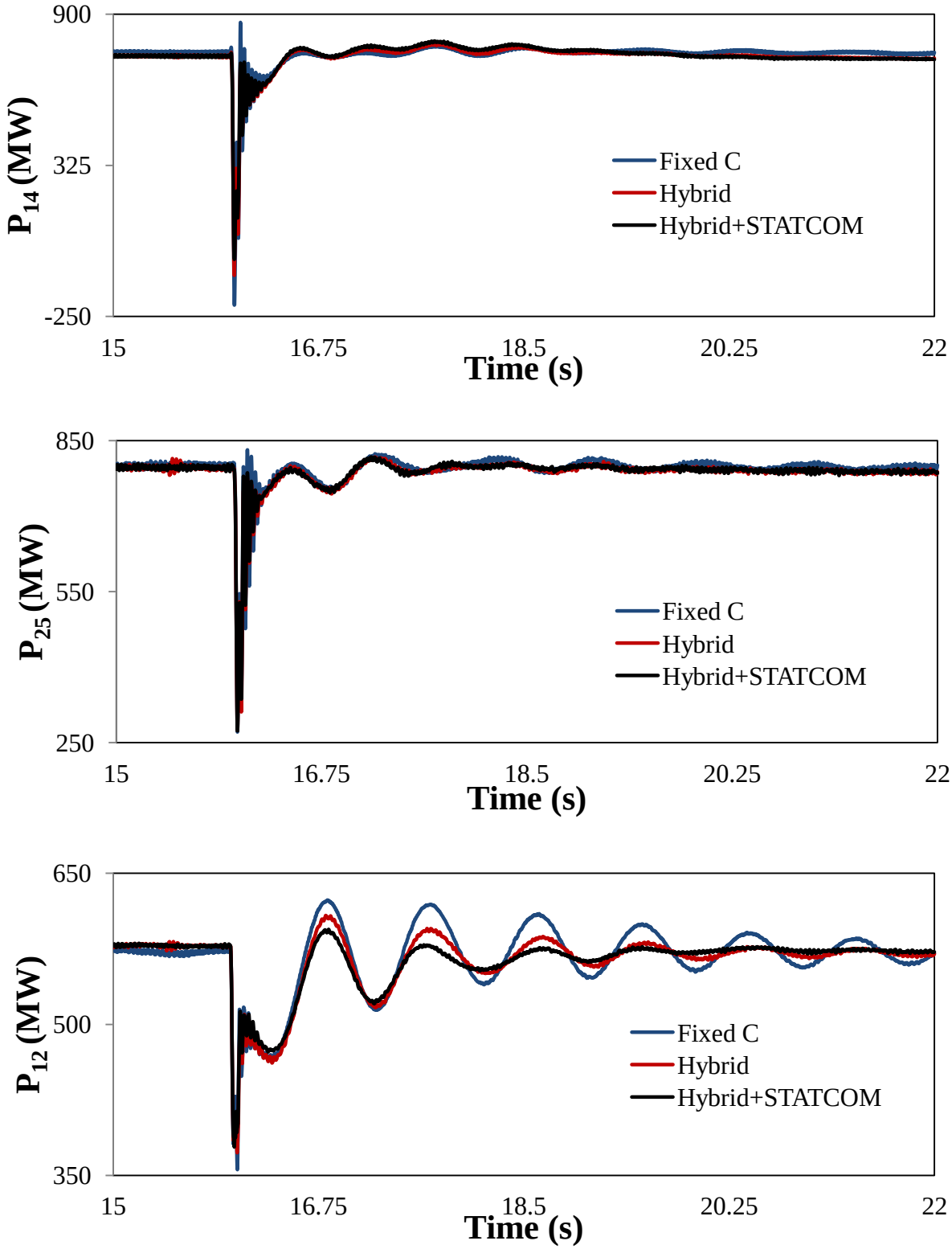


**Figure 4.6:** Transmission line real power flows during and after clearing a three-cycle, three-phase fault at bus 3 (case study1).

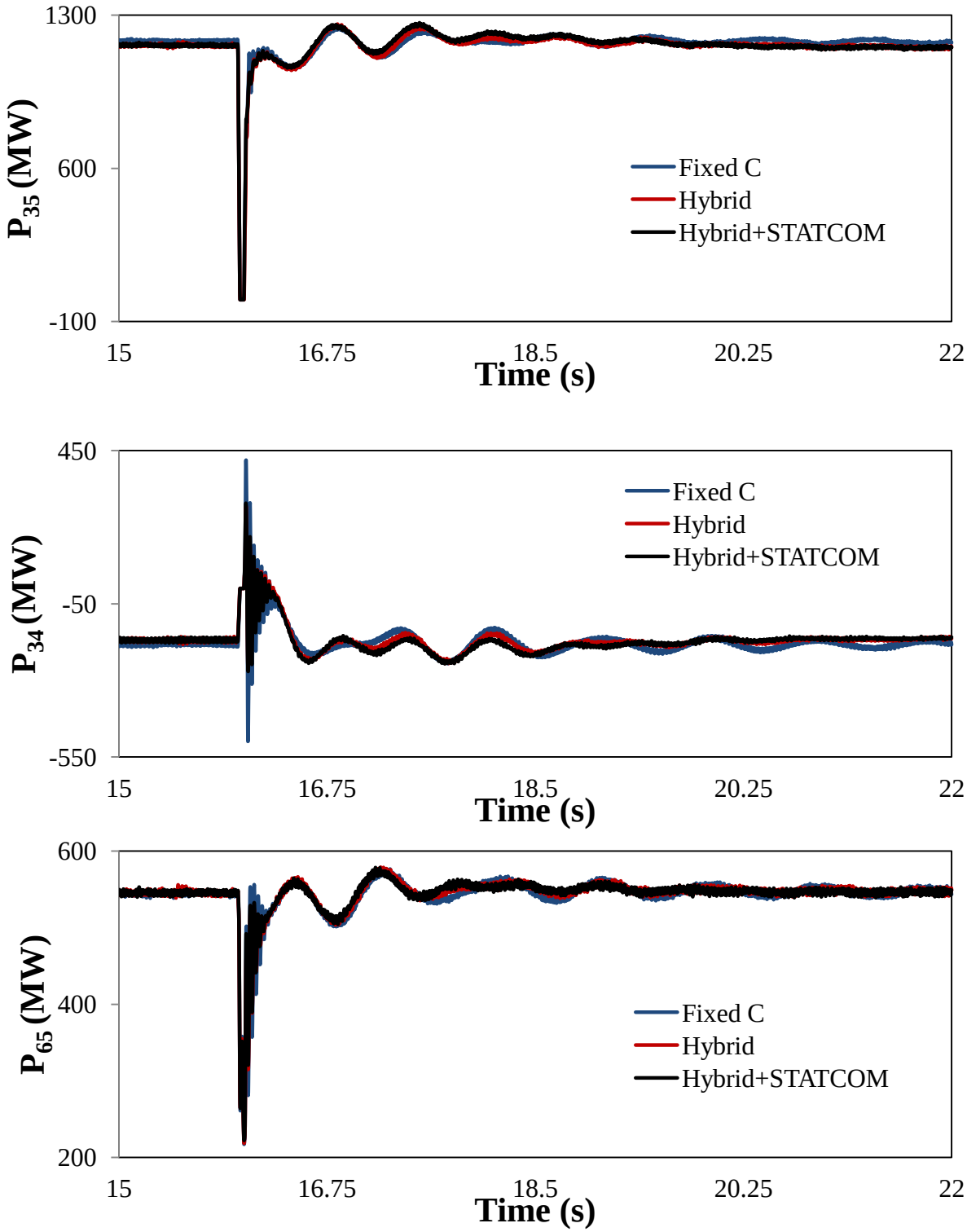


**Figure 4.6:** Continued.

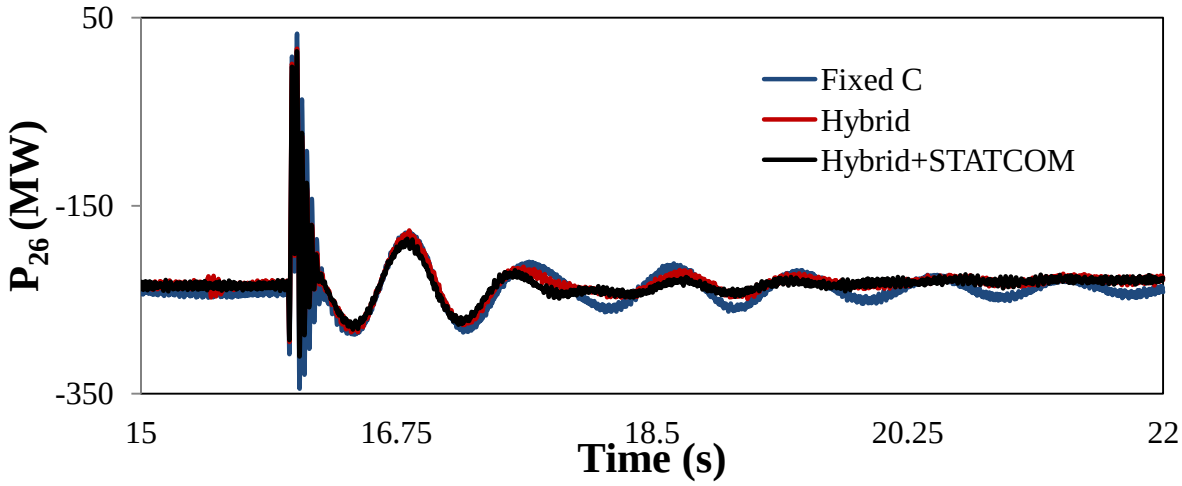


**Figure 4.6:** Continued.

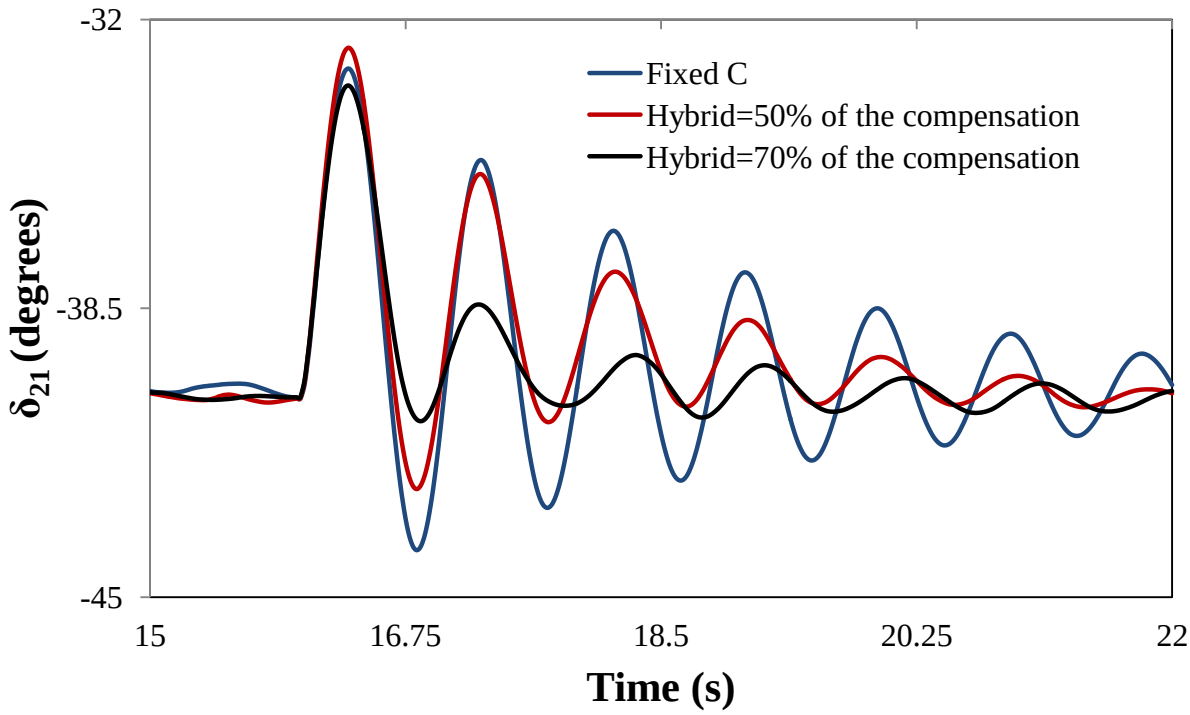


**Figure 4.7:** Generator load angles, measured with respect to generator 1 load angle, during and after clearing a three-cycle, three-phase fault at bus 3 (case study I- Effect of the ratio $X_{TCSC}/X_{Cc}$).

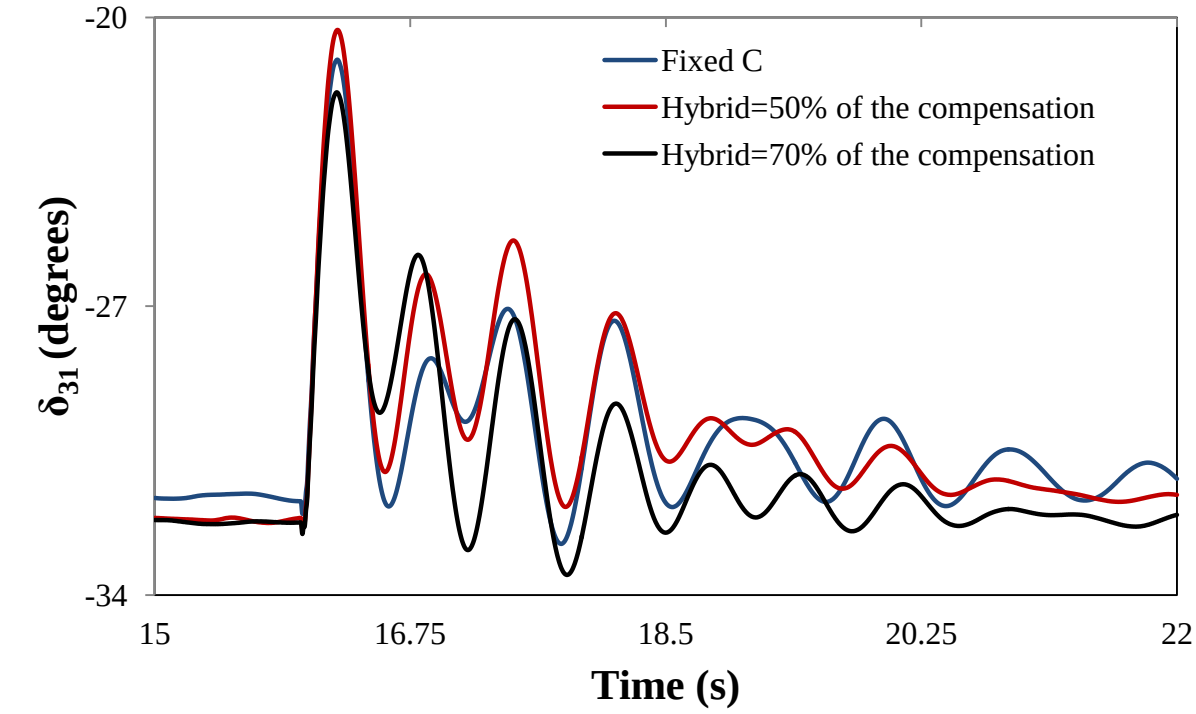


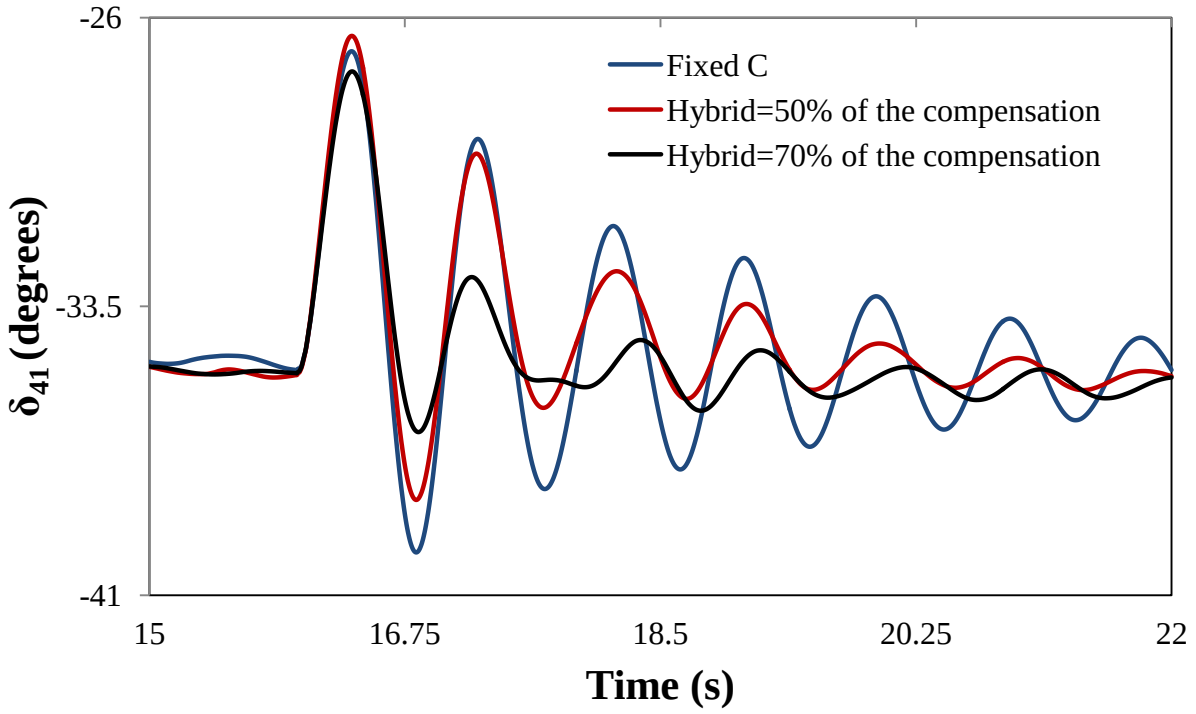


**Figure 4.7:** Continued

## 4.4 Case Study II: The Hybrid Single-Phase-TCSC Compensation Scheme is Installed in both Circuits of Line $L_2$

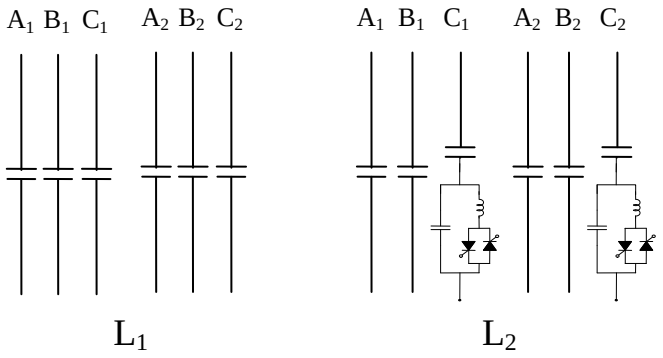


**Figure 4.8:** Case study II: the hybrid single-phase-TCSC compensation scheme is installed in both circuits of line $L_2$.

Each TCSC provides 50% of the total capacitive compensation ($X_{Cc} = X_{TCSC} = 0.5\ X_C$) and the stabilizing signal for their supplemental controllers as well as for the STATCOM supplemental controller is $\delta_{21}$. The generator load angles and speeds, measured with respect to generator 1 load angle and speed, and the transmission line real power flow responses during and after clearing a three-cycle, three-phase fault at bus 3 are illustrated in Figures 4.9 to 4.11 for the case when the TCSC supplemental controllers are of a proportional type with a transfer function given in Equation 4.4 and the STATCOM supplemental controller is not activated as well as for the case when the TCSC supplemental controllers are of a proportional type with a transfer function given in Equation 4.5 and the STATCOM supplemental controller given by Equation 4.6 is activated.

Comparing Figures 4.9 to 4.11 to Figures 4.4 to 4.6 reveals that the system transient time responses in case studies I and II are very similar. Moreover, Figure 4.9 shows that the hybrid single-phase TCSC at its new location along with the STATCOM supplemental controller are very effective in the damping of the system oscillations.

$$G_{P-\delta 21}(s) = -0.8\frac{0.5}{(s+0.5)}\frac{2s}{(2s+1)} \tag{4.4}$$

$$G_{P-\delta 21}(s) = -0.8\frac{0.5}{(s+0.5)}\frac{2s}{(2s+1)} \tag{4.5}$$

$$G_{P-\delta 21}(s) = 250\ \frac{80}{(s+80)}\frac{50\,s}{(50\,s+1)} \tag{4.6}$$

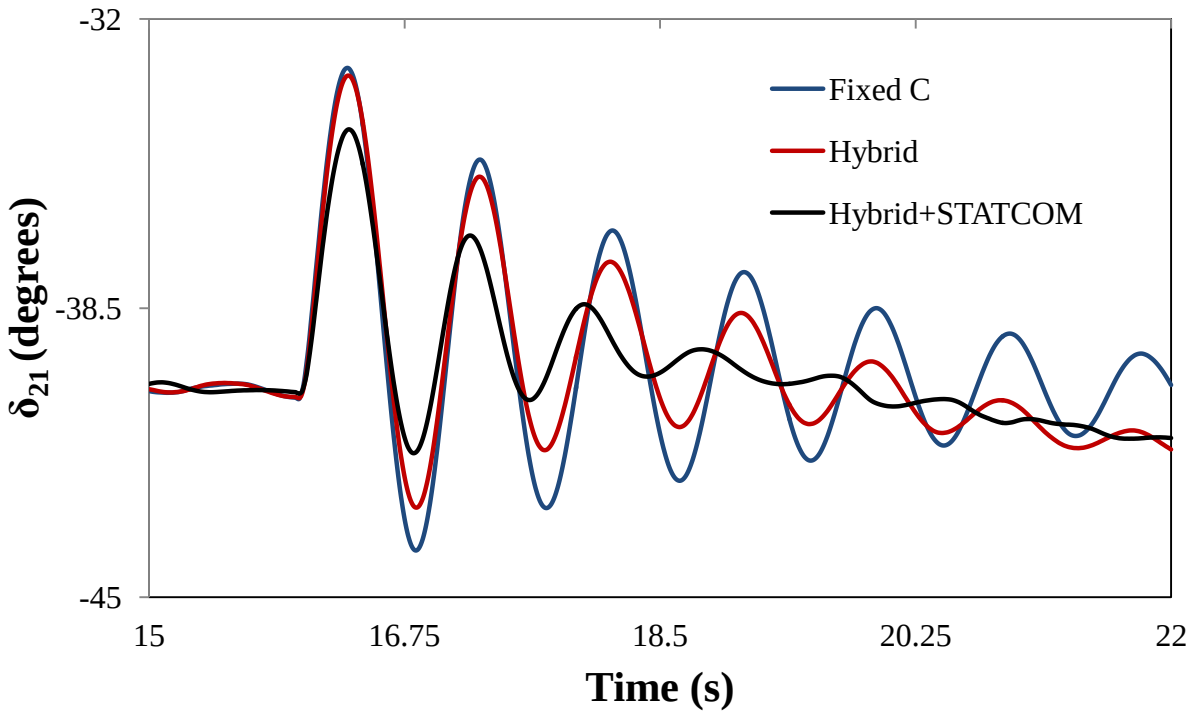


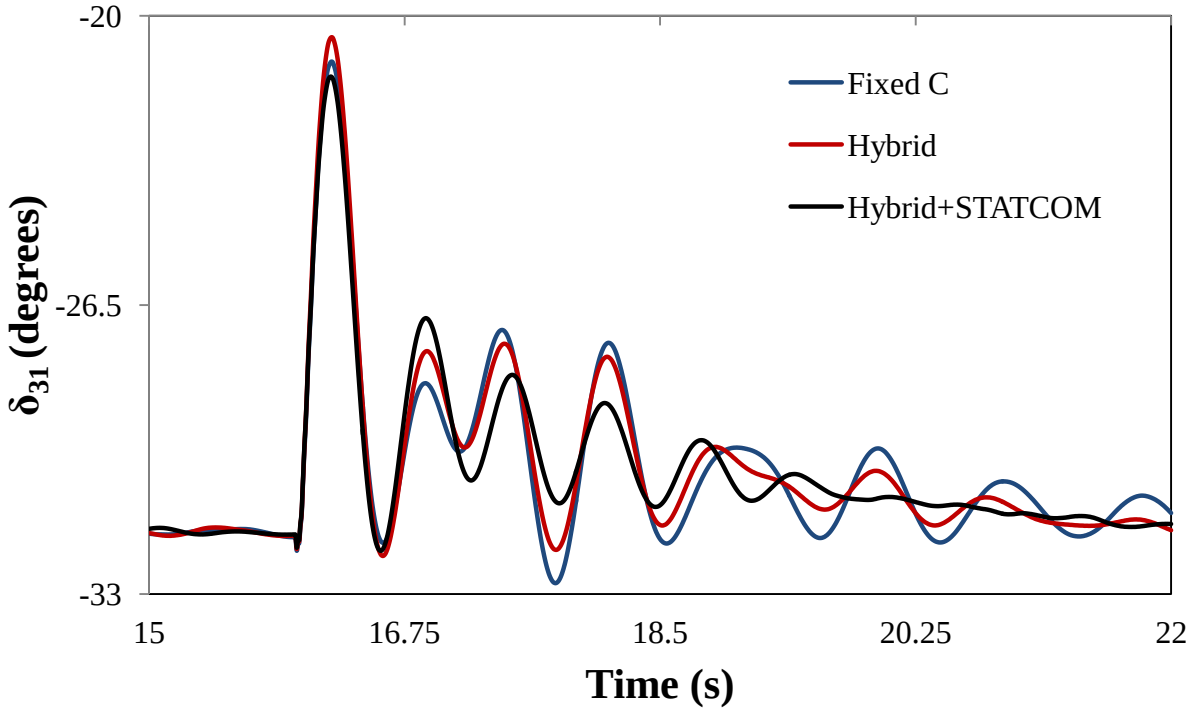


**Figure 4.9:** Generator load angles, measured with respect to generator 1 load angle, during and after clearing a three-cycle, three-phase fault at bus 3 (case study II).

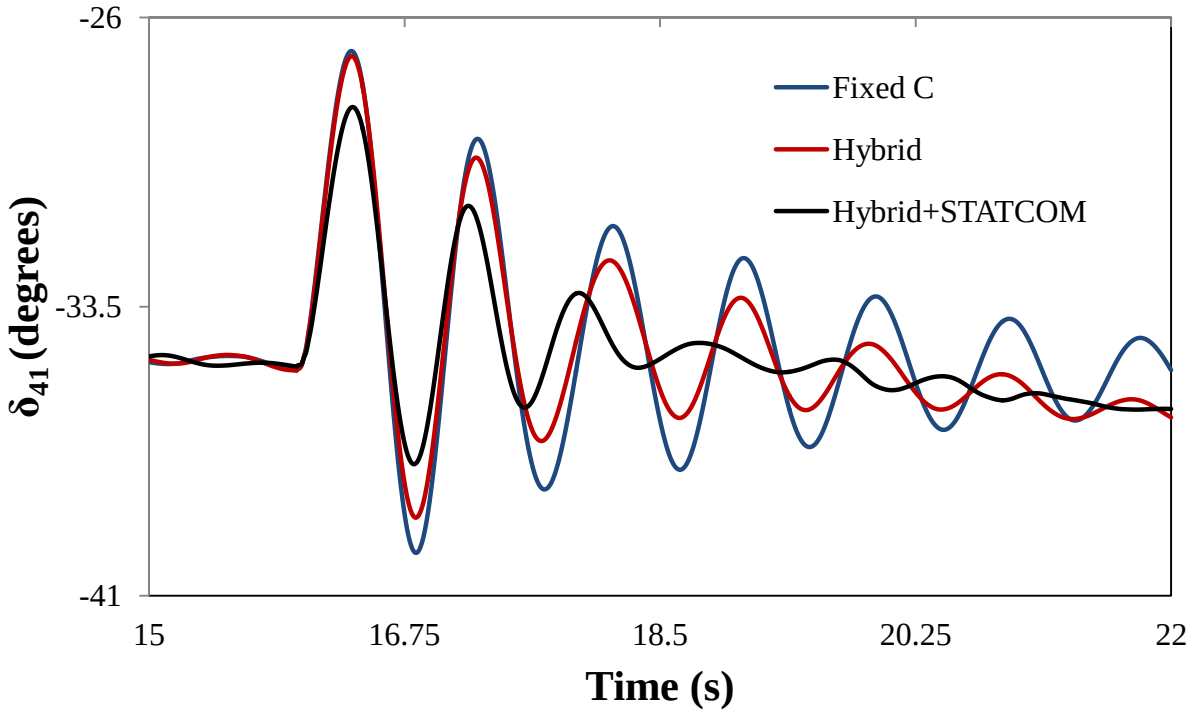


**Figure 4.9:** Continued.

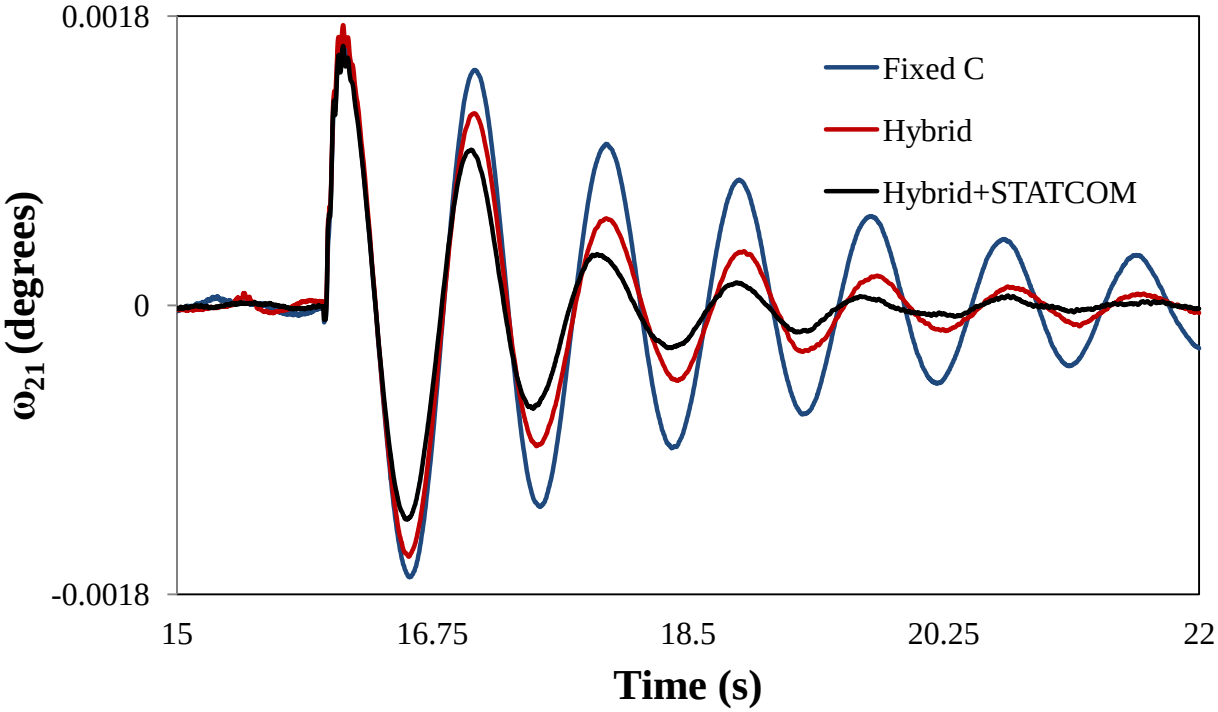


**Figure 4.10:** Generator speeds, measured with respect to generator 1 speed, during and after clearing a three-cycle, three-phase fault at bus 3 (case study II).

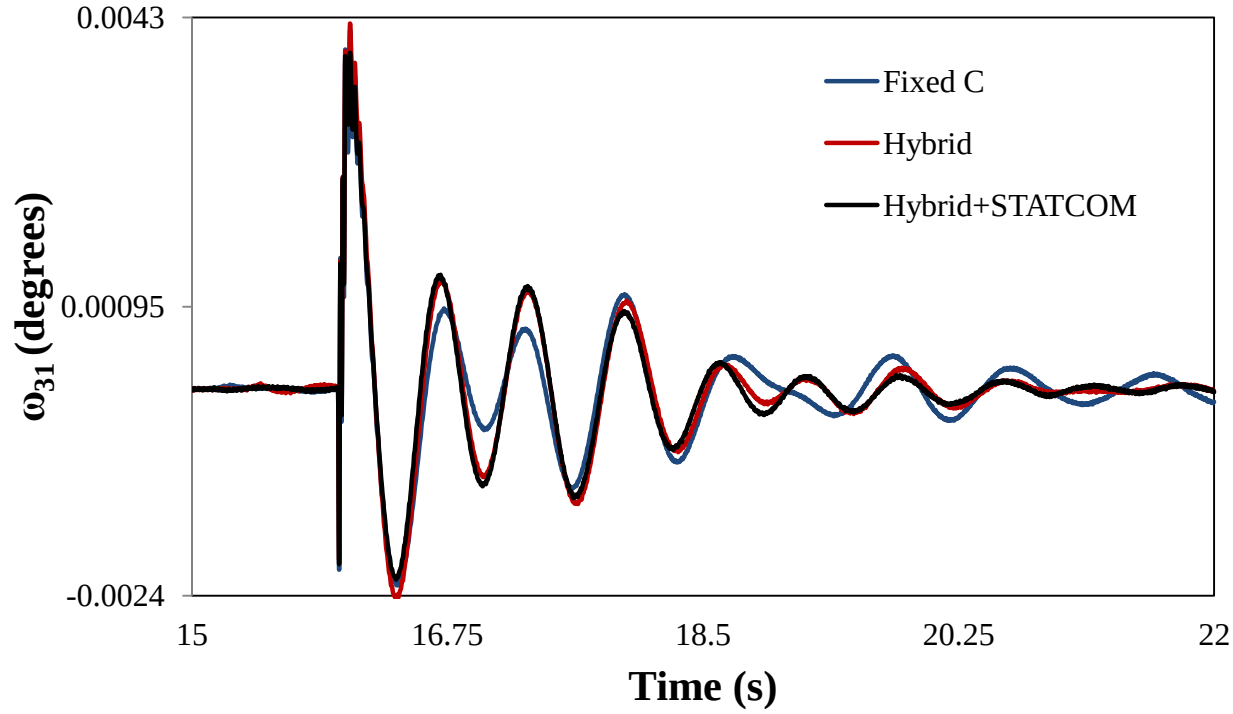


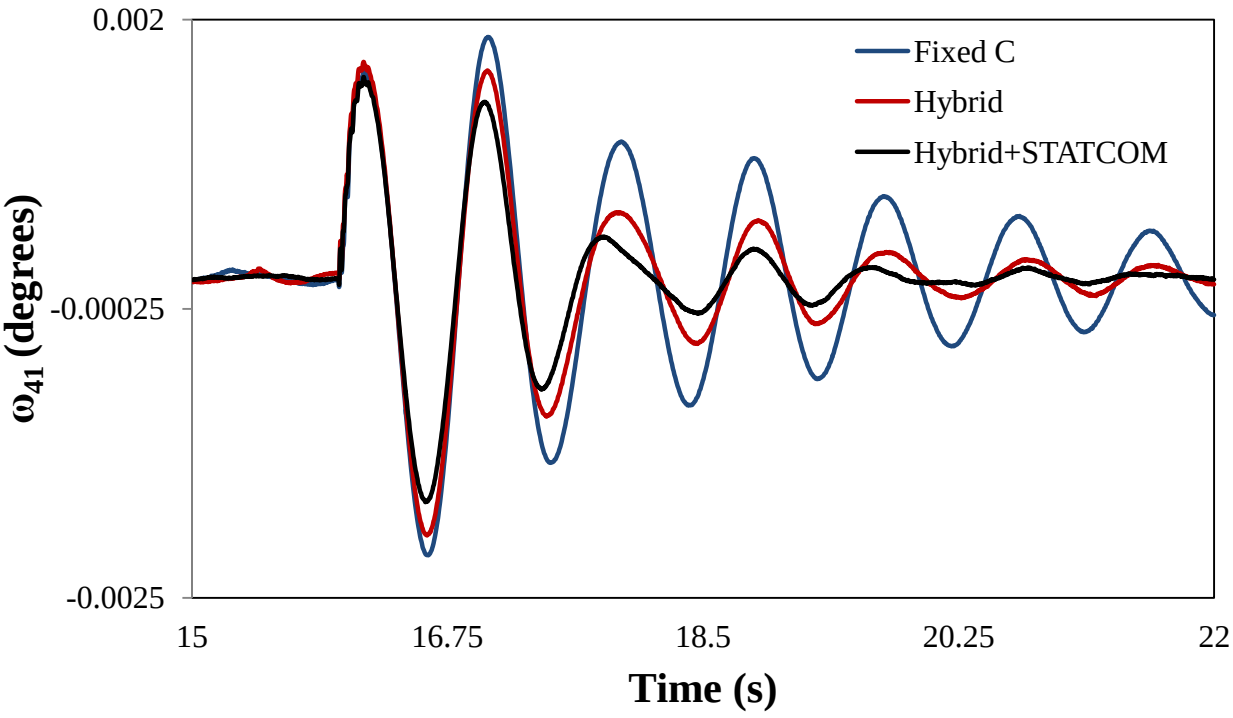


**Figure 4.10:** Continued.

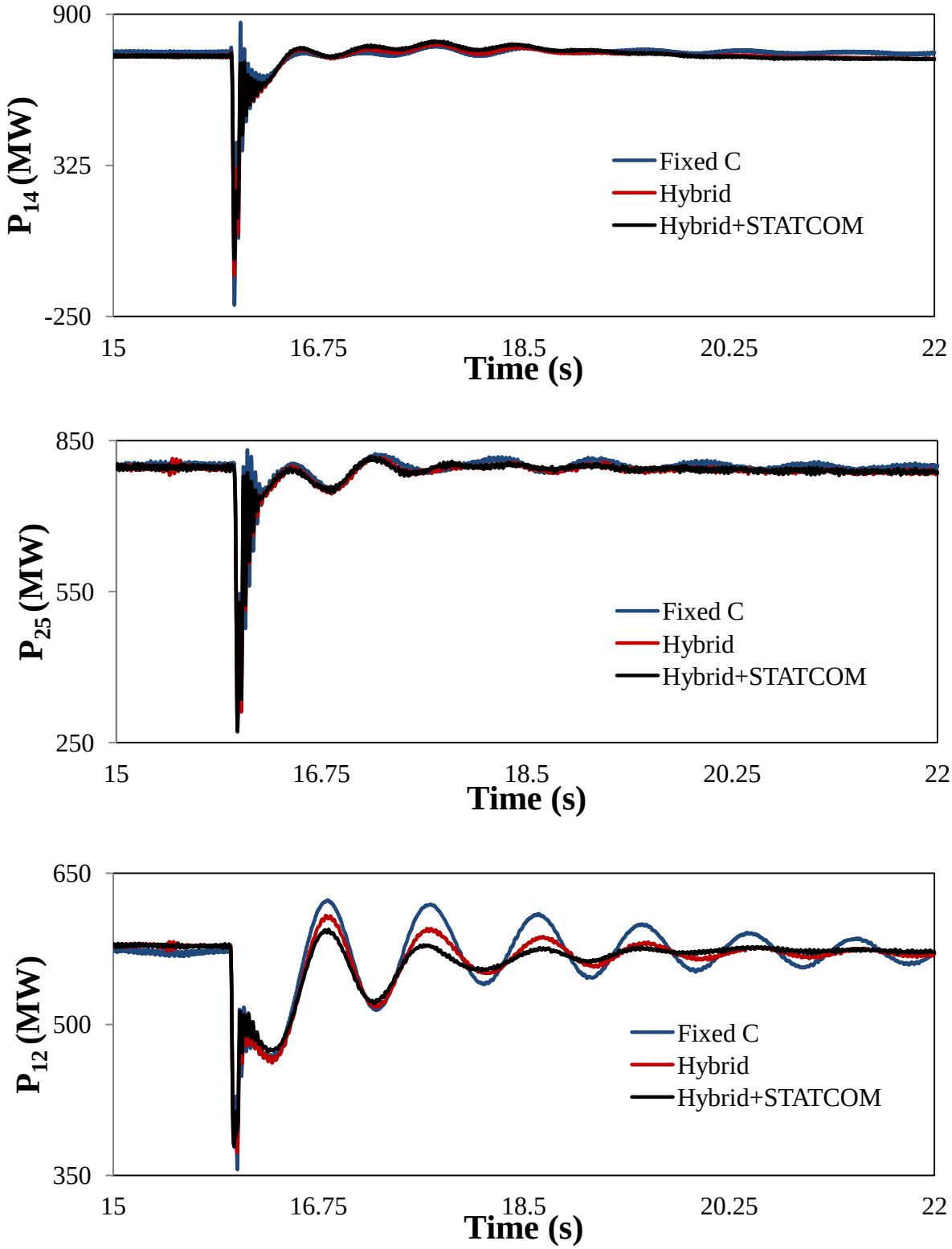


**Figure 4.11:** Transmission line real power flows during and after clearing a three-cycle, three-phase fault at bus 3 (case study II).

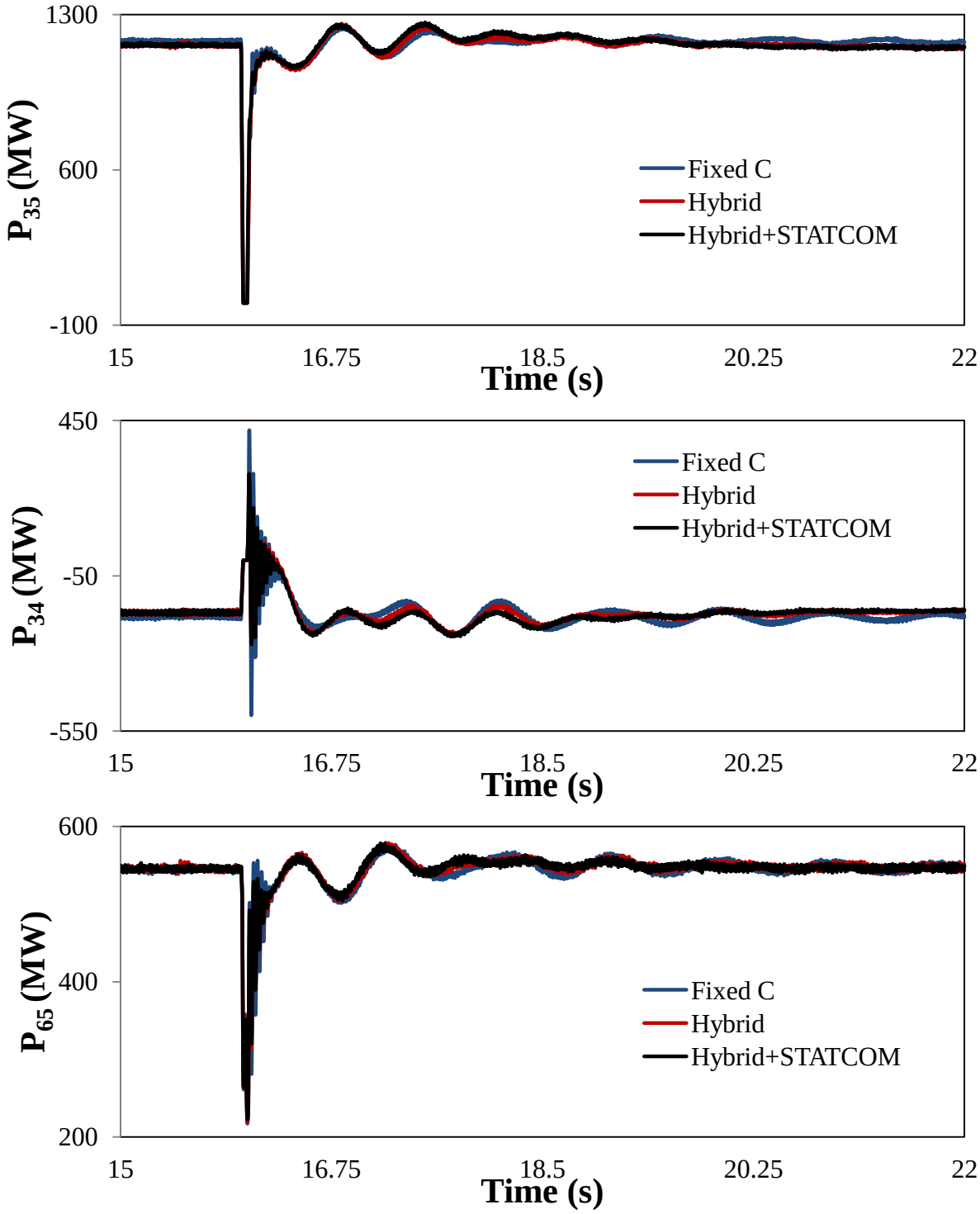


**Figure 4.11:** Continued.

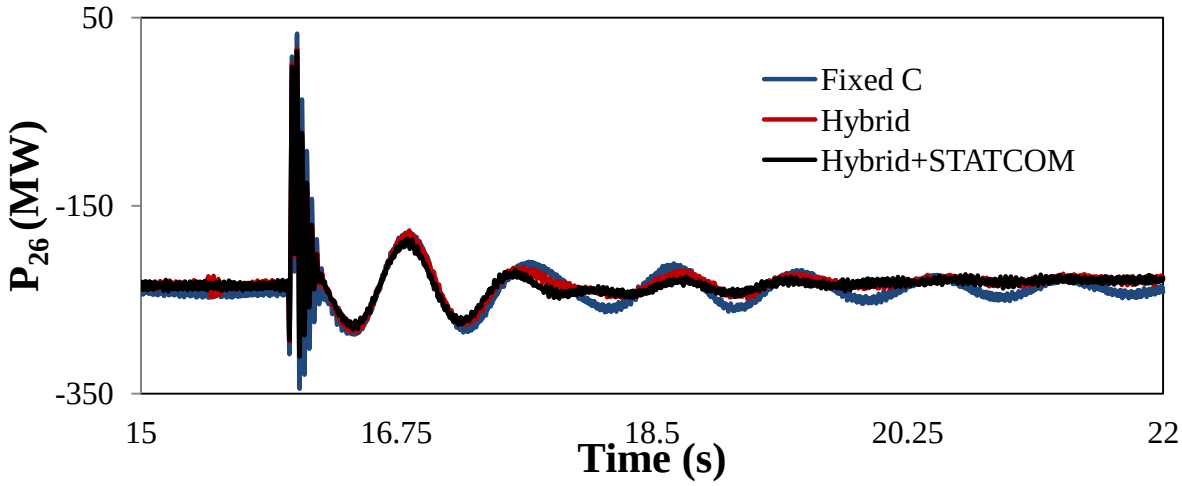


**Figure 4.11:** Continued.

## 4.5 Case Study III: The Hybrid Single-Phase-TCSC Compensation Scheme is Installed in all Circuits of Lines $L_1$ and $L_2$

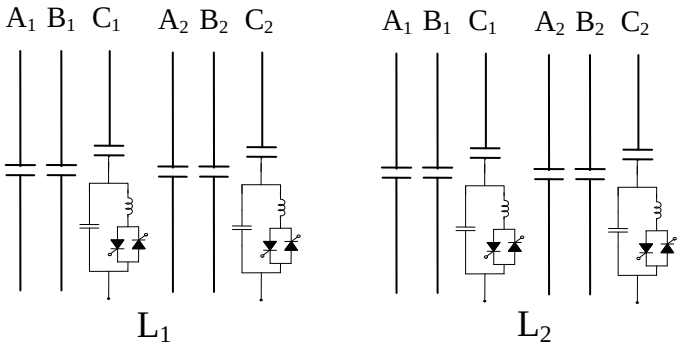


**Figure 4.12:** Case study III: the hybrid single-phase-TCSC compensation scheme is installed in all circuits of lines $L_1$ and $L_2$.

Each TCSC provides 50% of the total capacitive compensation and the disturbance is a three-cycle, three-phase fault at bus 3. Three different combinations of stabilizing signals (tabulated in Table 4.1) are examined in order to determine the combination that would result in the best system transient time responses. The final results of the time-domain simulation studies (controllers tuning) are shown in Figure 4.13 which illustrates the generator load angles, measured with respect to generator 1 load angle, during and after fault clearing. The transfer functions of the STATCOM and TCSC supplemental controllers for the three combinations are given in Tables 4.2 and 4.3.

**Table 4.1:** The three examined combinations of stabilizing signals.

| Combination | Each TCSC in $L_1$ | Each TCSC in $L_2$ | STATCOM |
|---|---|---|---|
| 1 | $\delta_{21}$ | $\delta_{21}$ | $\delta_{21}$ |
| 2 | $\delta_{21}$ | $\delta_{21}$ | $\delta_{31}$ |
| 3 | $\delta_{21}$ | $\delta_{21}$ | $\delta_{41}$ |

**Table 4.2:** Transfer functions of the TCSC supplemental controllers.

| Combination | Each TCSC in $L_1$ | Each TCSC in $L_2$ |
|---|---|---|
| 1 | $G(s) = 2\dfrac{0.5}{(s+0.5)}\dfrac{s}{(s+1)}$ | $G(s) = -0.07\dfrac{0.5}{(s+0.5)}\dfrac{s}{(s+1)}$ |
| 2 | $G(s) = 2\dfrac{0.5}{(s+0.5)}\dfrac{s}{(s+1)}$ | $G(s) = -0.07\dfrac{0.5}{(s+0.5)}\dfrac{s}{(s+1)}$ |
| 3 | $G(s) = 2\dfrac{0.5}{(s+0.5)}\dfrac{s}{(s+1)}$ | $G(s) = -0.07\dfrac{0.5}{(s+0.5)}\dfrac{s}{(s+1)}$ |

**Table 4.3:** Transfer functions of the STATCOM supplemental controller.

| Combination | STATCOM Transfer Function |
|---|---|
| 1 | $G(s) = 250\dfrac{50}{(s+50)}\dfrac{6s}{(6s+1)}$ |
| 2 | $G(s) = 250\dfrac{50}{(s+50)}\dfrac{6s}{(6s+1)}$ |
| 3 | $G(s) = 100\dfrac{50}{(s+50)}\dfrac{6s}{(6s+1)}$ |

It can be seen from this figure that the best damping of the relative load angle responses are achieved with the $\delta_{21}$- $\delta_{21} - \delta_{41}$ combination. The other two combinations yield almost to the same responses which are also very satisfactory. These results should be expected due to the direct relationship between the relative load angles and the generators that yield the problem.

Having established that $\delta_{21}$- $\delta_{21}$- $\delta_{41}$ are the best stablizing input signals, Figures 4.14 and 4.15 illustrate respectively, the transient time responses of the generator speeds (relative to the speed of generator 1) and the real power flow on the seven transmission lines.

Figure 4.16 illustrates the three-phase voltages, $V_{X\text{-}Y}$, across the hybrid compensation scheme on one of circuits of double-circuit transmission line $L_2$ during and after clearing the fault. The system phase imbalance during the disturbance is clearly noticeable, especially in phase C where the TCSC is installed.

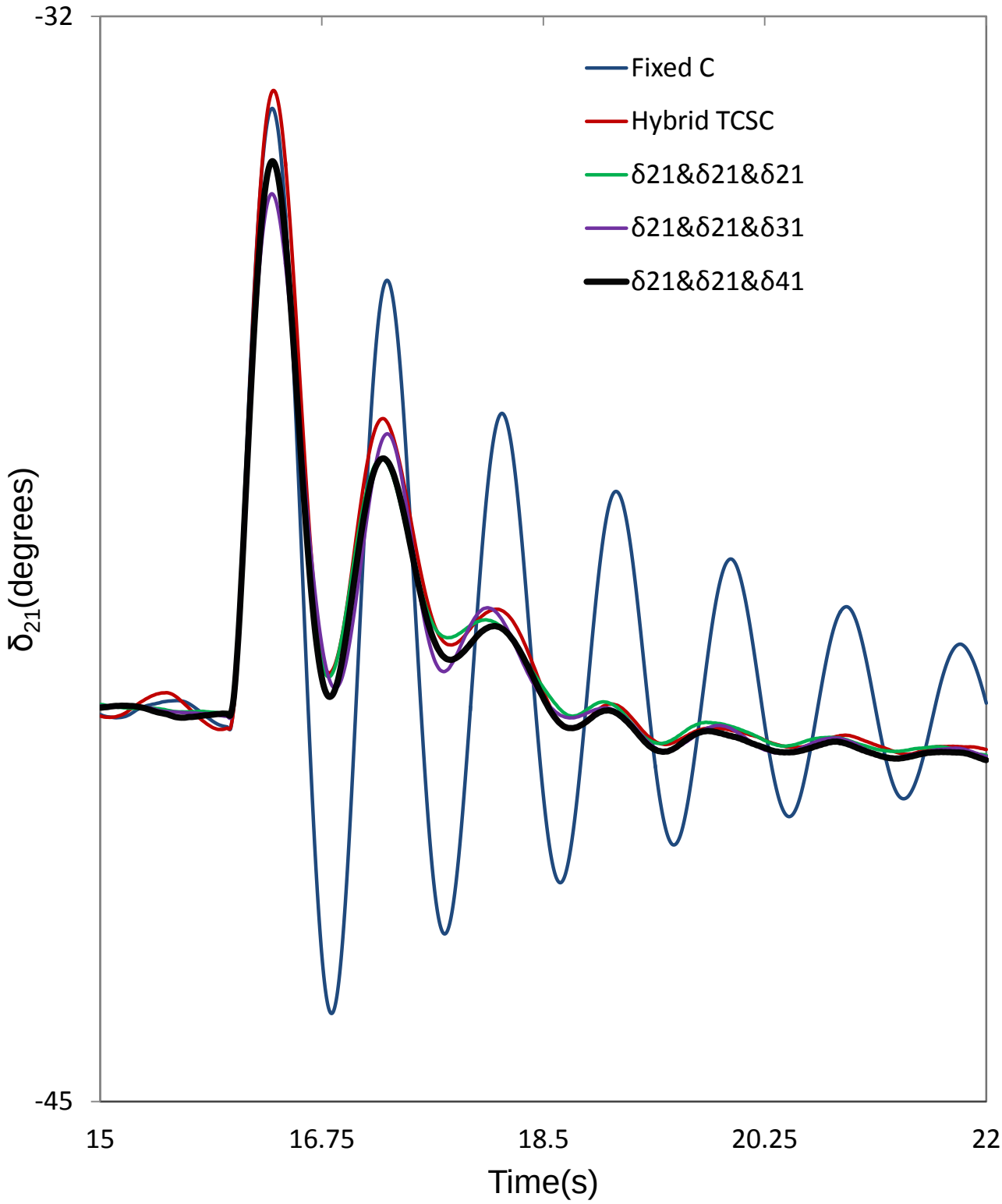


**Figure 4.13:** Generator load angles, measured with respect to generator 1 load angle, during and after clearing a three-cycle, three-phase fault at bus 3 (case study III).

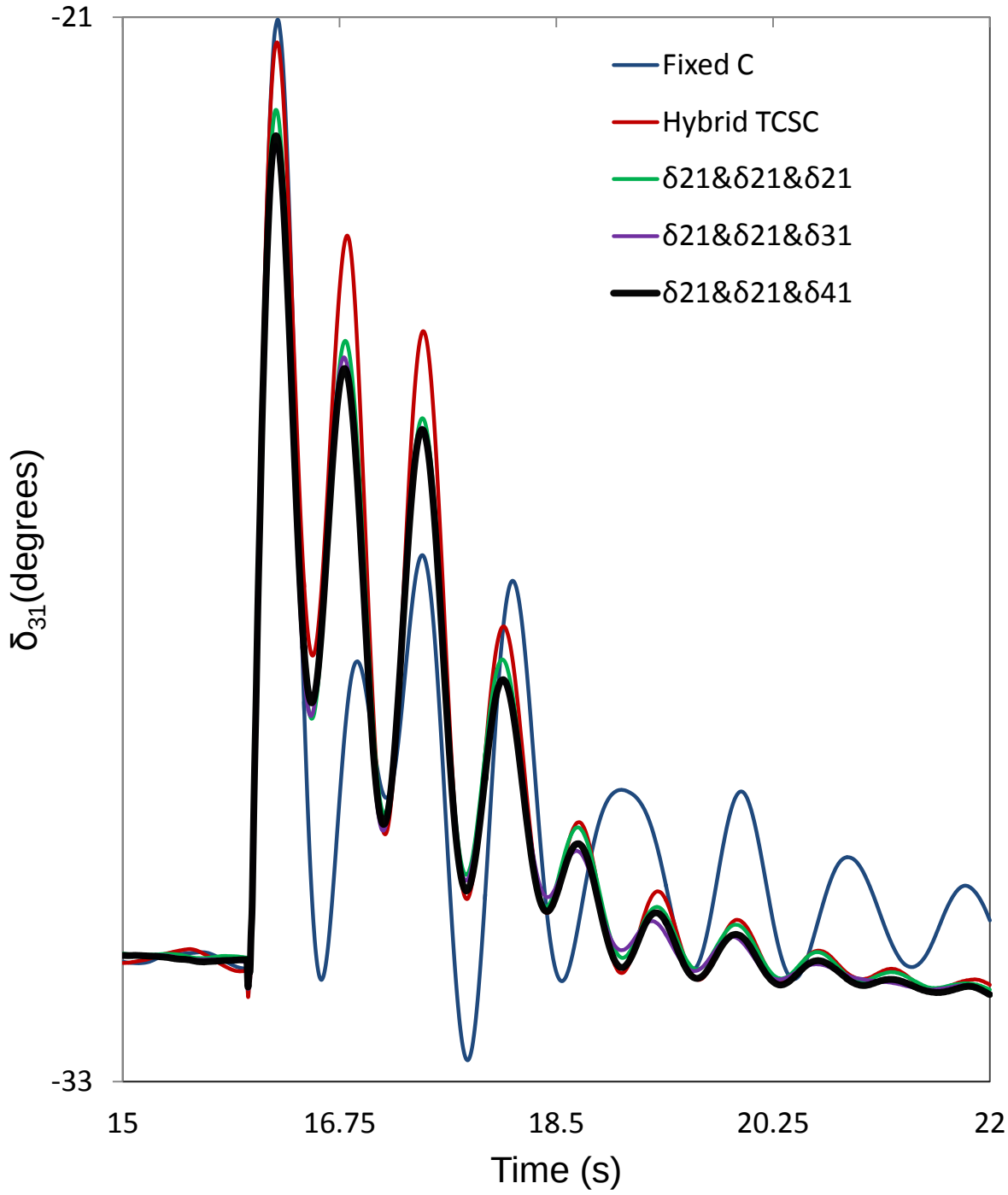


**Figure 4.13:** Continued.

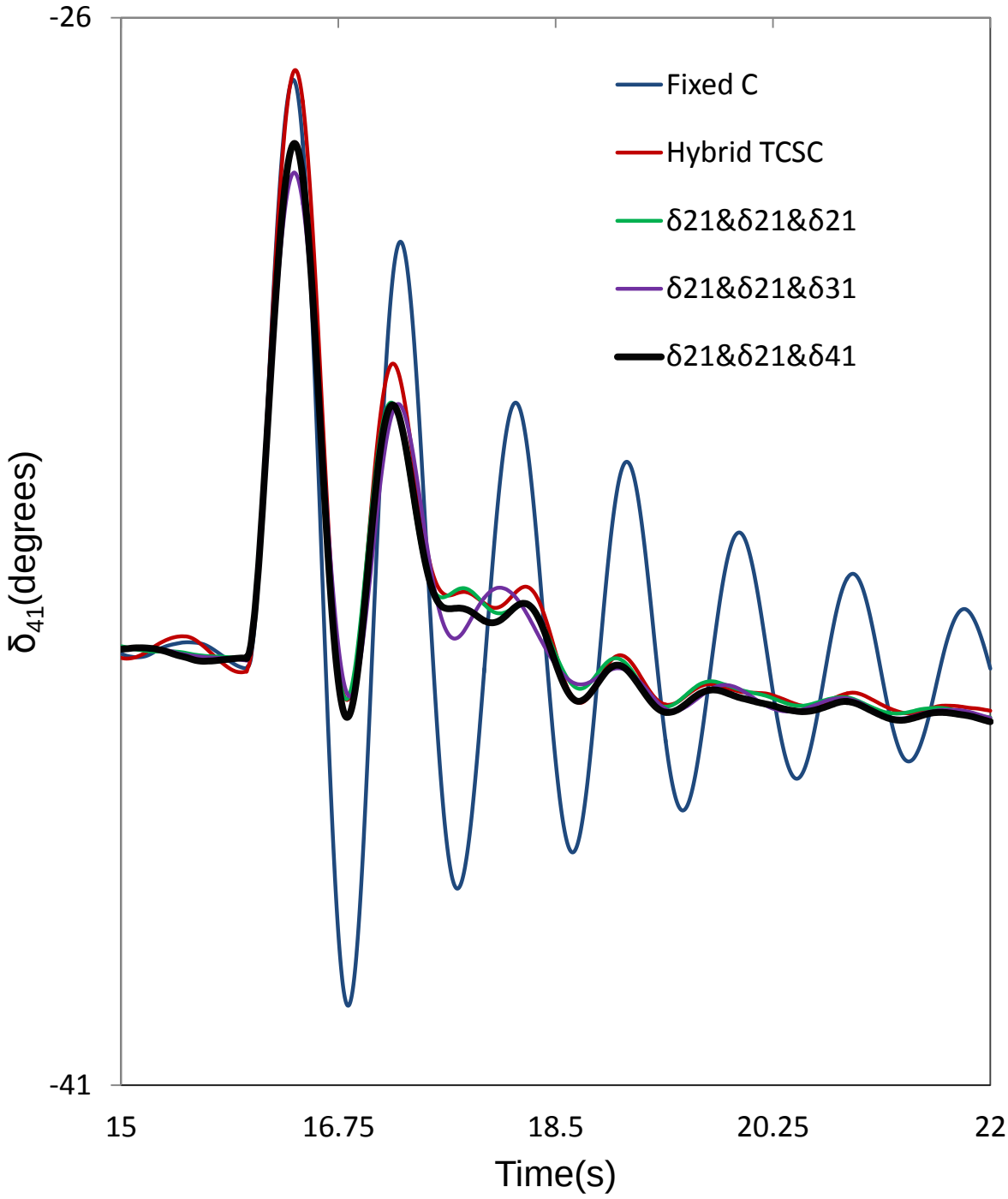


**Figure 4.13:** Continued.

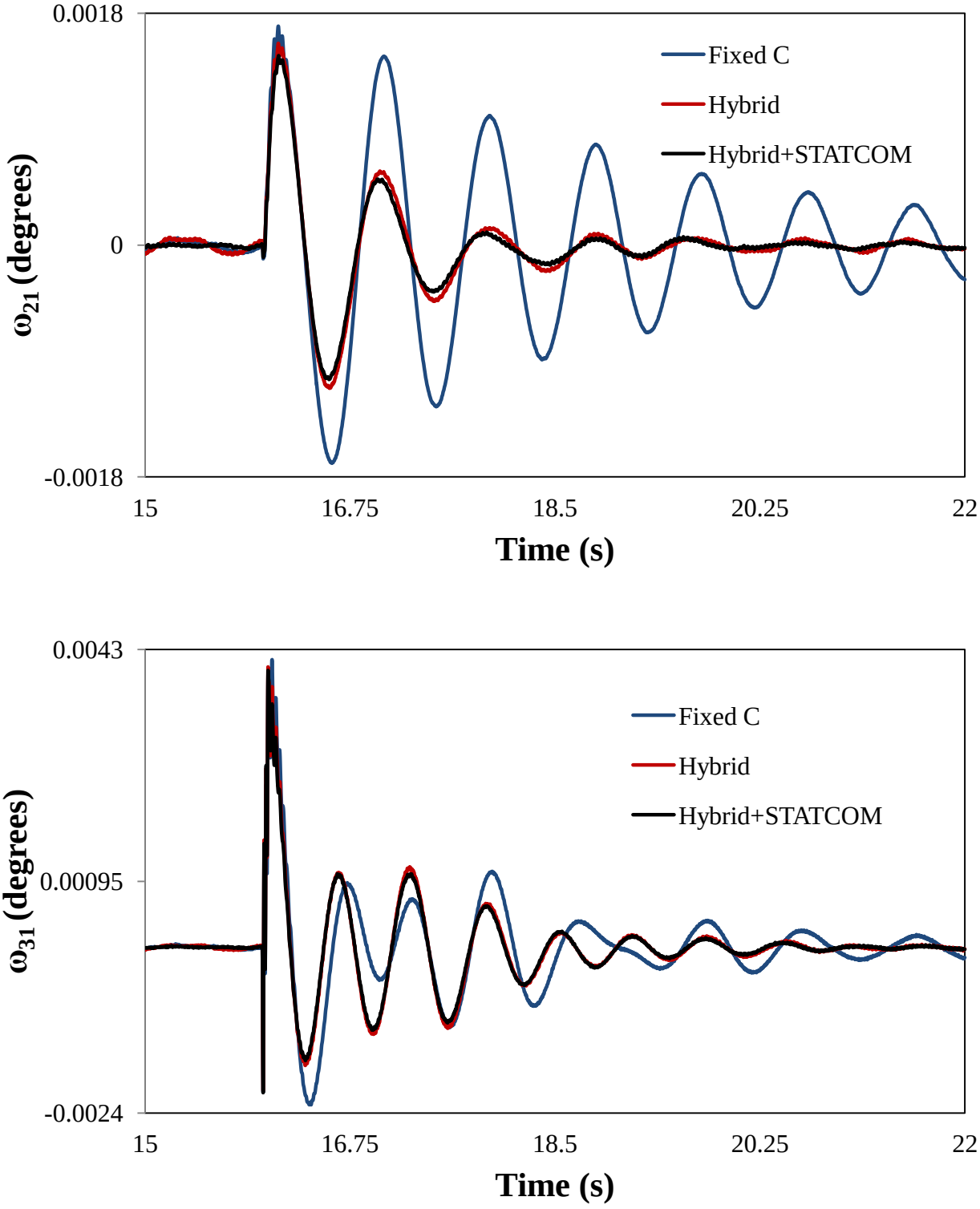


**Figure 4.14:** Generator speeds, measured with respect to generator 1 speed, during and after clearing a three-cycle, three-phase fault at bus 3 (case study III, stabilizing signals are $\delta_{21}$ for both TCSC controllers and $\delta_{41}$ for STATCOM controller).

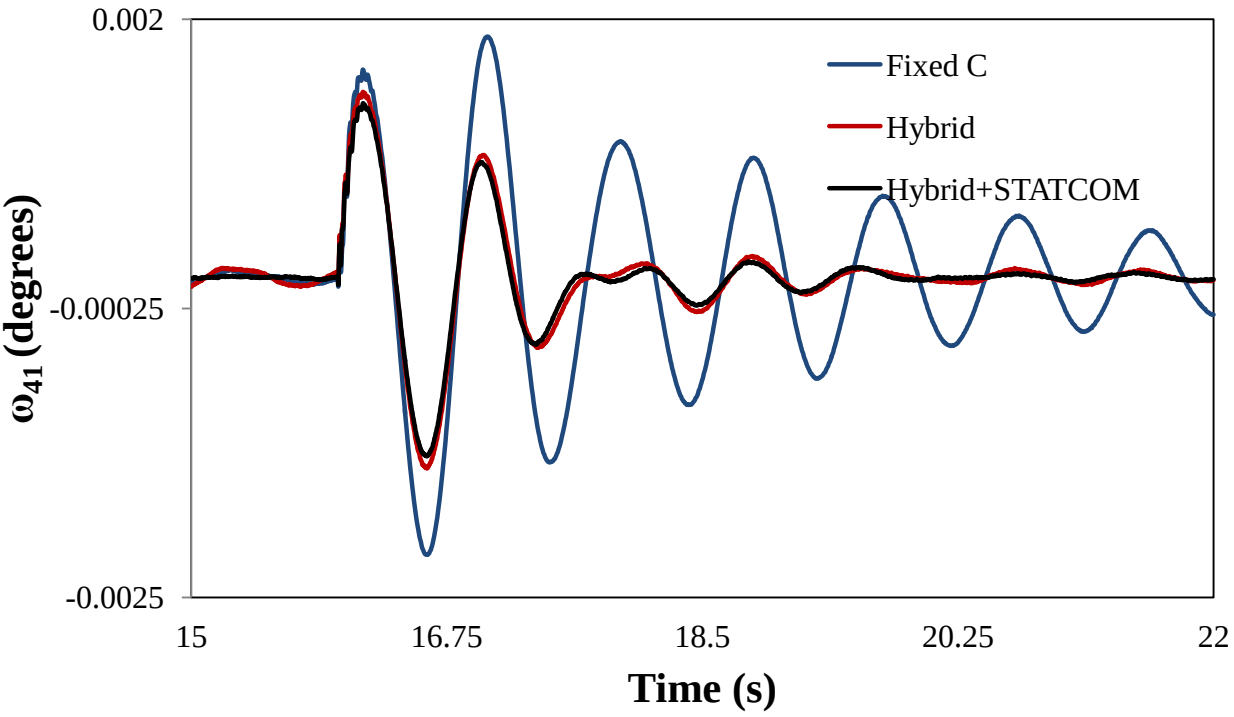


**Figure 4.14:** Continued.

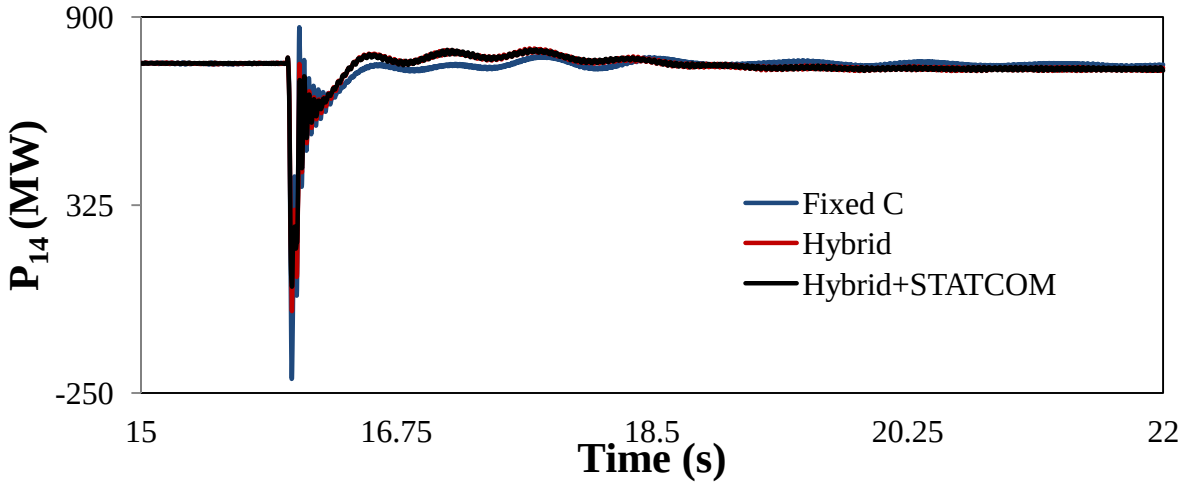


**Figure 4.15:** Transmission line real power flows during and after clearing a three-cycle, three-phase fault at bus 3 (case study III, input signals are $\delta_{21}$ for both TCSC controllers and $\delta_{41}$ for STATCOM controller).

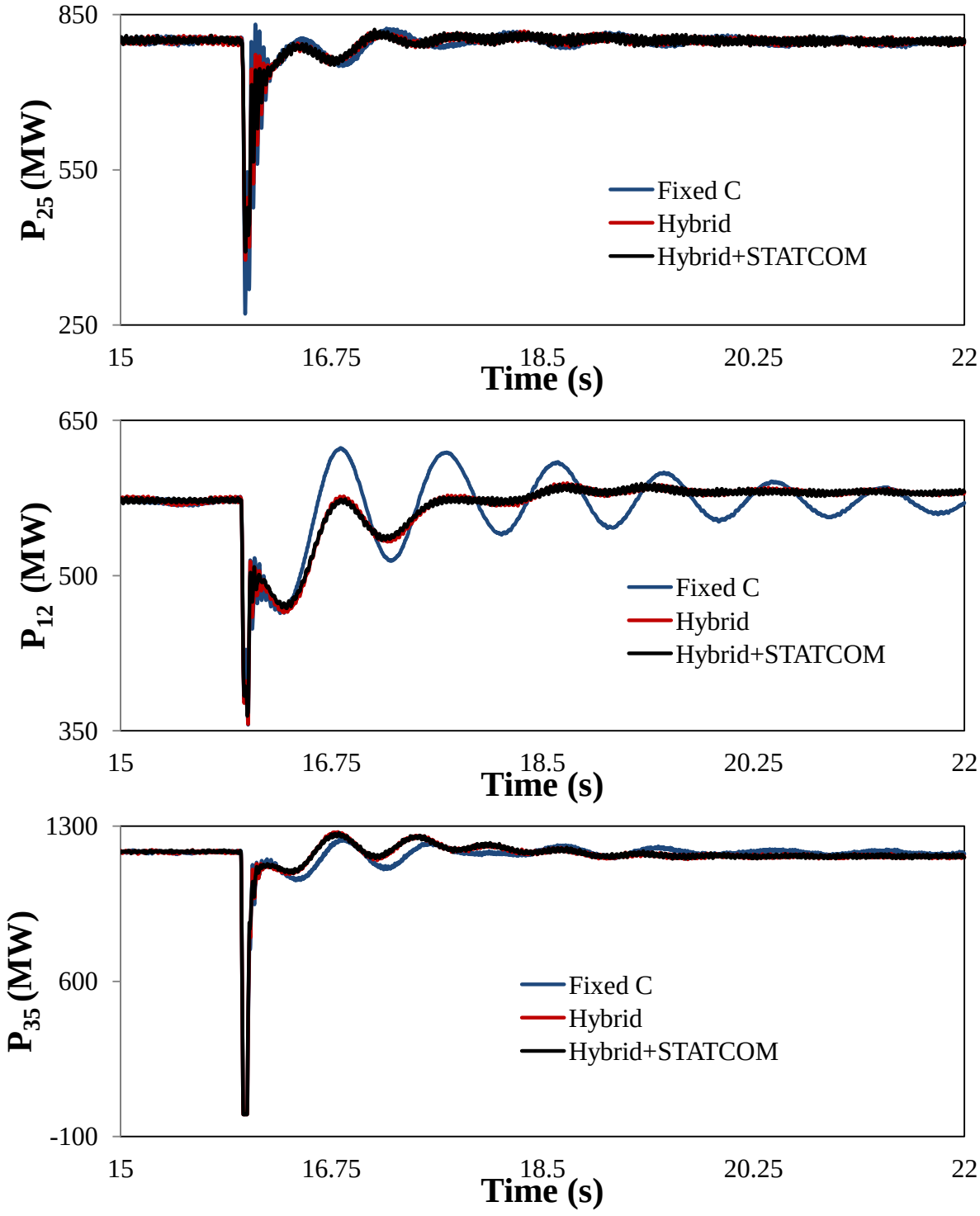


**Figure 4.15:** Continued.

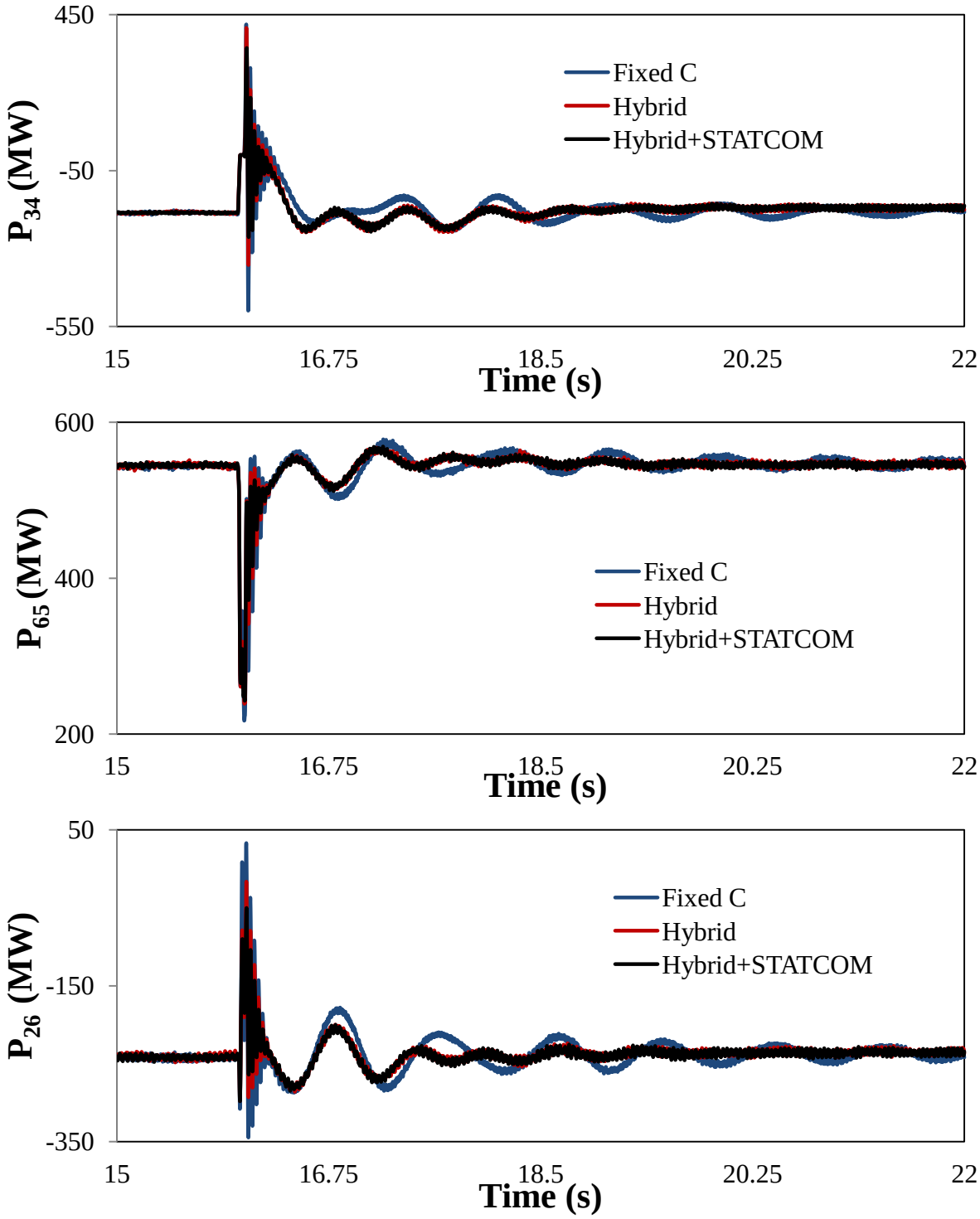


**Figure 4.15:** Continued.

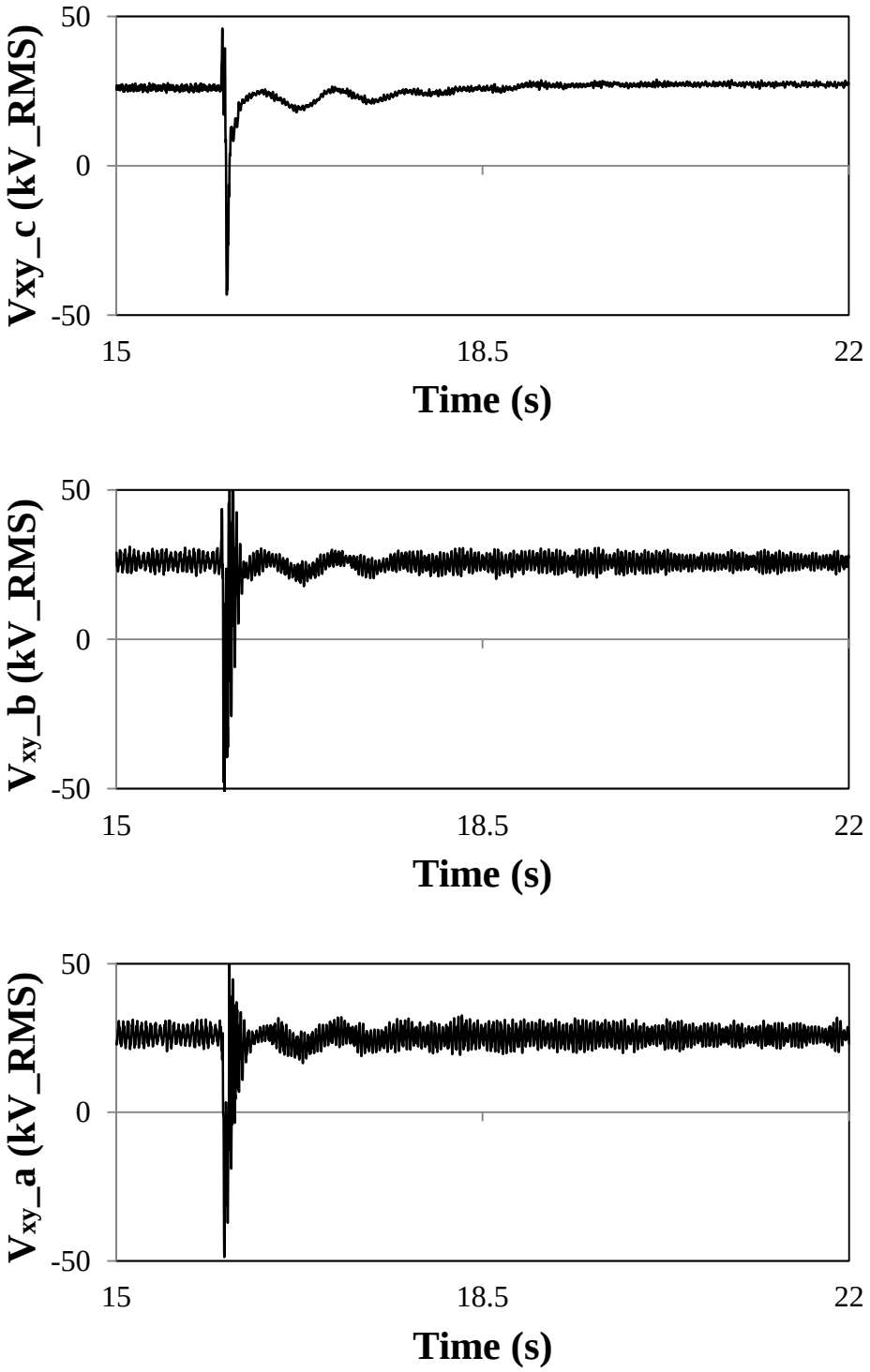


**Figure 4.16:** Phase voltages, $V_{X\text{-}Y}$ across the hybrid single-phase-TCSC of Fig. 3.5 during and after clearing a three-cycle, three-phase fault at bus 3 (case study III).

### 4.5.1 Effect of the Fault Clearing Time

Figure 4.17 illustrates the transient time responses of generator load angles, measured with respect to generator 1 load angle, during and after fault clearing a 4.5 cycle three - phase fault at bus 3. As it can be seen from this figure, the supplemental controllers are capable also of damping the system oscillations resulting from such a disturbance for the new fault clearing time.

### 4.5.2 Effect of the Fault Location

Figure 4.18 illustrates the transient time responses of the generator load angle, during and after fault clearing a 3 cycle three - phase fault at bus 2. As it can be seen from this figure, the supplemental controllers are capable also of damping the system oscillations resulting from such a disturbance at the new fault location.

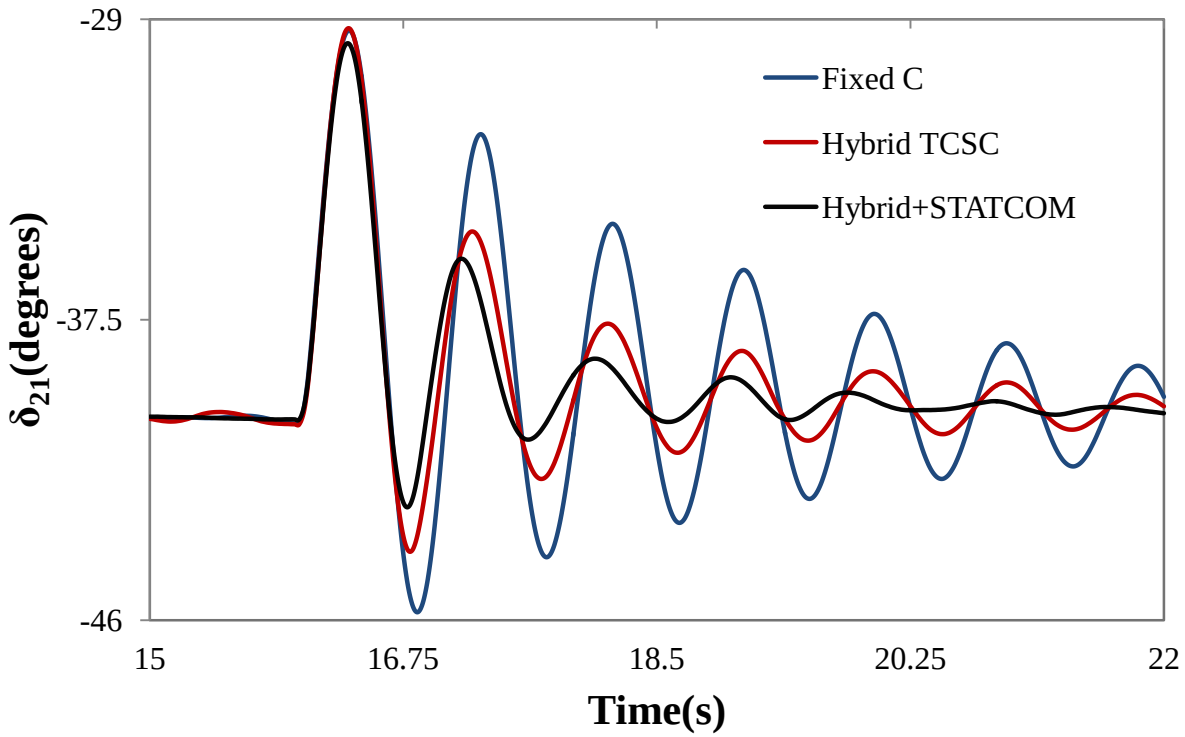


**Figure 4.17:** Generator load angles, measured with respect to generator 1 load angle, during and after clearing a 4.5-cycle, three-phase fault at bus 3 (case study III, input signals are $\delta_{21}$ for both TCSC controllers and $\delta_{41}$ for STATCOM controller).

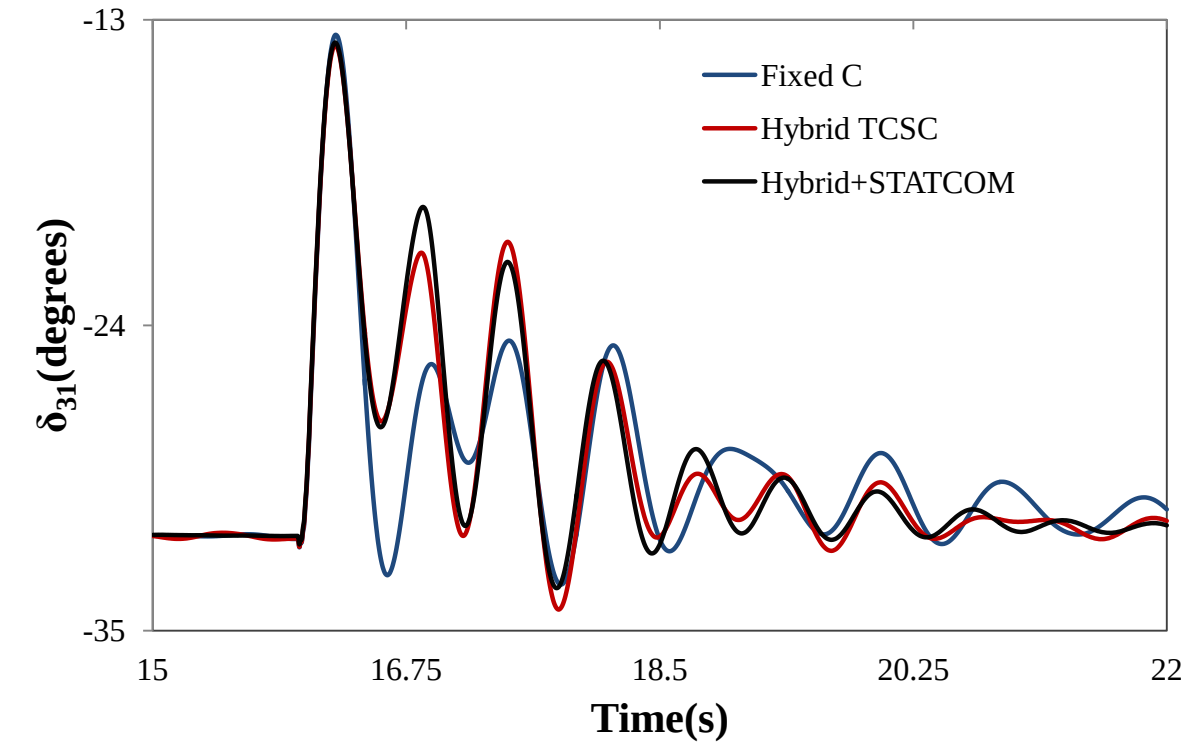


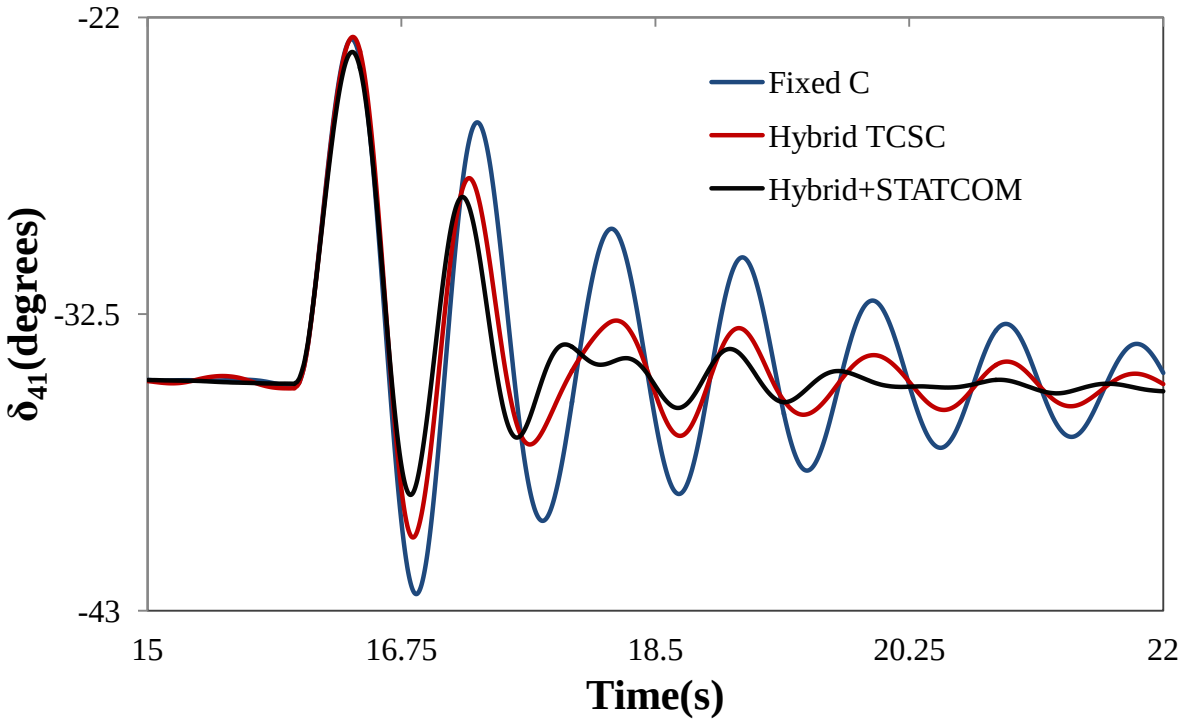


**Figure 4.17:** Continued.

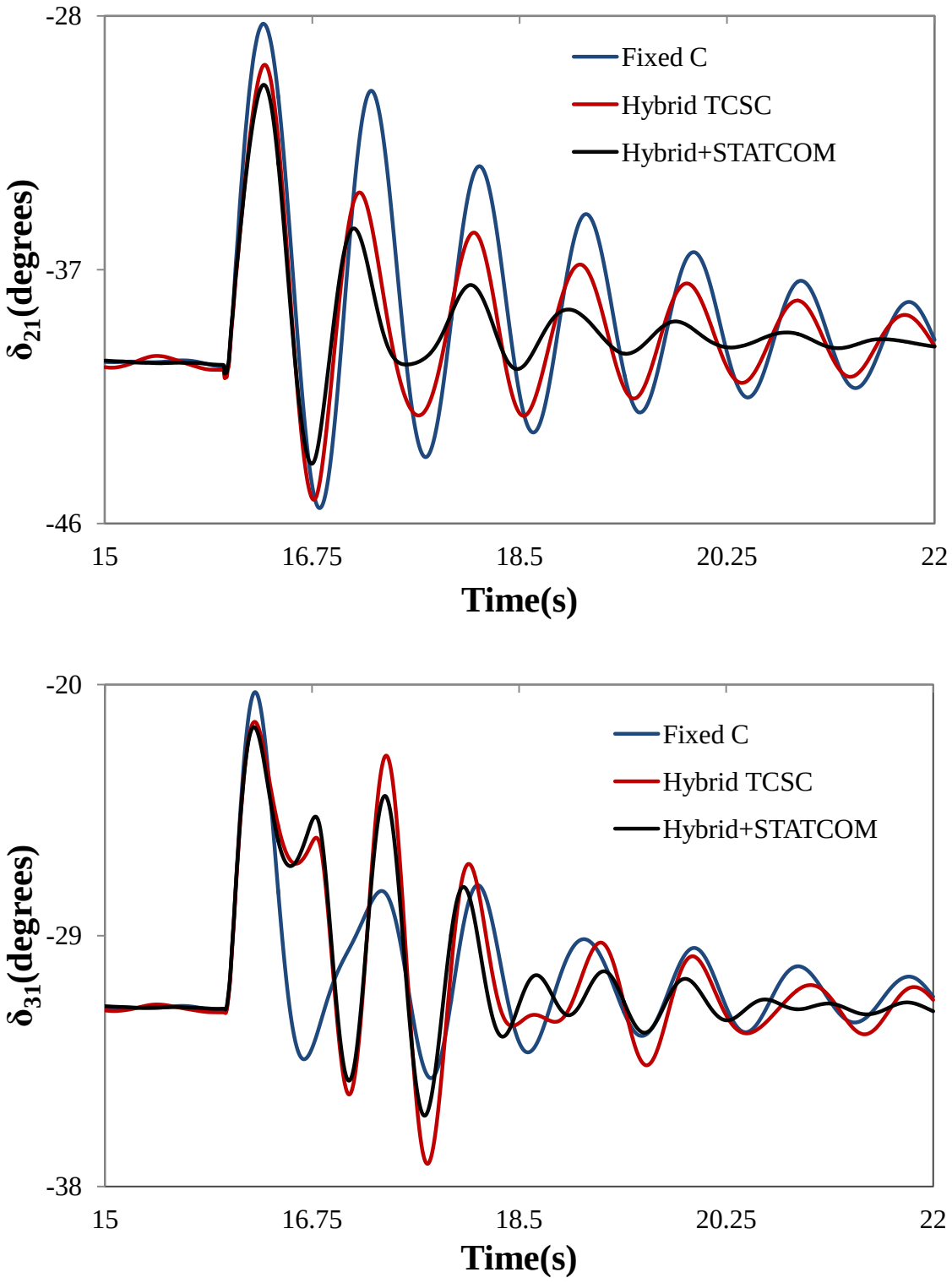


**Figure 4.18:** Generator load angles, measured with respect to generator 1 load angle, during and after clearing a 3-cycle, three-phase fault at bus 2 (case study III, input signals are $\delta_{21}$ for both TCSC controllers and $\delta_{41}$ for STATCOM controller).

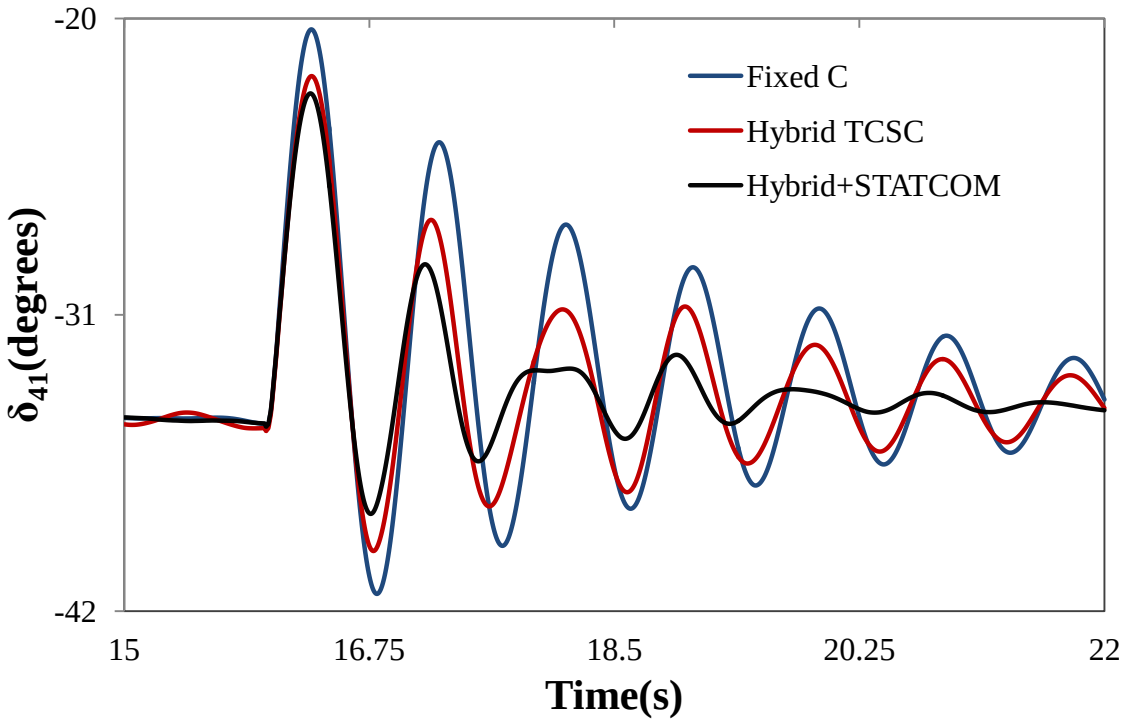


**Figure 4.18:** Continued.

## 4.6 Case Study IV: The Hybrid Single-Phase-TCSC Compensation Scheme is Installed in Lines $L_1$ and $L_3$

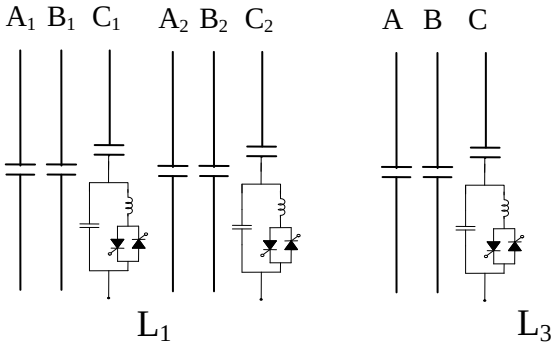


**Figure 4.19:** Case study IV: the hybrid single-phase-TCSC compensation scheme is installed in lines $L_1$ and $L_3$.

In this case study, the hybrid single-phase-TCSC compensation scheme is installed in the uncompensated line, $L_3$, for the purpose of system dynamic reinforcement. As it can be seen from Figure 2.9, line $L_3$ is the direct interconnection between $G_1$ and $G_2$. Controlling the real power flow of this line would have a direct impact on the oscillations between these two generators.

The system pre-fault load flow for this case is shown in Figure 4.20 where it is assumed that the degree of compensation of $L_3$ is 50% and that the single-phase-TCSC provides 50% of the total capacitive compensation. The disturbance is a three-cycle, three-phase fault at bus 3. The final results of the time-domain simulation studies (controller tuning) are compared with case study III and are shown in Figure 4.21. This figure illustrates the generator load angles, measured with respect to generator 1 load angle, during and after fault clearing. The transfer functions of the STATCOM and TCSC supplemental controllers with the stabilizing signal $\delta_{21}$ are given in Table 4.4.

**Table 4.4:** Transfer functions of the STATCOM and TCSC supplemental controllers with the stabilizing signal $\delta_{21}$ (case IV).

| | Transfer Function |
|---|---|
| Each TCSC in L1 | $G_{TCSC}(s) = \frac{0.5}{(s+0.5)}\frac{s}{(s+1)}$ |
| Each TCSC in L2 | $G_{TCSC}(s) = 2\frac{0.5}{(s+0.5)}\frac{s}{(s+1)}$ |
| STATCOM | $G_{STATCOM}(s) = 250\frac{50}{(s+50)}\frac{6s}{(6s+1)}$ |

As the result of the series compensation of $L_3$, the phase angles between buses 1 and 2, 1 and 3 as well as between buses 1 and 4 are reduced and the real power transmitted between buses 1 and 2 is increased (from 521 MW, Figure 2.9, to 665.5 MW, Figure 4.20). The reductions in these phase angles are directly reflected into reductions in the initial values of the relative generator load angles $\delta_{21}$, $\delta_{31}$ and $\delta_{41}$ as it is shown in Figure 4.21. The figure also shows that Scheme I and the STATCOM supplemental controllers provide very effective damping to system oscillations.

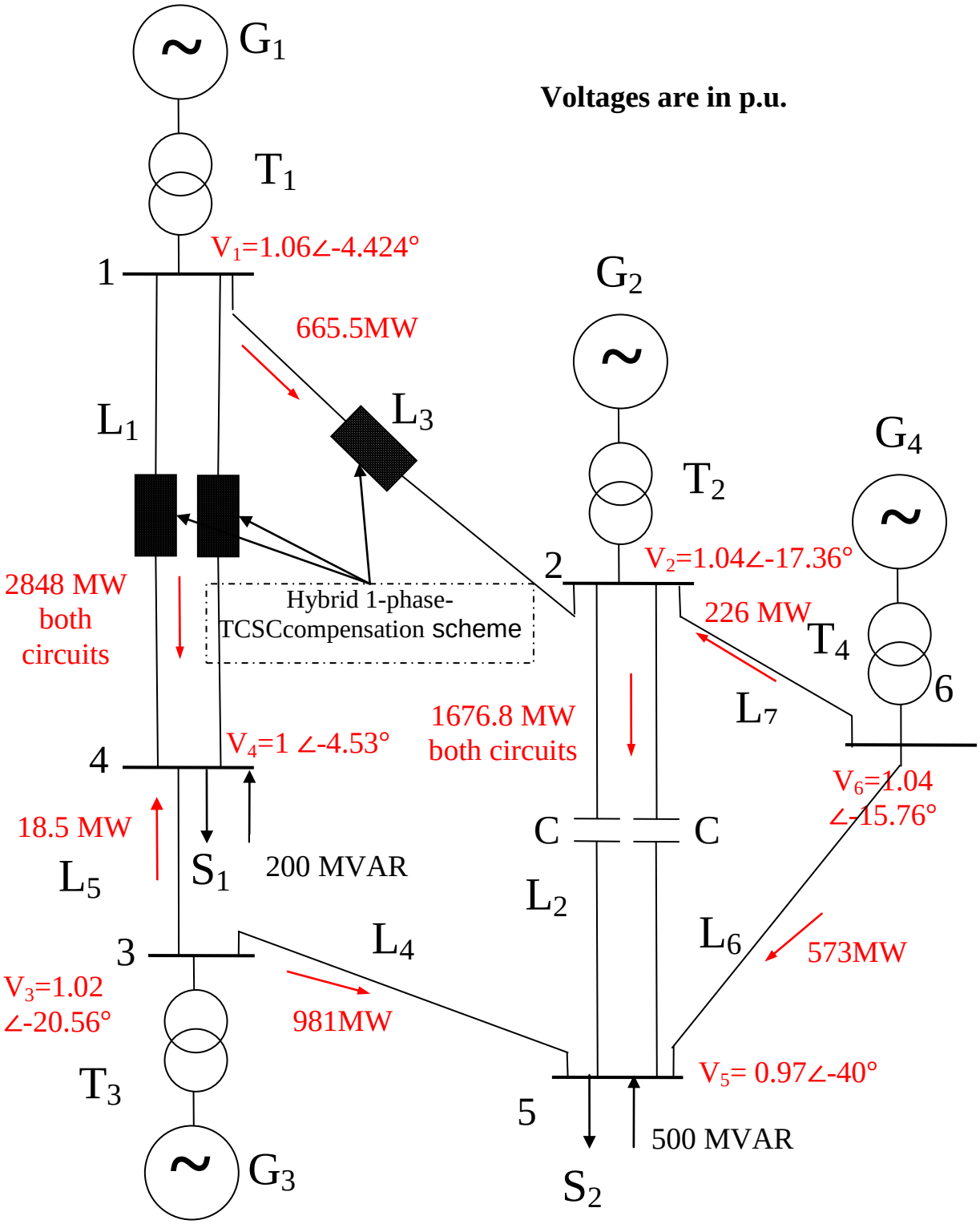


**Figure 4.20:** Power flow results of bus voltages and line real power flows of the system under study for case study IV.

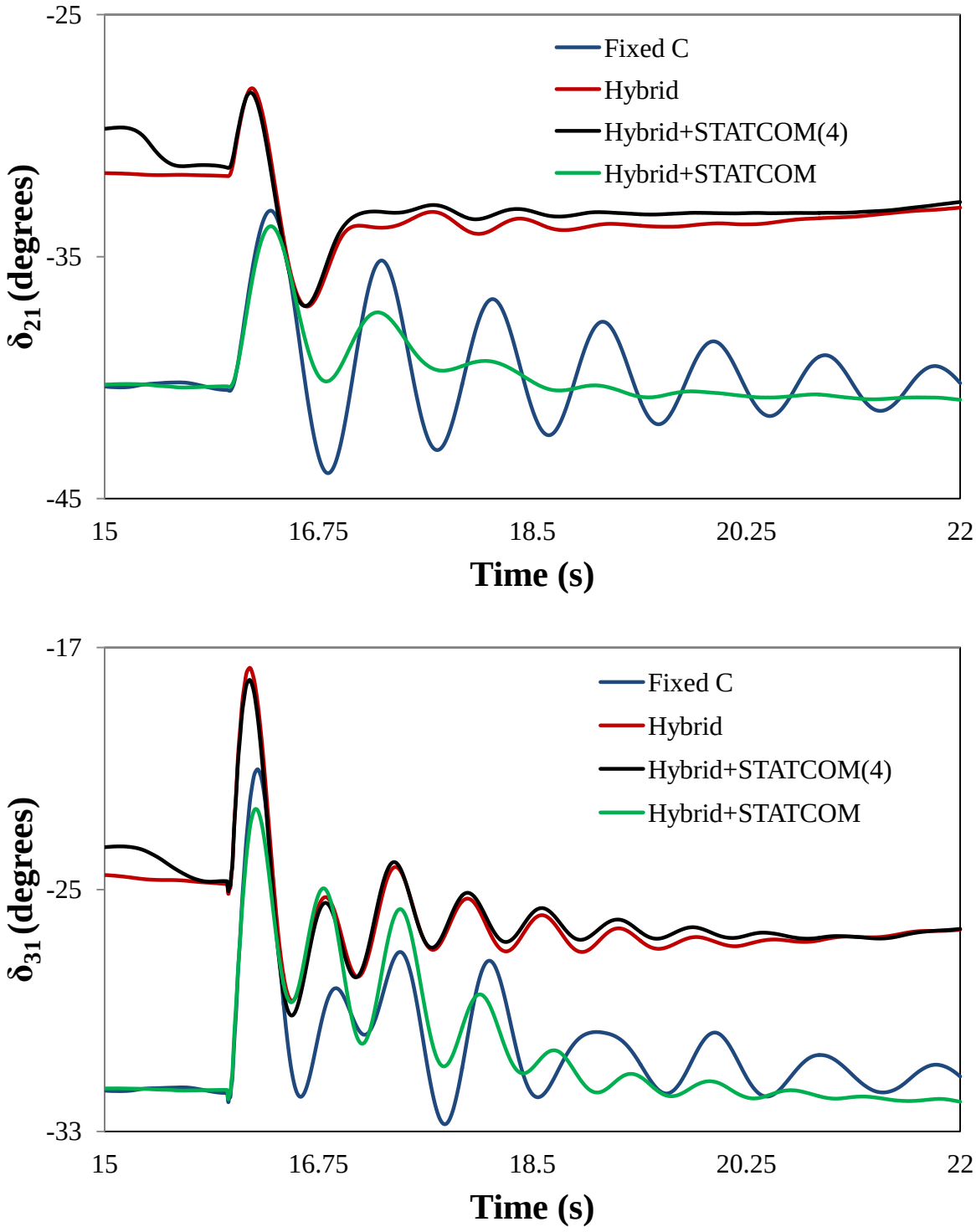


**Figure 4.21:** Generator load angles, measured with respect to generator 1 load angle, during and after clearing a three-cycle, three-phase fault at bus 4 (case study IV, stabilizing signals: $\delta_{21}$).

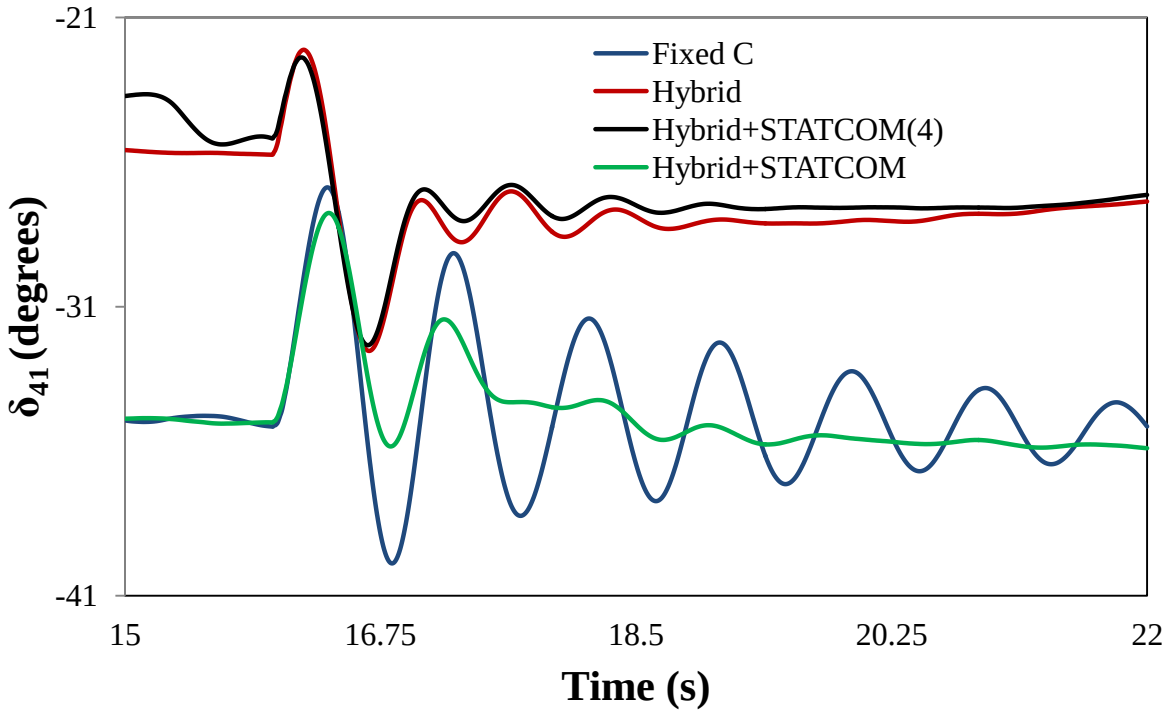


**Figure 4.21:** Continued.

## 4.7 Summary

This chapter investigates the potential use of a supplemental control of a STATCOM combined with a phase imbalanced hybrid series capacitive compensation scheme for damping power system oscillations. The capability to increase system damping and improve power transfer capabilities to supply load demand in two load centers using simple controllers is presented. The results of several case studies have demonstrated the effectiveness of the proposed supplemental controllers in improving the system dynamic performance.

# Chapter 5

# SUMMARY AND CONCLUSIONS

## 5.1 Summary

Oscillations of real power in power transmission systems may arise in corridors between generating areas as a result of poor damping of the interconnection, particularly during heavy power transfer. These oscillations can be excited by a number of reasons such as line faults, switching of lines or a sudden change of generator output. The existence of real power oscillations tends to limit the power transmission capacity of interconnections between areas or transmission regions.

As a result of the Flexible AC Transmission Systems (FACTS) initiative, considerable effort has been spent in the last two decades on the development of power electronic-based power flow controllers. The potential benefits of these FACTS controllers are now widely recognized by the power system engineering and the transmission and distribution communities. The TCSC and STATCOM have shown to be attractive and very effective controllers for power flow control, system oscillations damping and steady-state voltage profile enhancement. This thesis reports the results of the investigations that were carried out to explore the effectiveness of the hybrid single-phase-TCSC compensation scheme (Scheme I) and the STATCOM supplemental controllers in damping power system oscillations in multi-machine power systems.

A brief review of the benefits of series compensation of transmission lines is presented in Chapter 1. The inability of series capacitors in providing adequate damping to power system oscillations as well as their contribution to the subsynchronous resonance phenomenon are also discussed in this chapter.

In Chapter 2, the system used in the studies conducted in this thesis is introduced and the mathematical models of its components are presented. The results of digital time-domain simulations of a case study for the system with only fixed capacitance compensation during a three-phase fault are also presented in this chapter.

In Chapter 3, comprehensive descriptions of the TCSC, its three modes of operation and the analysis of its net reactance are presented. The phase imbalanced hybrid single-phase-TCSC compensation scheme and its modeling in the ElectroMagnetic Transient Program (EMTP-RV) are also presented.

In Chapter 4, several case studies investigating the effects of the location of the hybrid single-phase-TCSC compensation scheme, the degree of compensation provided by the scheme, the stabilizing signal, the fault clearing time, as well as the fault location on the damping of power system oscillations are documented. These studies are intended to demonstrate the effectiveness of Scheme I and the STATCOM supplemental controllers in damping power system oscillations resulting from clearing system faults.

## 5.2 Conclusions

The studies conducted in this thesis yield the following conclusions for the system under study:

1. The series capacitor compensated system is first swing stable for three-phase faults, but the post-contingency oscillations are not well damped.
2. Although the system has three natural modes of oscillation, generators 2, 3 and 4 tend to oscillate at a single frequency (approximately 1.4 Hz).
3. The hybrid single-phase-TCSC compensation scheme has shown to be, in general, very effective in damping power system oscillations at different loading profiles.
4. Increasing the proportion of the single-phase-TCSC to the fixed capacitor of its phase results in improving the damping of system oscillations. Increasing the proportion of the hybrid single-phase-TCSC compensation scheme to the total fixed capacitor compensation (i.e. installing the scheme in more transmission line circuits replacing fixed capacitor compensation) enhances significantly the damping of system oscillations. Choosing the values of such two proportion options can be considered as an optimization task between dynamic stability improvements and economical and reliability advantages of fixed series capacitors.
5. The performance of Scheme I supplemental controller when the deviation of generator 2 load angle, with respect to generator 1 load angle, is used as the stabilizing signal is better than when the deviations of generators 3 or 4 load angles with respect to generator 1 load

angle are utilized. This is true regardless of the fault location, fault clearing time or Scheme I location. On the other hand, the best stabilizing signal for the STATCOM controller is found to be either the deviation of generator 2 load angle, with respect to generator 1 load angle or the deviation of generator 4 load angle with respect to generator 1 load angle.

6. In all case studies, adequate power system oscillation damping is obtained with proportional-type TCSC and STATCOM supplemental controllers.
7. Overall, the best damping of the relative load angle responses are achieved when the hybrid single-phase-TCSC is installed in line $L_3$ as well as in the two circuits of line $L_1$.
8. The reduction of the generator first swings depends on the proportion of the hybrid single-phase-TCSC compensation scheme to the total fixed capacitor compensation in the system. It is observed, however, that in one case there is a slight increase in the first swing of one generator. It should be emphasized here that the main task of the supplemental controller of the hybrid single-phase-TCSC compensation scheme is to damp power system oscillations in the "already stable" system under study. For transient stability control of marginally stable power systems, different TCSC control methodologies are usually used.

# REFERENCES


[1] P.M. Anderson, *Subsynchronous resonance in power systems*, New York, IEEE Press, 1990.

[2] P.M. Anderson and R.G. Farmer, *Series Compensation of Power Systems*, PBLSH!, 1996.

[3] R. Billinton, M. Fotuhi-Firuzabad and S.O. Faried, "Power System Reliability Enhancement using a Thyristor Controlled Series Capacitor," IEEE Transactions on Power Systems, Vol. 14, No. 1, February 1999, pp. 369-374.

[4] J.L. Batho, J.E. Hardy and N. Tolmunen, "Series Capacitor Installations in the B.C. Hydro 500 kV System," IEEE Transactions on Power Apparatus and Systems, Vol. PAS-96, No. 6, November/December 1977, pp. 1767.1776.

[5] "Increased Power Transmission Capacity on 500 kV Grid by Installation and Refurbishing of Series Capacitors," ABB online web site, [http://www05.abb.com/global/scot/scot221.nsf/veritydisplay/7f8d670d8379cc50c1256fda003b4d0a/$File/McLeese%20A02-0159E.pdf].

[6] D.N. Kosterev, C.W. Taylor, W.A. Mittelstadt, "Model Validation for the August 10, 1996 WSCC System Outage," IEEE Transactions on Power Systems, Vol. 14, No. 3, August 1999, pp. 967-979.

[7] R. Witzmann, Damping of Interarea Oscillations in Large Interconnected Power Systems," Proceedings of the International Conference on Power Systems Transients (IPST01), Rio de Janeiro, Brazil, June 24-28, 2001, paper No. 197.

[8] Y.H. Song and A.T. Johns, *Flexible AC Transmission Systems (FACTS)*, London, Institution of Electrical Engineers, 1999.

[9] N.G. Hingorani and L. Gyugyi, *Understanding FACTS: Concepts and Technology of Flexible AC Transmission Systems*, New York, IEEE Press, 2000.

[10] C. Gama, "Brazilian North-South Interconnection Control-Application and Operating Experience with a TCSC," Proceedings of the 1999 IEEE PES Summer meeting, Edmonton, Alberta, Canada, July 18-22, 1999, Vol. 2, pp. 1103-1108.

[11] C. Gama and L. Angquist, "Commissioning and Operative Experience of TCSC for Damping Power Oscillation in the Brazilian North-South Interconnection," CIGRE, Session 2000, Paris, France, paper No. 14-104.

[12] D. Rai, S.O. Faried, G. Ramakrishna, and A. Edris," Damping Inter-Area Oscillations using Phase Imbalanced Series Compensation Schemes," IEEE Transactions on Power Systems, Vol. 26, No. 3, August 2011, pp. 1753-1761.

[13] D. Rai, G. Ramakrishna, S.O. Faried and A. Edris," Enhancement of Power System Dynamics Using a Phase Imbalanced Series Compensation Scheme," IEEE Transactions on Power Systems, Vol. 25, No. 2, May 2010, pp. 966-974.

[14] D. Rai, Power System Dynamics Enhancement Through FACTS Devices and Adaptive Control, Ph.D. thesis, University of Saskatchewan, 2012.

[15] H.A. Othman and L. Angquist, "Analytical Modeling of Thyristor-Controlled Series Capacitors for SSR Studies," IEEE Transactions on Power Systems, Vol. 11, No. 1, February 1996, pp. 119-127.

[16] B.K. Perkins and M.R. Iravani, "Dynamic Modeling of a TCSC with Application to SSR Analysis," IEEE Transactions on Power Systems, Vol. 12, No. 4, pp. 1619-1625, 1997.

[17] R.J. Piwko, C.W. Wegner, S.J. Kinney and J.D. Eden, "Subsynchronous Resonance Performance Tests of the Slatt Thyristor-Controlled Series Capacitor," IEEE Transactions on Power Delivery, Vol. 11, No. 2, April 1996, pp. 1112-1119.

[18] W. Zhu, R. Spee, R.R. Mohler, G.C. Alexander, W.A. Mittelstadt and D. Maratukulam, "An EMTP Study of SSR Mitigation Using the Thyristor- Controlled Series Capacitor," IEEE Transactions on Power Delivery, Vol. 10, No. 3, July 1995, pp. 1479-1485.

[19] Naoto Kakimoto and Anan Phongphanphanee, "Subsynchronous Resonance Damping Control of Thyristor-Controlled Series Capacitor," IEEE Transactions on Power Delivery, Vol. 18, No. 3, July 2003, pp. 1051-1059.

[20] R. Rajaraman, I. Dobson, R. H. Lasseter, and Y. Shern, "Computing the Damping of Subsynchronous Oscillations due to a Thyristor Controlled Series Capacitor," IEEE Transactions on Power Delivery, Vol. 11, No. 2, April 1996, pp. 1120–1127.

[21] P. Mattavelli, A.M. Stankovic`, and G.C. Verghese, "SSR Analysis with Dynamic Phasor Model of Thyristor-Controlled Series Capacitor," IEEE Transactions on Power Systems, Vol. 14, No. 1, February 1999, pp. 200–208.

[22] Alireza Daneshpooy and A.M. Gole, "Frequency Response of the Thyristor Controlled Series Capacitor," IEEE Transactions on Power Delivery, Vol. 16, No. 1, January 2001, pp. 53-58.

[23] J.F. Hauer, W.A. Mittelstadt, R.J. Piwko, B.L. Damsky, J.D. Eden, "Modulation and SSR Tests Performed on the BPA 500 kV Thyristor Controlled Series Capacitor Unit at Slatt Substation," IEEE Transactions on Power Systems, Vol. 11, No. 2. May 1996, pp. 801-806.

[24] P.S. Dolan, J.R. Smith and W.A. Mittelstadt, "A Study of TCSC Optimal Damping Control Parameters for Different Operating Conditions," IEEE Transactions on Power Systems, Vol. 10, No. 4, November 1995, pp. 1972-1978.

[25] J. Urbanek, R.J. Piwko, E.V. Larsen, B.L. Damsky, B.C. Furumasu and W. Mittlestadt, "Thyristor Controlled Series Compensation Prototype Installation at the Slatt 500 kV Substation," IEEE Transactions on Power Delivery, Vol. 8, No. 3, July 1993, pp. 1460-1469.

[26] S. Nyati, C.A. Wegner, R.W. Delmerico, R.J. Piwko, D.H. Baker and A. Edris, "Effectiveness of Thyristor Controlled Series Capacitor in Enhancing Power System Dynamics: An Analog Simulator Study," IEEE Transactions on Power Delivery, Vol. 9, No. 2, April 1994, pp. 1018-1027.

[27] X. R. Chen, N.C. Pahalawaththa, U.D. Annakkage and C.S. Kumble, "Design of Decentralised output Feedback TCSC Damping Controllers by Using Simulated

Annealing," IEE Proceedings, Generation, Transmission and Distribution, Vol. 145, No. 5, September 1998, pp. 553-558.

[28] Y.Y. Hsu and T.S. Luor, "Damping of Power System Oscillations using Adaptive Thyristor-Controlled Series Compensators Tuned by Artificial Neural Networks," IEE Proceedings, Generation, Transmission and Distribution, Vol. 146, No. 2, March 1999, pp. 137-142.

[29] X.X. Zhou and J. Liang, "Nonlinear Adaptive Control of TCSC to Improve the Performance of Power Systems," IEE Proceedings, Generation, Transmission and Distribution, Vol. 146, No. 3, May 1999, pp. 301-305.

[30] P. Kundur, *Power System Stability and Control*, New York, McGraw-Hill, 1994.

[31] Y. Yu, *Electric Power System Dynamics*, New York, Academic Press, 1983.

[32] O.I. Elgerd, *Electrical Energy Systems Theory*, McGraw-Hill, 1971.

[33] N. Mohan, T.M. Undeland and W.P. Robbins, *Power Electronics: Converters Applications, and Design*, Wiley, New York, 1995.

[34] R.M. Mathur and R.K. Varma, *Thyristor-Based FACTS Controllers for Electrical Transmission Systems*, Piscataway, NJ, IEEE, 2002.

[35] EMTP-RV website: www.emtp.com.

[36] A. Daneshpooy and A.M. Gole," Frequency Response of the Thyristor Controlled Series Capacitor," IEEE Transactions on Power Delivery, Vol. 16, No. 1, January 2001, pp. 53-58.

[37] K. Kabiri, S. Henschel and H.W. Dommel, "Resistive Behavior of Thyristor-Controlled Series Capacitors at Subsynchronous Frequencies," IEEE Transactions on Power Delivery, Vol. 19, No. 1, January 2004, pp. 374-379.

[38] H. Xie and L. Ängquist, "Synchronous Voltage Reversal control of TCSC – impact on SSR conditions," Proceedings of the Nordic Workshop on Power and Industrial Electronics (NORPIE), 2004.

[39] Lennart Ängquist, "Synchronous Voltage Reversal Control of Thyristor Controlled Series Capacitor," Royal Institute of Technology, TRITA-ETS-2002-07, ISSN 1650-674X.

[40] L. Angquist and C. Gama, "Damping Algorithm based on Phasor Estimation," Proceedings of the IEEE Power Engineering Society Winter Meeting, Columbus, Ohio, January 28 – February 1, 2001, Vol. 3, pp. 1160-1165.

[41] D. Rai, S.O. Faried, G. Ramakrishna, and A. Edris, "Hybrid Series Compensation Scheme Capable of Damping Subsynchronous Resonance," IET Generation, Transmission and Distribution, Vol. 4, No. 3, March 2010, pp. 456-466.

[42] A.M. Gole, S. Filizadeh, R.W. Menzies, and P.L. Wilson, "Optimization-enabled Electromagnetic Transient Simulation," IEEE Transactions on Power Delivery, Vol. 20, No. 1, January 2005, pp. 512–518.

[43] A.M. Gole, S. Filizadeh, and P.L. Wilson, "Inclusion of Robustness into Design using Optimization-enabled Transient Simulation," IEEE Transactions on Power Delivery, Vol. 20, No. 3, July 2005, pp. 1991–1997.

[44] R. Grünbaum and Jacques Pernot, "Thyristor Controlled Series Compensation: A State of the Art Approach for Optimization of Transmission over Power Links, ABB online web site: [http://www05.abb.com/global/scot/scot221.nsf/veritydisplay/d578889d05b3ba01c1256fda003b4cff/$File/SEE_FIILE2001_TCSC.pdf].

[45] N. Yang, Q. Liu and J. McCalley, "TCSC Controller Design for Interarea Oscillations," IEEE Transactions on Power Systems, Vol. 13, No. 4, November 1998, pp. 1304-1309.

[46] X. Chen, N. Pahalawaththa, U. Annakkage and C. Kumbe, "Output Feedback TCSC Controllers to Improve Damping of Meshed Multi-Machine Power Systems," IEE Proceedings, Generation, Transmission and Distribution, Vol. 44, No. 3, May 1997, pp. 243-248.

[47] J. Machowski, S. Robak and J. Bialek, "Damping of Power Swings by Optimal Control of Series Compensators," Proceedings of the 10th International Conference on Power System Automation and Control *PSAC'97*, Bled, Slovenia, October 1-3, 1997, pp. 39-44.

[48] J.F. Hauer, M.K. Donnelly, W.A. Mittelstadt, W. Litzenberger and D.J. Maratukulam, "Information Functions and Architecture for Networked Monitoring of Wide Area Power System Dynamics: Experience with the Evolving Western System Dynamic Information Network," Proceedings of the Sixth Symposium of Specialists on Electric Operational and Expansion Planning (VI SEPOPE), Bahia, Brazil, May 24-29, 1998.

[49] B. Bhargava and A. Salazar, "Use of Synchronized Phasor Measurement System for Monitoring Power System Stability and System Dynamics in Real-Time," Proceedings of the 2008 IEEE PES GM, Pittsburgh, PA, July 20 – 24, 2008, pp. 1-8.

[50] H. Ni, G.T. Heydt and L. Mili, "Power System Stability Agents using Robust Wide Area Control, "IEEE Transactions on Power Systems, Vol. 17, No. 4, November 2002, pp. 1123-1131.

[51] X. Xie, J. Xiao, C. Lu and Y. Han, "Wide-Area Stability Control for Damping Interarea Oscillations of Interconnected Power Systems," IEE Proceedings, Generation, Transmission and Distribution, Vol. 153, No. 5, September 2006, pp. 507-514.

[52] C.W. Taylor, D.E. Erickson, K.E. Martin, R.E. Wilson and V. Venkatasubramanian," WACS-Wide-Area Stability and Voltage Control System: R&D and Online Demonstration," Proceedings of IEEE, Vol. 93, No. 5, May 2005, pp. 892-906.

[53] X. Zhou and J. Liang, "Overview of Control Schemes for TCSC to Enhance the Stability of Power Systems," IEE Proceedings, Generation, Transmission and Distribution, Vol. 146, No. 2, March 1999, pp. 125-130.

# APPENDIX A

## DATA OF THE SYSTEM UNDER STUDY

### A.1 Synchronous Generators

**Table A.1:** Synchronous generator data.

| | $G_1$ | $G_2$ | $G_3$ | $G_4$ |
|---|---|---|---|---|
| Rating, MVA | 2400 | 1000 | 1100 | 1100 |
| Rated voltage, kV | 26 | 26 | 26 | 26 |
| Armature resistance, $r_a$ , p.u. | 0 | 0.0045 | 0.0045 | 0.0045 |
| Leakage reactance, $x_l$ , p.u. | 0.13 | 0.14 | 0.12 | 0.12 |
| Direct-axis synchronous reactance, $x_d$ , p.u. | 1.79 | 1.65 | 1.54 | 1.54 |
| Quadrature-axis synchronous reactance, $x_q$ , p.u. | 1.71 | 1.59 | 1.5 | 1.5 |
| Direct-axis transient reactance, $x_d^{'}$ , p.u. | 0.169 | 0.25 | 0.23 | 0.23 |
| Quadrature-axis transient reactance, $x_q^{'}$ , p.u. | 0.228 | 0.46 | 0.42 | 0.42 |
| Direct-axis subtransient reactance, $x_d^{''}$ , p.u. | 0.135 | 0.2 | 0.18 | 0.18 |
| Quadrature-axis subtransient reactance, $x_q^{''}$ , p.u. | 0.2 | 0.2 | 0.18 | 0.18 |
| Direct-axis transient open-circuit time constant, $T_{do}^{'}$ , s | 4.3 | 4.5 | 3.7 | 3.7 |
| Quadrature-axis transient open-circuit time constant, $T_{qo}^{'}$ , s | 0.85 | 0.55 | 0.43 | 0.43 |
| Direct-axis subtransient open-circuit time constant, $T_{do}^{''}$ , s | 0.032 | 0.04 | 0.04 | 0.04 |
| Quadrature-axis subtransient open-circuit time constant, $T_{qo}^{''}$ , s | 0.05 | 0.09 | 0.06 | 0.06 |
| Zero-sequence reactance, $x_o$ , p.u. | 0.13 | 0.14 | 0.12 | 0.12 |
| Inertia constant, H, s | 7 | 3.7 | 3.12 | 3.12 |

## A.2 Transformers

**Table A.2:** Transformer data.

| | $T_1$ | $T_2$ | $T_3$ | $T_4$ |
|---|---|---|---|---|
| Rating, MVA | 2400 | 1000 | 1100 | 1100 |
| Rated voltage, kV | 26/500 | 26/500 | 26/500 | 26/500 |
| Resistance, $r_T$ , p.u. | 0 | 0 | 0 | 0 |
| Leakage reactance, $x_T$ , p.u. | 0.1 | 0.1 | 0.1 | 0.1 |

## A.3 Transmission Lines

All transmission lines have the same series impedance and shunt admittance per unit length.

$$Z_{T.L.series} = 0.01864 + j\,0.3728 \quad \Omega / km$$

$$Y_{T.L.shunt} = j\,4.4739 \quad \mu S / km$$

Transmission voltage = 500 kV

## A.4 System Loads

$$S_1 = 1400 + j\,200 \quad MVA$$

$$S_2 = 3137 + j\,500 \quad MVA$$

## A.5 Excitation System

**Table A.3:** Excitation system data.

| | |
|---|---|
| $K_A$ = 2 | $K_E$ = 1.0 |
| $K_{FE}$ = 0.03 | $T_A$ = 0.04 s |
| $T_{FE}$ = 1.0 s | $T_E$ = 0.01s |
| *Lim_max* = 4.75 p.u. | *Lim_min* = -4.75 p.u. |

# APPENDIX B

## THE VOLTAGE SOURCE CONVERTER

### B.1 Voltage-Source Converter

The Voltage-Source Converter (VSC) is the basic building block of many of the modern FACTS devices such as STATCOM, SSSC, and UPFC. The voltage-source converter uses switching gates that have turn-on and turn-off capability such as Gate Turn-Off Thyristor (GTO), Insulated Gate Bipolar Transistor (IGBT), MOS Turn-Off Thyristor (MTO) and Insulated Gate-Commutated Thyristor (IGCT). The voltage-sourced converter generates ac voltage from a dc voltage. With a voltage-source converter, the magnitude, the phase angle and the frequency of the output voltage can be controlled. It has the capability to transfer power in either direction by just reversing the polarity of the current. A typical topology of a GTO–based three-phase two level voltage-source converter is shown in Figure B.1 (also known as six-pulse converter). The voltage-source converter dc voltage is supported by capacitor(s) large enough to at least handle a sustained charge/discharge current without a significant change in the dc voltage.

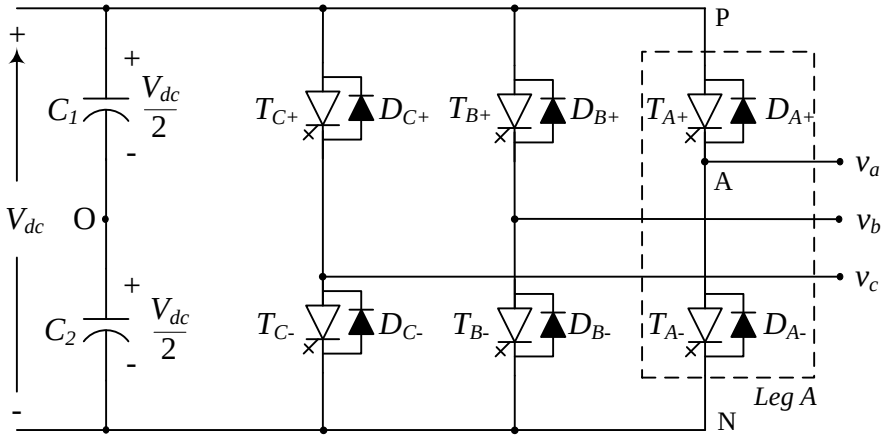


**Figure B.1:** Topology of a three-phase, two-level, voltage-source converter.

The operating principle of a converter can be explained with the help of GTO and diode switching operation. For example, when GTO $T_{A+}$ is switched '*on*', the phase *a* ac voltage would jump to $+V_{dc}/2$. If the current happens to flow from P to A through GTO $T_{A+}$ (shown in the dotted box in Figure B.1), the power would flow from the dc side to the ac side acting as an inverter. On the other hand, if the current happens to flow from A to P, it would flow through

diode $D_{A+}$ even if GTO $T_{A+}$ is switched '*on'*, and the power would flow from the ac side to dc side acting as a rectifier.

There are many types of converter concepts within the voltage-sourced converter category for example: multi pulse, multi level, and cascade concept. As all the converter topologies operate by turn-on and turn-off of power electronic gates, they require some sort of switching circuitry. The inverter switching strategies used at present can be classified into two main categories [33]:

1. ***Fundamental frequency switching***: In this technique, the switching of each semiconductor device is limited to one turn-on and one turn-off per power cycle. The six-pulse converter shown in Figure B.1 produces a quasi-square-wave output with this method, which has an unacceptably high harmonic content. In practice, a number of six-pulse units are combined in series and/or parallel to achieve a better waveform quality and higher power ratings.
2. ***Pulse-Width Modulation* (*PWM*)**: In this technique, the semiconductor switches are turned '*on'* and '*off*' at a rate considerably higher than the power frequency. The output waveform has multiple pulses per half-cycle. This shifts the undesirable harmonics in the output to higher frequencies and filtering is possible with smaller components. This method suffers, however, from higher switching losses compared to the previous switching technique. The PWM method is described in detail in the following section.

### B.1.1 Pulse Width Modulation

The Pulse Width Modulation based switching scheme creates a train of switching pulses by comparing a reference wave "$v_{ref}$" and a carrier wave "$v_{carrier}$". The *ac* output voltage of the converter consists of multiple pulses per half-cycle and the width of the pulses can be varied to change the amplitude of the fundamental frequency of the output voltage. The PWM converter related basic terms that are used throughout this thesis are given below:

$V_{ref}$ = Reference sinusoidal waveform peak magnitude, volts.

$f_r$ = Reference sinusoidal wave frequency, Hz, 60 Hz in general.

$V_{carrier}$ = Triangular carrier wave peak magnitude, volts, generally kept constant.

$f_c$ = Triangular carrier wave frequency, Hz.

MI $= V_{ref}/V_{carrier}$, amplitude modulation ratio, or modulation index.

$m_f = f_c/f_r$ , frequency modulation ratio.

Figure B.2 shows one leg of a six-pulse converter and Figure B.3 shows the generation of the switching pulses by comparing the reference wave with the high frequency triangular carrier wave. The turn-on and turn-off of the GTOs takes place corresponding to the crossing points of the saw-tooth wave and the sine wave. For example, when the rising slope of the triangular wave crosses the sinusoidal wave, GTO $T_{A+}$ switches '*on'* and GTO $T_{A-}$ switches '*off*'. Similarly, when the negative slope of the triangular wave crosses the sine wave, GTO $T_{A-}$ turns '*on'* and GTO $T_{A+}$ turns '*off*'. The switching pair $T_{A+}$ and $T_{A-}$ are complement to each other.

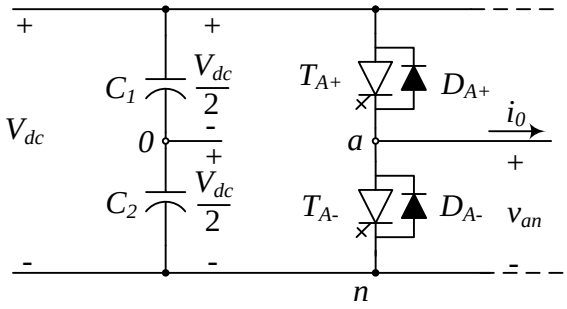


**Figure B.2:** One leg of a voltage-source converter.

The output voltage "$v_{an}$" of the PWM converter contains a fundamental frequency component "$v_{a0}$" and harmonics. Furthermore, the output voltage is symmetrical about the zero crossing of the sine wave (if the triangular wave frequency is chosen to be an odd multiple of the reference wave). In general, the magnitude of the triangular carrier wave is kept constant and the magnitude of the sinusoidal reference wave is either increased or decreased (i.e. increase or decrease of modulation index, *MI*), to increase or decrease the amplitude of the fundamental component of the ac output voltage. When the sinusoidal reference wave amplitude, $V_{ref}$ is less than $V_{carrier}$, the *ac* output voltage changes linearly with modulation index, and when $V_{ref}$ is greater than $V_{carrier}$ , the output voltage tends to become a square wave.

The magnitude of the PWM converter output voltage can be controlled from zero to the maximum value and the phase angle and/or frequency can be controlled by controlling the reference wave phase and/or frequency almost instantaneously [2], [33]. The PWM method has certain advantages such as faster response and capability for harmonic elimination [2], [33] compared to the fundamental switching method. The PWM method is used to model the voltage-source converter in this research work.

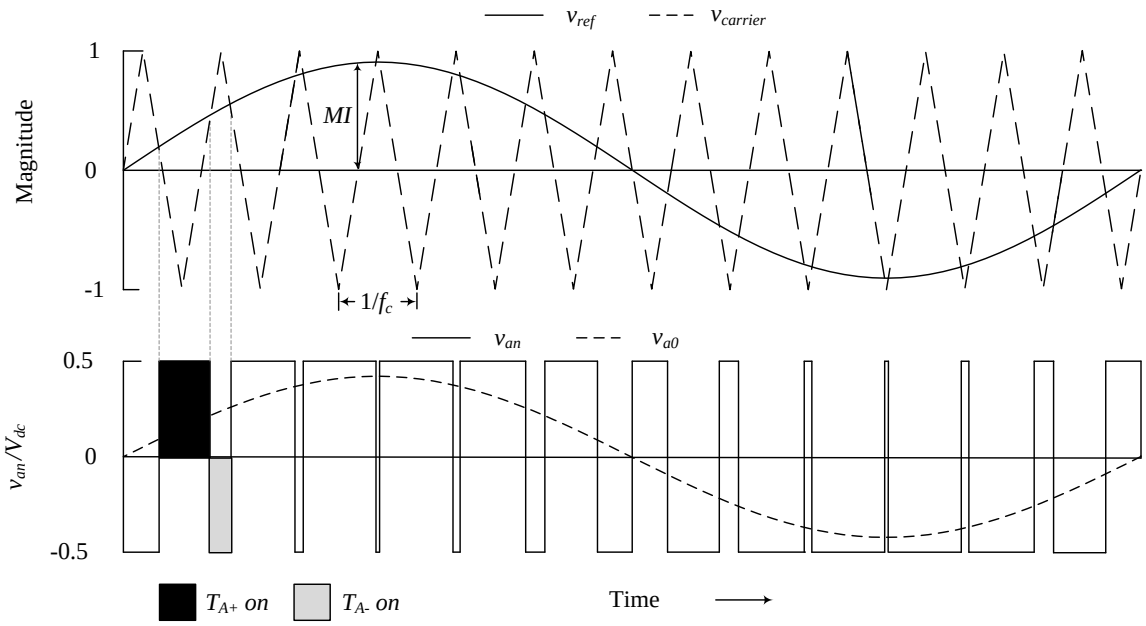


**Figure B.3:** Pulse-width modulation switching signal generation and output voltage.

## B.2 Principle of Voltage Source Converter Operation

Consider a VSC connected to an AC system through a lossless reactor as illustrated in Figure B.4. The converter produces an AC voltage with a fundamental frequency equal to that of the AC reference voltage. The voltage at the supply bus is assumed to be $V_s \angle 0^0$, and the AC voltage produced by the VSC is taken to be $V_{sh} \angle \delta_{sh}$. $X_l$ is the reactance of the converter reactor.

The active and the reactive power can be expressed respectively as

$$P = \frac{V_{sh} V_s}{X_l} \sin \delta_{sh} \tag{B.1}$$

$$Q = \frac{V_{sh} V_s}{X_l} \cos \delta_{sh} - \frac{V_s^2}{X_l} \ . \tag{B.2}$$

With respect to these two Equations, the following observations are noticed:

1. The active power flow between the AC source and the VSC is controlled by the phase angle $\delta_{sh}$. The active power flows into the AC source from the VSC for $\delta_{sh} > 0$, and flows out of the AC source from the VSC for $\delta_{sh} < 0$,

2. The reactive power flow is determined mainly by the amplitude of the AC source voltage, $V_s$, and the VSC output fundamental voltage, $V_{sh}$, as the angle $\delta_{sh}$ is generally small. For $V_{sh} > V_s$, the VSC generates reactive power and while it consumes reactive power when $V_{sh} < V_s$.

Because of its key steady-state operational characteristics and impact on system voltage and power flow control, the VSC is becoming the basic building block employed in the new generation of FACTS Controllers.

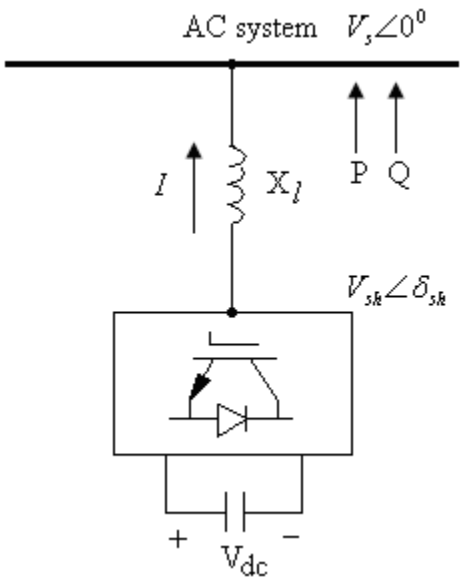


**Figure B.4:** A VSC connected to an AC system.